

**RIGA TECHNICAL UNIVERSITY**

Faculty of Civil Engineering  
Institute of Heat, Gas and Water Technology

**Renārs Millers**

Doctoral Student of the Study Programme “Heat, Gas and Water Technology”

**SIMULATION MODEL FOR COOLING PANELS  
WITH INTEGRATED LATENT THERMAL  
STORAGE SYSTEM**

**Doctoral Thesis**

Scientific Supervisor  
Professor Dr. sc. ing.  
ARTURS LEŠINSKIS

RTU Press  
Riga 2021

Millers, R. Simulation Model for Cooling Panels with Integrated Latent Thermal Storage System. Doctoral Thesis. Riga: RTU Press, 2021. 105 p.

Published in accordance with the decision of the Promotion Council "RTU P-12" of 23. February 2021, Minutes No. 1/21.

# **DOCTORAL THESIS PROPOSED TO RIGA TECHNICAL UNIVERSITY FOR THE PROMOTION TO THE SCIENTIFIC DEGREE OF DOCTOR OF SCIENCE**

To be granted the scientific degree of Doctor of Science (Ph. D.), the present Doctoral Thesis has been submitted for the defence at the open meeting of RTU Promotion Council on 3 September 2021 at 15.00 at the Faculty of Civil Engineering of Riga Technical University, 6B Kipsalas Street, Room 106.

## **OFFICIAL REVIEWERS**

Asoc. prof., Dr.sc.ing. Jurgis Zemītis  
Riga Technical University, Latvia

Asoc. prof. Dr.sc.ing. Sandra Gusta  
Latvia University of Life Sciences and Technology, Latvia

Prof. Dr.sc.ing. Martin Thalfeldt  
Tallinn University of Technology, Estonia

## **DECLARATION OF ACADEMIC INTEGRITY**

I hereby declare that the Doctoral Thesis submitted for the review to Riga Technical University for the promotion to the scientific degree of Doctor of Science (Ph. D.) is my own. I confirm that this Doctoral Thesis had not been submitted to any other university for the promotion to a scientific degree.

Renārs Millers ..... (signature)

Date: .....

The Doctoral Thesis has been written in English. It consists of an Introduction; 7 Chapters; Conclusion; 47 figures; 17 tables; the total number of pages is 105. The Bibliography contains 162 titles.

## ANNOTATION

This thesis focuses on the development of an experimentally validated equation based simulation model of a cooling panel with integrated latent thermal storage system for utilization in Nearly Zero-Energy Buildings (NZEB) buildings. Development of such model is necessary in order for this technology to achieve industry-readiness.

The thesis is composed of a literature review and an experimental study.

The literature review focuses on NZEB requirements in European Union (EU) member countries, previous research in the field of passive cooling technologies and latent thermal storage systems. The passive cooling technologies described in the literature review are considered potential cooling energy sources to be coupled with the researched cooling panel. A combination of these technologies may be used to address overheating issues in NZEB buildings.

The experimental study is focused on the development and validation of the aforementioned cooling panel simulation model. The numerical model is developed by using dynamic simulation software IDA ICE and is composed of sub-models written in *Neutral Model Format (NMF)*. The simulation model is validated against experimental measurements carried out in a test chamber that was developed specially for this study. Moreover a comparative study is carried out where the results generated by the developed and validated simulation model are compared against a previous CFD simulation study results acquired by a different research team.

The accuracy of the results generated by the simulation model when compared with experimental measurements is a maximum deviation of 2.2 °C and a root mean square error of 1.01 °C. The results indicate that the accuracy reached by the simulation model is equal or higher than reported in other similar studies, therefore the accuracy is considered suitable for energy, thermal comfort and cooling load simulation in whole building scale simulation studies.

The experimental study also provides several limitations for the proposed simulation model that shall be respected in order to reach the accuracy claimed in this study.

## ANOTĀCIJA

Šī promocijas darba fokuss ir vērsts uz vienādojumiem balstīta simulācijas modeļa izstrādi dzesēšanas panelim ar integrētu latentu termālās enerģijas akumulatoru, kas ir eksperimentāli validēts un paredzēts izmantošanai gandrīz nulles enerģijas ēkās. Šāda modeļa izstrāde ir nepieciešama, lai šī tehnoloģija būtu gatava izmantošanai būvniecības industrijā.

Promocijas darbs sastāv no literatūras apskata un eksperimentāla pētījuma.

Literatūras apskatā ir iekļauts pārskats par gandrīz nulles enerģijas ēku prasībām Eiropas Savienības dalībvalstīs, iepriekšējiem pētījumiem pasīvās dzesēšanas tehnoloģiju jomā un latentu termālās enerģijas akumulatoru tehnoloģijām. Pasīvās dzesēšanas sistēmas, kas ir aplūkotas literatūras apskatā, tiek uzskatītas par potenciāliem dzesēšanas enerģijas avotiem, kuri var tikt izmantoti kopā ar iepriekš minētajiem dzesēšanas paneļiem. Šo tehnoloģiju kombinācija var tikt izmantota, lai reaģētu uz telpu pārkaršanas problēmām gandrīz nulles enerģijas ēkās.

Eksperimentālais pētījums ir fokusēts uz iepriekš minētā paneļa simulācijas modeļa izstrādi un validāciju. Šī pētījuma ietvaros izmantotais matemātiskais modelis ir izstrādāts, izmantojot dinamisko simulāciju rīku *IDA ICE* un sastāv no apakšmodeļiem, kuri ir rakstīti *NMF (Neutral model format)* programmēšanas valodā. Simulāciju modelis ir validēts pret eksperimentāliem mērījumiem, kas ir veikti testa kamerā, kura ir izstrādāta speciāli šim pētījumam. Eksperimentālā pētījuma ietvaros ir veikts arī salīdzinošais pētījums, kurā tiek savstarpēji salīdzināti izstrādātā simulācijas modeļa rezultāti ar rezultātiem, kas iegūti no plūsmas dinamikas simulācijas (CFD), ko iepriekš izstrādājusi cita pētnieku komanda.

Izstrādātā simulācijas modeļa precizitāte attiecībā pret eksperimentālajiem mērījumiem testa kamerā ir maksimālā novirze 2,2 °C un vidējā kvadrātiskā kļūda 1,01 °C. Rezultāti norāda uz to, ka izstrādātā modeļa precizitāte ir līdzvērtīga vai augstāka par precizitāti, kas ir tikusi ziņota citos, līdzīgos pētījumos. Līdz ar to var uzskatīt, ka šī modeļa precizitāte ir pietiekama, lai to izmantotu enerģijas patēriņa, termālā komforta un dzesēšanas slodžu simulācijās, kas ietver pilnu ēkas apjomu.

Eksperimentālajā pētījumā arī ir norādīti vairāki izstrādātā modeļa ierobežojumi, kuri būtu jāņem vērā, lai sasniegtu precizitāti, kas ziņota šajā pētījumā.

# CONTENTS

ANNOTATION .....	4
ANOTĀCIJA .....	5
CONTENTS .....	6
ABBREVIATIONS.....	9
1 INTRODUCTION.....	10
1.1 Novelty and motivation.....	10
1.2 Aim and scope.....	11
1.3 Thesis task.....	11
1.4 Thesis practical value.....	12
1.5 Arguments for the defence of the thesis .....	12
1.6 List of conferences .....	13
1.7 List of publications .....	13
1.8 Thesis composition and outline .....	14
2 REVIEW OF NEARLY ZERO-ENERGY BUILDING REQUIREMENTS IN EUROPEAN UNION.....	15
2.1 Background of nearly zero-energy building concept.....	15
2.2 Examples of nearly zero-energy building requirements in EU member countries .....	16
2.3 Conclusion .....	20
3 REVIEW OF PASSIVE COOLING TECHNOLOGIES FOR APPLICATION IN BUILDINGS .....	22
3.1 Night cooling .....	22
3.2 Radiant nocturnal cooling .....	24
3.3 Radiant cooling using “the window of transparency” in the Earth’s atmosphere .....	25
3.4 Adiabatic or evaporative cooling .....	27
3.5 Desiccant cooling.....	30
3.6 Passive geothermal cooling.....	31
3.7 Earth to air heat exchangers .....	32
3.8 Earth to liquid heat exchangers.....	32
3.9 Conclusion .....	32

4	REVIEW OF PHASE CHANGE MATERIALS .....	34
4.1	Different types of PCM materials .....	35
	Solid-liquid PCMs .....	36
	Paraffin based PCMs.....	38
	Fatty acid based PCMs.....	41
	Inorganic solid-liquid PCMs .....	41
	Eutectic PCMs .....	42
4.2	Conclusion .....	43
5	REVIEW OF THERMAL STORAGE SYSTEMS BASED ON PCM APPLICATION.....	44
5.1	Passive PCM thermal storage systems.....	44
	PCM integration into plasterboards .....	45
	PCM integration into external envelope .....	47
5.2	Active PCM thermal storage systems .....	48
	PCM to air heat exchangers .....	48
	PCM storage tanks .....	52
	Cooling panels with integrated PCM thermal storage .....	52
5.3	Conclusion .....	58
6	REVIEW OF THE HEAT TRANSFER THEORY .....	59
6.1	Conduction.....	59
6.2	Convection .....	62
6.3	Radiation.....	65
6.4	Conclusion .....	66
7	METHODOLOGY .....	68
7.1	Experimental set-up .....	68
	Experimental test chamber.....	68
	The cooling panel.....	71
	Simulated heat gains .....	72
	Simulation model for validation .....	73
	Total heat transfer coefficients.....	74
	Container walls and fixed air gap .....	75
	PCM layer .....	76
	Hydronic circuit .....	78

7.2	Simulation model for performance modelling.....	81
8	RESULTS AND DISCUSSION.....	83
8.1	Verification of the simulation model.....	83
	Statistical analyses of experimental results.....	83
	Simulation model without a PCM cooling panel.....	84
	Simulation model with a PCM cooling panel and a cooling water connection.....	85
	Performance modelling - comparative Case.....	88
8.2	Summary of the results.....	90
8.3	Limitations of the developed model.....	91
	Surface heat transfer coefficients.....	91
	PCM layer.....	92
	Hydronic circuit.....	92
9	CONCLUSION.....	93
10	BIBLIOGRAPHY.....	96

## ABBREVIATIONS

EBSM	Equation based simulation model
CFD	Computational fluid dynamics
PCM	Phase change materials
ODP	Ozone depleting potential
GWP	Global warming potential
HVAC	Heating, ventilation and air-conditioning
EU	European Union
EPBD	Energy performance buildings directive
NZEB	Nearly zero-energy building
RES	Renewable energy source
TABS	Thermally active building structure
DHW	Domestic hot water
MEP	Mechanical, electrical and plumbing systems
SEER	Seasonal energy efficiency ratio
SFP	Specific fan power
IR	Infra-red spectrum
EER	Energy efficiency ratio
DEC	Direct evaporative cooling
IEC	Indirect evaporative cooling
EATHE	Earth to air heat exchanger
COP	Coefficient of performance
SCOP	Seasonal coefficient of performance
TES	Thermal energy storage system
AC	Air conditioning
<i>NMF</i>	Neutral model format
<i>IDA ICE</i>	IDA Indoor Climate and Energy
RMSE	Root mean square error
3D	Three-dimensional
ZEB	Zero-energy building

# 1 INTRODUCTION

## 1.1 Novelty and motivation

For the last decades the need for cooling of indoor premises has increased in Central European as well as Northern European climate. This phenomenon is caused by:

- highly insulated building envelopes (especially with light-weight structures [1]);
- higher thermal comfort levels required by occupants;
- the climate change;
- thermal island effect in large cities [2–5];
- the use of large glazed surfaces that in many cases are required to achieve optimal daylight levels [6,7].

According to the estimations this trend will continue. It is reflected by the fact that the worldwide final energy consumption for cooling has more than tripled in the time period from 1990 to 2016 and according to estimations the energy consumed by cooling equipment will triple again by year 2050 [8]. Particularly large increases in cooling energy growth have been observed in the residential sector.

Currently mechanical cooling is responsible for approximately 20 % of total energy consumption in buildings in Europe [8].

It is clear that the increase of cooling demand is in conflict with the EU movement towards reducing greenhouse gas emissions. New passive cooling technologies are essential to address overheating issues and avoid the increase of installation of cooling equipment that contains refrigerants with high ODP and GWP potentials.

It is known that in most cases passive cooling technologies are not sufficient to cover all cooling requirements in a building. This issue at least partly can be addressed by incorporating thermal energy storage systems.

Thermal energy storage systems (TES) systems can be divided into passive and active systems.

Passive systems usually rely on incorporating PCMs in building structures that act as thermal mass and help to stabilize room temperature. Often these systems fail to serve the purpose because the PCM thermal storage does not have a sufficient heat sink and the PCM thermal storage fails to undergo melting/solidification cycles rendering the system useless.

Active systems, on the other hand, employ some type of mechanism that extracts thermal energy from the PCM material in a controlled way greatly increasing the overall efficiency. Despite the fact that the active type TES are more complex, they are recognized as suitable candidates to be coupled with passive cooling systems.

The most common type of active thermal storage systems are PCM to air heat exchangers that are installed in ventilation systems and ceiling based cooling panels with integrated latent thermal storage.

This thesis focuses on the second type of aforementioned active type TES systems. The main focus of the research is set on the development of a validated equation based simulation

model for a ceiling based cooling panels with integrated latent thermal storage system for a previously developed cooling panel.

The development and validation of such simulation model is necessary to accurately predict the behaviour of these panels in modern NZEB buildings using dynamic energy simulation tools preparing this system to be industry-ready.

Validated numerical based simulation models for this type of cooling panel with integrated thermal storage system that utilises bulk PCM have not been developed before and, therefore, can be considered novel.

## 1.2 Aim and scope

This thesis aims to develop a calibrated simulation model of a cooling panel with integrated PCM storage and test its applicability for adaptation in full scale building simulation models. The simulation model was developed in *IDA Indoor climate and energy* software. The hydronic cooling panel with integrated PCM storage was developed in the scope of a previous *European Regional Development Fund* research project *No.1.1.1.1/16/A/007 “A New Concept for Sustainable and Nearly Zero-Energy Buildings.”*

This thesis attempts to demonstrate that it is possible to reach a reasonable accuracy reproducing measurements from a physical experiment in a test chamber and a more sophisticated CFD simulation model using a simulation model developed in *IDA ICE*.

This approach was chosen because despite the fact that CFD simulation methods are the most accurate mathematical representations of physical processes their applicability for practical heating/cooling load calculations as well as whole year energy calculations in buildings is very limited. The use of CFD simulations for this purpose is impractical due to labour intensity and very significant computing power required. Nevertheless, dynamic simulation tools allow simulating large systems in relatively small time periods and such simulation tools are widely used in the industry.

### Hypothesis

Experimentally validated equation based numerical simulation model of a hydronic cooling panel with integrated latent thermal storage can produce simulation results with accuracy suitable for application in construction industry to support other passive cooling technologies.

## 1.3 Thesis task

To achieve the aim of the thesis several tasks are laid out:

- To perform state a of art literature review for:
  - NZEB requirements in different EU member states;
  - previous studies regarding passive cooling technologies;
  - different PCM materials and their properties;

- different latent thermal storage applications in buildings and existing numerical models;
- fundamentals of heat transfer in HVAC systems;
- To describe the methodology, experimental set-up and numerical models used for the study;
- To perform experiments and gather data;
- To perform calibration and validation of the elaborated model against experimental results and results acquired from a CFD simulation;
- To analyse the results in context of other similar studies.

#### **1.4 Thesis practical value**

Without a reliable thermal storage it is difficult for the majority of currently existing passive cooling technologies to provide sufficient cooling in buildings. This result in increased energy consumption and lowered thermal comfort levels in new buildings. Currently only CFD simulations can accurately describe this particular type of cooling panel with integrated latent thermal storage system.

CFD simulation models are used in many industries and are known to be accurate representations of actual systems also in the case of PCM cooling panels and other HVAC systems. However, this approach is impractical and not industry-ready for application in construction industry due to high complexity and vast computation power required to calculate even simple cases. The developed equation based numerical model can be applied by industry professionals for practical whole building scale simulations for HVAC system sizing, thermal comfort and annual energy simulations.

The key results of this thesis and the developed equation based simulation model have been published in an open access journal *Energies* by *Multidisciplinary Digital Publishing Institute* [9].

#### **1.5 Arguments for the defence of the thesis**

- The experimental results demonstrate a reasonable agreement between the measured and simulated results;
- Results produced by the developed model demonstrate reasonable agreement with results produced by CFD simulation in a comparative study. Time required for the same simulation case is several orders of magnitude smaller;
- The accuracy of the results produced by the simulation model are equal or more accurate than reported in other similar studies.

## 1.6 List of conferences

26.05.2019 – 29.05.2019

Renars Millers, Aleksandrs Korjakins, Arturs Lesinskis, Thermally Activated Concrete Slabs with Integrated PCM Materials CLIMA 2019, Romania, Bucharest

05.10.2016 – 07.10.2016

Renars Millers, Uldis Pelite, Survey of Control Characteristics of Circular Air Dampers in Variable Air Volume Ventilation Systems, SBE16 Tallinn and Helsinki Conference; Build Green and Renovate Deep, Estonia, Tallinn

22.05.2016 – 25.05.2016

Galina Stankevica, Andris Kreslins, Anatolijs Borodinecs, Renars Millers, Achieving Deep Energy Retrofit in Latvian Public Building – Simulation Study CLIMA 2016, Denmark, Aalborg

## 1.7 List of publications

### Paper 1

Millers, R.; Korjakins, A.; Lešinskis, A.; Borodinecs, A. Cooling Panel with Integrated PCM Layer: A Verified Simulation Study. *Energies* 2020, doi:10.3390/en13215715.

### Paper 2

Millers, R., Korjakins, A., Lešinskis, A. Thermally Activated Concrete Slabs with Integrated PCM Materials. No: *E3S Web of Conferences*, Romania, Bucharest, 26.-29. May, 2019. Bucharest: CLIMA 2019 Congress, 2019, 1.-6.lpp. ISSN 2555-0403. Available: doi:10.1051/e3sconf/201911101080

### Paper 3

Prozuments, A., Vanags, I., Borodinecs, A., Millers, R., Tumanova, K. A Study of the Passive Cooling Potential in Simulated Building in Latvian Climate Conditions. From: *IOP Conference Series: Materials Science and Engineering*, Latvia, Riga, 27.-29. September, 2018. UK: IOP Publishing, 2017, 1.-8.lpp. ISSN 1757-8981. Available: doi:10.1088/1757-899X/251/1/012052

### Paper 4

Ovchinnikov, P., Borodinecs, A., Millers, R. Utilization Potential of Low Temperature Hydronic Space Heating Systems in Russia. *Journal of Building Engineering*, 2017, Vol.13, 1.-10.lpp. ISSN 2352-7102. Available: doi:10.1016/j.job.2017.07.003

### **Paper 5**

Stankeviča, G., Krēsliņš, A., Borodiņecs, A., Millers, R. Achieving Deep Energy Retrofit in Latvian Public Building – Simulation Study. From: CLIMA 2016: Proceedings of the 12th REHVA World Congress. Vol.10, Denmark, Aalborg, 22.-25. May, 2016. Aalborg: Aalborg University, Department of Civil Engineering, 2016, 1.-9.lpp. e-ISBN 87-91606-35-7.

### **Paper 6**

Millers, R., Pelīte, U. Survey of Control Characteristics of Circular Air Dampers in Variable Air Volume Ventilation Systems. Energy Procedia, 2016, Vol.96, 294.-300.lpp. ISSN 1876-6102. Available: doi:10.1016/j.egypro.2016.09.152

## **1.8 Thesis composition and outline**

This thesis is structured in nine chapters:

- Chapter 1 presents the motivation and novelty of the research, defines the aim and scope of the thesis, formulates the hypothesis, describes the tasks and demonstrates the practical value. Additionally publications and participation in conferences are listed in this chapter.
- Chapter 2 outlines underlying principles of nearly zero-energy buildings (NZEBs) and examples of the requirements for different EU member states and how overheating issues are addressed in these countries;
- Chapter 3 describes previous research of passive cooling technologies that can be considered as candidates for application in NZEB buildings together with latent thermal storage systems in order to address overheating;
- Chapter 4 includes a review of available PCM materials, their properties and suitability for application in PCM cooling panels. Moreover, this chapter acknowledges property decay over time for different PCMs;
- Chapter 5 describes previous research of latent thermal storage systems and reported performance for different types of TES systems, previously developed numerical models and highlights the most visible experimental and simulation studies;
- Chapter 6 outlines the fundamentals behind heat transfer in HVAC systems in relation to cooling panels that is important to understand to apply, develop and model TES system components;
- Chapter 7 presents experimental methods used in the study and describes the equation based numerical model of the cooling panel with integrated latent thermal storage systems;
- Chapter 8 presents validation of the developed simulation model against experimentally measured values and previous CFD study as well as statistical analyses. Moreover this chapter describes the limitations of the developed numerical model.
- Chapter 9 summarizes the conclusions of the work done and confirms the hypothesis.

## 2 REVIEW OF NEARLY ZERO-ENERGY BUILDING REQUIREMENTS IN EUROPEAN UNION

### 2.1 Background of nearly zero-energy building concept

In European Union as well as in many other parts of the world building energy codes are becoming stricter each year. This is how governments are attempting to comply with CO<sub>2</sub> reduction targets set by global treaties such as the Kyoto Protocol [10] and Paris agreement [11].

EU aims to limit CO<sub>2</sub> emissions in building sector by 55 % (compared to 1990 levels) by year 2030 and reach net zero greenhouse gas emissions by year 2050 [12]. Currently building segment contributes to around 40 % of total CO<sub>2</sub> emissions in EU and represents the largest source of emissions in Europe [13].

The main tool for reducing energy consumption in buildings and reaching net zero greenhouse emissions by 2050 in EU is the Directive 2010/31/EU of the European Parliament and of the Council on the energy performance of buildings. This directive states that by 2020 December 31 all new buildings must be “nearly zero-energy buildings”. The definition of a “nearly zero-energy building” according to the directive is as follows:

*“Nearly zero-energy building” means a building that has a very high energy performance, as determined in accordance with Annex I. The nearly zero or very low amount of energy required should be covered to a very significant extent by energy from renewable sources, including energy from renewable sources produced on-site or nearby.*

The directive provides only general framework for the calculation methodology of NZEBs as well as minimum energy requirements for NZEBs – these details are to be described in the building codes of all the member states and shall be cost-optimal.

NZEB requirements and definition differs country by country due to climatic, economic and historical differences.

Heating energy consumption can be significant especially in the northern and central part of Europe and this has been extensively addressed in the past decades. Many countries have adopted requirements in building codes that result in highly insulated, airtight buildings to minimize heating energy consumption. Ovchinnikov et al. [14] also have emphasized the benefits of low temperature hydronic heating.

For northern and central part of Europe where NZEB and low energy buildings are usually airtight with highly insulated envelopes the accumulated internal and solar heat gains can be trapped within the thermal envelope that can lead to increased overheating in rooms.

This overheating side-effect of modern northern European buildings must be addressed in the building codes and handled in efficient manner. Many countries have already incorporated some type of limitations for maximum indoor temperatures. The next chapter describes examples of NZEB requirements and how overheating is addressed in some EU member states.

## 2.2 Examples of nearly zero-energy building requirements in EU member countries

**Austria** had building codes with relatively well defined energy performance requirements for new buildings and major renovations already before the Energy Performance Buildings Directive (EPBD) came into power. This can be partly contributed to the “Passive house” movement before the introduction of the NZEB concept. In 2010 there were more than 11 800 “Passive houses” already in use in Austria and as early as 2008 around 13 % of newly built residential units were “Passive houses” [15] .

NZEB in Austria is defined as an energy efficient building with good thermally insulated envelope and an environment-friendly heating system. Energy performance is measured by four indicators:

- Space heating demand HWB (kWh/m<sup>2</sup> a year);
- Primary energy demand EEB (kWh/m<sup>2</sup> a year);
- CO<sub>2</sub> emissions (kg/m<sup>2</sup> a year);
- Total energy efficiency factor  $f_{GEE}$ .

Compliance to NZEB performance can be demonstrated in two ways:

- Through meeting the space heating demand requirement;
- Through meeting the total energy efficiency factor  $f_{GEE}$ .

For both cases also maximum primary energy consumption and CO<sub>2</sub> emissions are limited. For space heating demand calculation also building shape factor  $l_c$  is considered. For minimum energy performance levels of new residential and new non-residential buildings see Table 2.1 and Table 2.2.

Overheating in residential buildings in Austria is addressed as a limitation of maximum operative temperature of 25 °C and 27 °C depending on room type and time of the day. The compliance is calculated with a simplified calculation according to ÖNORM B 8110-3 [16].

Table 2.1

Minimum energy requirements for new residential NZEBs in Austria [17]

		New construction	Reconstruction
HWB <sub>Ref,RK,zul</sub> in [kWh/m <sup>2</sup> a]	valid until 01.01.2021	12 x (1 + 3.0 / $l_c$ )	19 x (1 + 2.7 / $l_c$ )
	valid from 01.01.2021	10 x (1 + 3.0 / $l_c$ )	17 x (1 + 2.9 / $l_c$ )
EEB <sub>RK,zul</sub> in [kWh/m <sup>2</sup> a]	valid	EEB <sub>WG,RK,zul</sub>	EEB <sub>WGsan,RK,zul</sub>
HWB <sub>Ref,RK,zul</sub> in [kWh/m <sup>2</sup> a]	valid	16 x (1 + 3.0 / $l_c$ )	25 x (1 + 2.5 / $l_c$ )
$f_{GEE,RK,zul}$	valid until 01.01.2021	0.80	1.00
	valid from 01.01.2021	0.75	0.95

Table 2.2

## Minimum energy requirements for new non-residential NZEBs in Austria [17]

		New construction	Reconstruction
$HWB_{Ref,RK,zul}^{(1)}$ in [kWh/m <sup>2</sup> a]	valid until 01.01.2021	$12 \times (1 + 3.0 / I_c)$	$19 \times (1 + 2.7 / I_c)$
	valid from 01.01.2021	$10 \times (1 + 3.0 / I_c)$	$17 \times (1 + 2.9 / I_c)$
$KB^*_{RK,zul}$ in [kWh/m <sup>3</sup> a]	valid	1.0	2.0
$EEB^*_{RK,zul}^{(1)}$ in [kWh/m <sup>2</sup> a]	valid	$EEB_{NWG,RK,zul}$	$EEB_{NWGsan,RK,zul}$
$HWB_{Ref,RK,zul}^{(1)}$ in [kWh/m <sup>2</sup> a]	valid	$16 \times (1 + 3.0 / I_c)$	$25 \times (1 + 2.5 / I_c)$
$KB^*_{RK,zul}$ in [kWh/m <sup>3</sup> a]	valid	1.0	2.0
$f_{GEE,RK,zul}$	valid until 01.01.2021	0.80	1.00
	valid from 01.01.2021	0.75	0.95
<sup>(1)</sup> ... based on the floor height from 3.00 m with the following usage profile: building category 2 with gross floor area ≤ 1000 m <sup>2</sup> , building category 3 with gross floor area > 1000 m <sup>2</sup>			

NZEB requirements in **Denmark** are primarily set by limiting primary energy consumption, however other factors such as overheating, envelope heat transmittance, building air tightness and the use of RES is also limited.

Maximum primary energy consumption in new buildings has been tightened in 2010, 2015 and 2020. Each time by approximately 25 % arriving to NZEB levels in 2020. The NZEB requirements for primary energy consumption are 20 kWh/m<sup>2</sup> a year for residential buildings and 25 kWh/m<sup>2</sup> a year for non-residential buildings (see Figure 2.1). This primary energy consumption limit is independent from the size of the building.

Additionally to primary energy consumption the design transmission loss through building envelope is also limited and must not exceed 3.7 W/m<sup>2</sup> for single story buildings, 4.7 W/m<sup>2</sup> for two-storey buildings and 5.7 W/m<sup>2</sup> for three and more storey buildings.

If the DHW consumption for a building outside district heating area exceeds 2000 l/day the use of RES is mandatory [18].

Apart from the energy consumption it also must be demonstrated (using dynamic simulation software or “Be10” (a national calculation tool [19])) that the indoor temperature in residential buildings does not exceed 26 °C for more than 100 hours and 27 °C for more than 25 hours a year. If the indoor temperature exceeds these values an overheating penalty is calculated as an imaginary cooling system that maintains 26 °C inside the rooms [18].

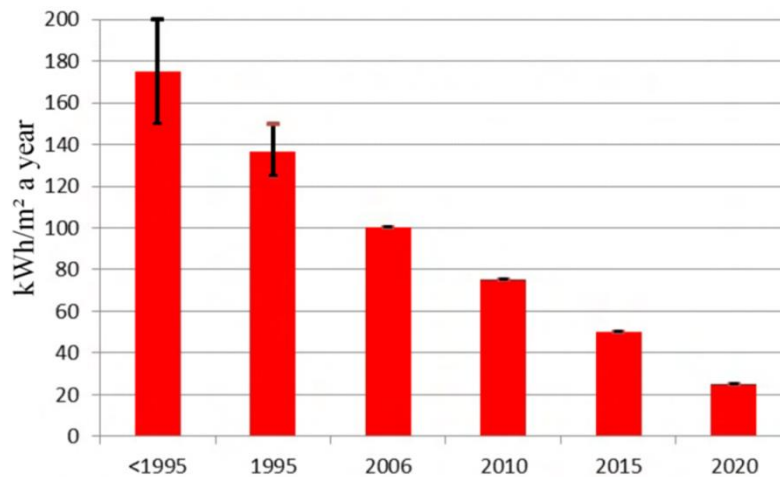


Figure 2.1 Primary energy consumption in new buildings in Denmark since 1995 [18]

NZEB requirements in **Estonia** are set by limiting primary energy consumption in buildings. There are separate requirements for different building types (see Table 2.3). The primary energy consumption includes:

- space heating;
- DHW;
- Cooling;
- lighting;
- ventilation;
- electrical appliances.

There are no minimum requirements for U-values the building has to meet in order to comply with NZEB requirements.

Apart from energy consumption a limit for overheating in summer (from 1 June to 31 August) is also set to a maximum of 150 degree-hours over 27 °C for residential buildings and 25 °C for non-residential [20].

Compliance to the aforementioned primary energy consumption and thermal comfort in summer period must be demonstrated using dynamic simulation software. Energy consumption for residential buildings can also be calculated using monthly method.

In addition to primary energy consumption there are also mandatory energy efficiency levels for MEP systems [21]:

- For heating and DHW systems the efficiency of the heat source divided by the primary energy factor must be at least 0.8;
- SEER of a cooling system must be at least 5.1;
- Heat recovery efficiency of a ventilation system must be at least 70 % (50 % for liquid coupled heat exchangers);
- SFP of a ventilation system must not exceed 2.5 kW/(m³/s)

Table 2.3

Primary energy performance requirements for NZEB and Low-energy buildings in Estonia  
[18]

No.	Building type	Energy performance requirements (kWh/m <sup>2</sup> ) (primary energy)	
		NZEB	Low-energy building
1	Detached houses	50	120
2	Apartment buildings	100	120
3	Office buildings and libraries	100	130
4	Commercial buildings	130	160
5	Public buildings	120	150
6	Shopping malls and terminals	130	160
7	Schools, universities	90	120
8	Kindergartens	100	140
9	Hospitals and medical buildings	270	300

Until 2015 in **Latvian** building codes energy efficiency in buildings was regulated mainly by limiting maximum envelope heat transmission (U-values). From 2015 onwards requirement regarding maximum heating energy consumption was added.

NZEB requirements in Latvia are set by limiting [22]:

- Heating energy requirement (40 kWh/m<sup>2</sup> a year for residential buildings and 45 kWh/m<sup>2</sup> for non-residential);
- Primary energy consumption (95 kWh/m<sup>2</sup> a year for heating, cooling, DHW, fan energy, and lighting);
- Minimum ventilation heat recovery efficiency (at least 75 % during heating season);
- Mandatory use of RES (However there is no requirement how much of building energy need should be covered by RES).

Apart from the energy consumption there is also a limit for maximum U-values for different structures (see Table 2.4) and building air tightness (1.5 m<sup>3</sup>/m<sup>2</sup>·h of envelope area at 50 Pa pressure difference) [23]. However, there is no obligation for the building owner or the contractor to demonstrate compliance to this air tightness requirement.

There is no direct requirement for maximum indoor temperatures, however, there is a requirement that during the design stage the client must be informed if indoor air temperature can exceed 28 °C. However, there is no further information how this must be calculated and how the compliance must be demonstrated [24].

Table 2.4

Maximum U values for different structures in Latvia [23]

No.	Construction	Residential buildings, retirement houses, hospitals and kindergartens	Non – residential buildings	Industrial buildings
		$U_{RM}$ value, $W/(m^2 \cdot K)$	$U_{RM}$ value, $W/(m^2 \cdot K)$	$U_{RM}$ value, $W/(m^2 \cdot K)$
1.	Floors:			
1.1.	Slabs and walls adjacent to ground	0.20	0.25	0.35
1.2.	Slab/floor above unheated basement or floor with ventilated underfloor space	0.30	0.35	0.40
2.	External walls			
2.1.	External walls	0.23	0.25	0.30
2.2.	In traditional log buildings without insulation layers	0.65	0.65	0.65
3.	Roofs and slabs in contact with external air	0.20	0.23	0.25
4.	External doors and gates	1.80	2.00	2.20
5.	Windows and balcony doors	1.10	1.10	1.30
6.	Thermal bridges ( $W/m \cdot K$ )	0.20	0.20	0.35

## 2.3 Conclusion

This chapter of the literature review provides a background for NZEB requirements in the EU member countries and examples how NZEB principles are incorporated on a national level. These requirements are the main driving force for the construction industry to apply passive cooling and thermal storage technology in order to meet required building energy performance.

Different EU member countries have chosen different ways to adopt NZEB requirements. All countries have limited the primary and/or other type of energy consumption but most countries have additional requirements regarding:

- Minimum HVAC and other system efficiencies;
- Minimum thermal envelope requirements;
- Maximum CO<sub>2</sub> emissions;
- Some other combined performance indicator.

Most countries have also acknowledged the current problem of overheating in modern buildings and incorporated some kind of measures to address this problem. In most cases there is a limitation of maximum temperature in rooms, defined as maximum temperature or a maximum degree-hour threshold above some room temperature.

Denmark has also introduced an overheating penalty in terms of energy consumption, where overheating is calculated as additional energy consumption.

In Latvia overheating is addressed only in principle without describing how the compliance must be demonstrated. This opens a window to confusion and a wide range of possible interpretations.

It can be concluded that in most of the central and northern EU countries airtight and highly insulated envelopes are required to meet energy requirement demands, but on the other hand this increases the overheating in buildings that needs to be addressed without compromising the overall energy consumption of the building.

### **3 REVIEW OF PASSIVE COOLING TECHNOLOGIES FOR APPLICATION IN BUILDINGS**

From the previous chapter (chapter 2) it can be concluded that extensive use of passive cooling technologies in buildings is essential for reaching NZEB or even net-zero energy consumption levels in buildings. Many technologies have been previously described in literature, but have not yet seen large scale application in buildings due to high cost, complexity, technical limitations and other factors.

Passive cooling technologies described in this chapter are seen as potential cooling energy sources that can be coupled with PCM storage to address overheating issues and minimize cooling energy requirements in NZEBs, ZEBs.

PCM application for passive cooling has been extensively researched in the past decades and is the central topic of this thesis therefore it is addressed in separate chapters (see chapters 4 and chapter 5).

#### **3.1 Night cooling**

Night cooling is a passive or semi-passive cooling technique that relies on temperature swings during day and night. The basic concept is to increase the air change in the building during night to utilise the cooler air as a heat-sink. This can be done using natural ventilation principles or mechanical ventilation if the utilization of thermal buoyancy or wind is not sufficient or possible.

Night cooling usually is used as a supplement to mechanical cooling to reduce energy consumption or in many cases is coupled with or assisted by other strategies like phase change materials [25–28].

Givoni [29–31] has suggested that night-time ventilation is feasible in climatic zones where day-time air temperature is below 36 °C and night time temperature is below 20 °C. Roaf et al. [32] found similar criteria: a minimum night-time temperature of 20 °C and maximum day-time temperature of 31 °C.

Artman et al. [33] elaborated a map of Europe based on “Meteonorm” data [34] with mean daily minimum temperatures and mean differences between minimum and maximum temperatures in July for estimating the feasibility for night cooling in different regions in Europe (See Figure 3.1 and Figure 3.2). Most of Northern and Central Europe is suitable for this cooling technique.

Prozuments et al. [35] performed a simulation study for night cooling potential in Latvian climate. The team found that it is not possible to provide comfortable indoor temperature using exclusively night cooling, however night cooling can provide approximately 8 % energy saving.

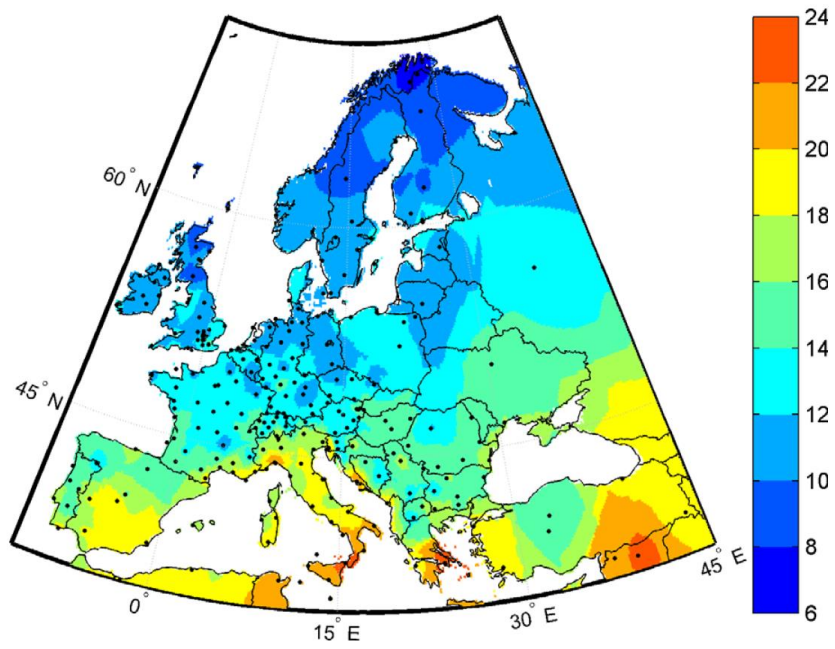


Figure 3.1 Mean daily minimum temperatures ( $^{\circ}\text{C}$ ) for July [33]

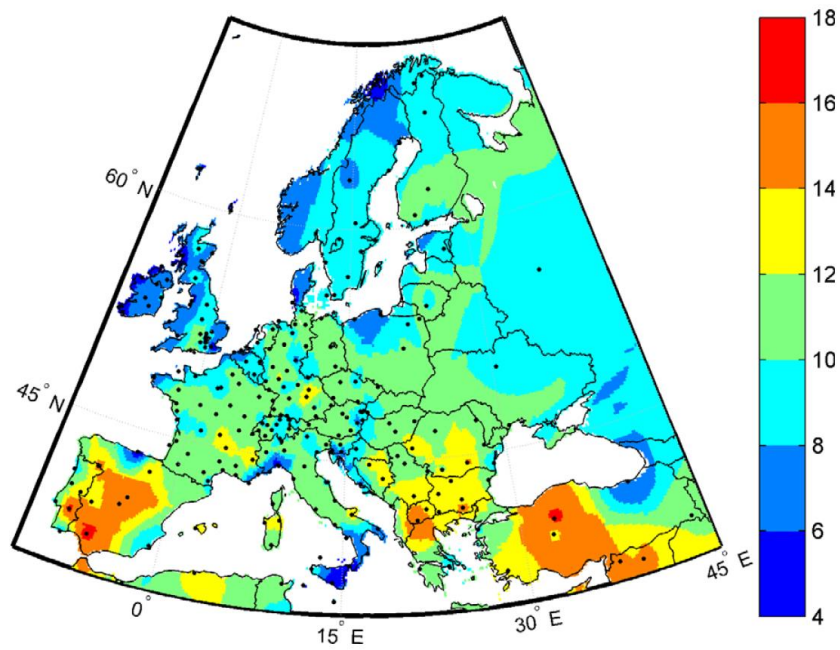


Figure 3.2 Mean differences between daily minimum and maximum temperatures (K) in July [33]

### 3.2 Radiant nocturnal cooling

Radiant nocturnal cooling is a cooling technique that utilises radiant heat exchange with the sky as a heat sink during the night. The heat exchange takes place because the night sky is cooler than the surfaces on the Earth. In principle the same mechanism is present also during day time, however the solar radiation coming from the Sun is absorbed and the net heat exchange is positive in the direction of the surfaces on the Earth.

Meir et al. reported that it is possible to cover a significant fraction of a single-family house cooling requirements with radiative cooling system [36]. Ecker and Dalibard [37] found that photovoltaic-thermal collectors can deliver up to 120 W/m<sup>2</sup> of radiative cooling and similar values were reported also by Thibault et al. [38].

Meir et al. [36] theoretically described the process of nocturnal cooling for a radiator. The total heat exchange can be calculated with Equation (3.1).

$$P_C = P_{rad} + P_{conv} + P_{cond}, \quad (3.1)$$

where  $P_C$  – total cooling power, W;

$P_{rad}$  – radiant cooling power, W;

$P_{conv}$  – convective cooling power, W;

$P_{cond}$  – conductive cooling power, W.

Conductive cooling power is insignificant and can be neglected. Convective cooling power can be calculated by applying Equation (3.2).

$$P_{conv} = h_{conv} \cdot A \cdot (T_{rad} - T_a), \quad (3.2)$$

where  $h_{conv}$  – convective heat exchange coefficient, W/m<sup>2</sup>·K;

$A$  – area, m<sup>2</sup>;

$T_{rad}$  – temperature of the radiator, K;

$T_a$  – temperature of the surrounding air, K.

The convective heat exchange coefficient is difficult to estimate and is dependent on air velocity, shape and other parameters [39].

Radiant cooling power can be calculated by applying Stefan-Boltzmann law for black body radiation (see Equation (3.3)).

$$P_{rad} = A \cdot \sigma \cdot \varepsilon \cdot (T_{rad}^4 - T_{sky}^4), \quad (3.3)$$

where  $\sigma$  – the Stephan-Boltzmann constant, 5.670374419·10<sup>-8</sup> W/m<sup>2</sup>·K<sup>4</sup>;

$\varepsilon$  – total emissivity;

$T_{sky}$  – sky temperature that represents the behaviour of a black body, K.

$T_{sky}$  can be represented with Equation (3.4)

$$T_{sky} = \varepsilon_{sky}^{1/4} \cdot T_a, \quad (3.4)$$

where  $\varepsilon_{sky}$  – the emissivity of the sky that depends on air temperature, air humidity and cloudiness [40,41].

### 3.3 Radiant cooling using “the window of transparency” in the Earth’s atmosphere

The importance and potential of the daytime radiative cooling using the atmospheric window in the infra-red spectrum between 8  $\mu\text{m}$  and 13  $\mu\text{m}$  was emphasised already a few decades ago [42–44]. Only recently daytime radiative cooling significantly below ambient temperatures was demonstrated due to advances in nanophotonics. The key to these advances is the ability for a material to possess a combination of high solar reflectance and strong infra-red emission between 8  $\mu\text{m}$  and 13  $\mu\text{m}$  (Figure 3.3).

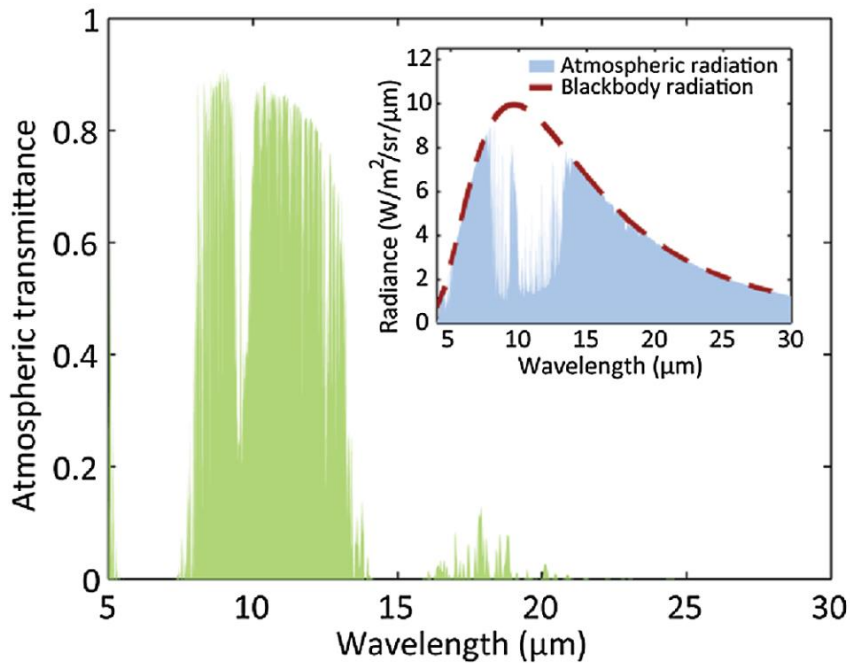


Figure 3.3 Atmospheric transmittance with the downward atmospheric radiation (Figure from [45], data from [46])

Material with the previously mentioned properties can achieve net positive radiant cooling power even when exposed to solar radiation. This has sparked extensive research in this field after Raman et al. [47] for the first time demonstrated radiant cooling of 5 °C below ambient temperature with the capacity of 40 W/m<sup>2</sup> under direct sunlight in 2014. Since then radiant cooling capacities of more than 100 W/m<sup>2</sup> have been achieved utilising “the window of transparency” in the Earth’s atmosphere (See Table 3.1).

Table 3.1

## Summary of recent research in the field of daytime passive cooling

Authors	Methodology	Solar Reflectance	IR Emissivity	Conditions	Temperature reduction below ambient, °C	Net Cooling power, W/m <sup>2</sup>
Bao et al. [48]	Numerical and Field Investigation	0.907	0.90	Non-vacuum	5	25
Chen et al. [49]	Numerical and Field Investigation	0.967	0.56	Vacuum	42	60
Jeong et al. [50]	Numerical and Field Investigation	0.942	0.84	Non-vacuum	7.2	14.3
Kecebas et al. [51]	Numerical	0.96	0.69	N.A.	N.A.	103
Kecebas et al. [51]	Numerical	0.965	0.54	N.A.	N.A.	85.8
Kou et al. [52]	Numerical and Field Investigation	0.975	0.92	Non-vacuum	8.2	127
Raman et al. [47]	Numerical and Field Investigation	0.970	0.65	Non-vacuum	4.9	40.1
Zhai et al. [53]	Numerical and Field Investigation	0.969	0.93	Non-vacuum	N.A.	93
Jeong et al. [54]	Numerical and Field Investigation	0.975	0.98	Non-vacuum	6.2	19.7

Hossain and Gu [45] has theoretically described principles of daytime radiative cooling. Taking into consideration all governing heat exchange processes net cooling capacity of a radiative cooling device can be described as follows (see Equation (3.5)).

$$P_{net} = P_{rad} - P_{atm} - P_{nonrad} - P_{sun}, \quad (3.5)$$

where  $P_{net}$  – net radiative cooling power, W;  
 $P_{rad}$  – radiant cooling power, W;  
 $P_{atm}$  – incident atmospheric radiation absorbed by the radiator, W;  
 $P_{nonrad}$  – nonradiative heat gains (conduction and convection), W;  
 $P_{sun}$  – solar radiation, W.

Radiative power emitted by the radiative device  $P_{rad}$  can be calculated with Equation (3.6).

$$P_{rad} = 2\pi \int_0^{\pi/2} \sin\theta \cos\theta d\theta \int_0^{\infty} U_B(\lambda, T_{rad}) e_{rad}(\lambda, \theta) d\lambda, \quad (3.6)$$

where  $\pi$  – mathematical constant 3.14159;  
 $\theta$  – zenith angle of the surface, rad;  
 $U_B(\lambda, T_{rad})$  – spectral radiance of the radiator (function of absolute temperature of the radiator and wavelength), W;

$\lambda$  – wavelength, m;  
 $T_{rad}$  – absolute temperature of the radiator, K;  
 $e_{rad}(\lambda, \theta)$  – angle dependent spectral emissivity of the radiator (function of wavelength and zenith angle).

The amount of the incident atmospheric radiation absorbed by the radiative device  $P_{atm}$  is calculated with Equation (3.7).

$$P_{atm} = 2\pi \int_0^{\pi/2} \sin\theta \cos\theta d\theta \int_0^{\infty} U_B(\lambda, T_{atm}) e_{rad}(\lambda, \theta) e_{atm}(\lambda, \theta) d\lambda, \quad (3.7)$$

where  $U_B(\lambda, T_{atm})$  – spectral radiance of the atmosphere (function of absolute temperature of the atmosphere and wavelength), W;

$T_{atm}$  – absolute temperature of the atmosphere, K;  
 $e_{atm}(\lambda, \theta)$  – angle dependent spectral emissivity of the atmosphere (function of wavelength and zenith angle).

The spectral radiance of a black body is calculated with Planck's law (3.8).

$$U_B(\lambda, T) = \frac{2hc^2}{\lambda^5} \frac{1}{e^{\frac{hc}{\lambda k_B T}} - 1}, \quad (3.8)$$

where  $U_B(\lambda, T)$  – spectral radiance of the black body radiator (function of absolute temperature and wavelength), W;

$h$  – Planck's constant,  $6.62607015 \cdot 10^{-34}$  J·s;  
 $c$  – speed of light in vacuum,  $2.99792 \cdot 10^8$  m/s;  
 $k_B$  – Boltzmann constant,  $1.380649 \cdot 10^{-23}$  J/K;  
 $T$  – absolute temperature of the black body, K;  
 $e$  – mathematical constant, 2.71828.

The emissivity of the radiative device can be defined by its absorptivity  $e_{atm}(\lambda, \theta)$  according to Kirchhoff's law. The angle dependent emissivity of the atmosphere is given by (see Equation (3.9)).

$$e_{atm}(\lambda, \theta) = 1 - t(\lambda)^{1/\cos\theta}, \quad (3.9)$$

where  $t(\lambda)$  – is the atmospheric transmittance in the zenith direction (function of wavelength).

### 3.4 Adiabatic or evaporative cooling

A very common passive cooling technology is adiabatic or evaporative cooling. The principle of adiabatic or evaporative cooling relies on the latent phase change energy of evaporating water. The cooling energy is extracted from the process with faster moving water

molecules that have enough energy to escape the Knudsen layer or evaporative layer and the rest of the molecules are left with lower kinetic energy. Since the average kinetic energy of the molecules is proportional to temperature the liquid cools. The molecules of the liquid in a closed system will eventually return to the evaporative surface. When the number of water molecules in the vapour reach a certain concentration where the number of molecules leaving the liquid and the number of molecules entering are the same an evaporative equilibrium is reached. For a system consisting of pure vapour and liquid substance the evaporative equilibrium is described by a Clausius-Clapeyron relation (see Equation (3.10)).

$$\ln\left(\frac{P_{S_2}}{P_{S_1}}\right) = -\frac{\Delta H_{vap}}{R}\left(\frac{1}{T_2} - \frac{1}{T_1}\right), \quad (3.10)$$

- where  $T_1$  – temperature at first point of coexistence curve, K;  
 $T_2$  – temperature at second point of coexistence curve, K;  
 $P_{S_1}$  – vapour pressure at absolute temperature  $T_1$ , Pa;  
 $P_{S_2}$  – vapour pressure at absolute temperature  $T_2$ , Pa;  
 $\Delta H_{vap}$  – enthalpy of evaporation, J;  
 $R$  – universal gas constant, 8.31446 J/K·mol.

The equilibrium state of the Clausius-Clapeyron relation for air and water would represent 100 % humidity in air. The liquid cooling process can continue until 100 % relative air humidity is reached. During this cooling process the total enthalpy of the thermodynamic system does not change therefore this principle is called adiabatic cooling (cooling at constant enthalpy).

This technology is typically not sufficient to provide enough cooling power all year round so it is usually supplemented with other technologies.

Millers et al. [55] in a simulation study demonstrated that it is possible to maintain comfortable indoor temperature in Baltic Sea region if adiabatic cooling is combined with PCM thermal storage. Duan et al. [56] reported EER values of 30 to 80 for indirect adiabatic cooling equipment. Amer [57] found evaporative roof cooling was the most effective of the researched passive cooling techniques for arid areas.

Santamouris and Kolokotsa [58] performed a state of the art passive cooling review for different types of evaporative cooling systems (see Table 3.2).

Table 3.2

Comparison of different evaporative cooling systems [58]

Authors	Type	Configuration	Cooling effect
Heidarinejad et al. [59]	Two stage DEC-IEC	A two-stage evaporative cooling experimental setup consisting of an indirect evaporative cooling stage (IEC) followed by a direct evaporative cooling stage (DEC).	The effectiveness of the two stage system is 108–111 % while the IEC' effectiveness is 55–61 %. 60 % power savings.

Heidarinejad et al. [60]	Hybrid system including DEC coupled with of nocturnal radiative cooling, cooling coil	The cold water is stored in a storage tank. During next day, hot outdoor air is pre-cooled by the cooling coil unit and then it enters the direct evaporative cooling unit.	The results obtained demonstrate that overall effectiveness of hybrid system is more than 100 %.
Heidarinejad et al. [61]	Hybrid ground-assisted DEC.	A ground circuit provides pre-cools the air and then a DEC cools the air even below its wet-bulb temperature.	The results obtained demonstrate that overall effectiveness of hybrid system is more than 100 %.
Phillips [62]	Chilled-water coil in conjunction with a DEC pad	A DEC is used as an additional component to air-handling unit.	Using a DEC in conjunction with a chilled coil results to 35 % energy savings comparing the chilled coil For a LEED rated building, this corresponds to four credits for energy conservation.
Sheng and Hnanna [63]	DEC	Testing the speed of frontal air, the dry-bulb temperature of frontal air, and the temperature of the incoming water versus cooling efficiency.	DEC cooling efficiency increases with frontal air dry-bulb temperature and decreases with frontal air velocity and incoming water temperature correspondingly.
Kim et al. [64]	DEC/IEC	100 % outdoor air system integrates DEC/IEC.	The proposed system shows a 16–25 % less annual cooling coil load and an 80–87 % reduced annual heating coil load with respect to a conventional variable air volume system.
Glanville et al. [65]	Dew point evaporative cooling	5 ton rooftop unit with Heat exchanger and flow path arrangement, provide unhumidified air below wet bulb temperatures.	80 % energy savings relative to a conventional vapour compression system.
Farmahini-Farahani and Heidarinejad [66]	Multi-step system of nocturnal radiative cooling and two-stage evaporative cooling	During the night, water is passed by the radiative panels and is stored. During the day, the stored cold water in the storage tank is used as coolant for a cooling coil unit and a two-stage evaporative cooler.	Higher effectiveness than conventional two-stage evaporative coolers. Energy savings 75 and 79 % compared to mechanical vapour compression systems.
Gomez et al. [67]	IEC by polycarbonate with a total heat exchange area of 6 m <sup>2</sup>	Tested in laboratory while enabling different climatic conditions to a climatic chamber.	The heat transfer through the heat exchanger polycarbonate wall improves the overall effectiveness.
Robinson et al. [68]	Passive Down-draught Evaporative Cooling (PDEC)	Micronisers that are located close to high level air inlets.	Savings between 50 and 83 %-depending upon occupancy and set-point. Thermal comfort could not be achieved by PDEC only.
Nasr and Hassan [69]	DEC	Evaporative condenser for residential refrigerator was introduced. Sheets of cloth are wrapped around condenser to suck the water from a water basin by capillary effect.	The condenser temperature increases 0.45 °C for each degree increase in evaporator temperature when the air velocity is 2.5 m/s, and the ambient condition is 29 °C and the relative humidity is 37.5 %.

### 3.5 Desiccant cooling

Desiccant cooling process consists of dehumidifying an air stream by running it through a desiccant that absorbs or adsorbs the water vapour of the air stream. In a parallel process the same desiccant from a previous cycle is being regenerated by heating it with another airstream to its regeneration temperature that is specific to each desiccant.

After the incoming airstream is being dehumidified it must be cooled to pre-dehumidification temperature (a common approach is to use air to air heat recovery device). Then the air stream can be cooled with a cooling coil or evaporative humidifier.

In order for a desiccant cooling system to work three components are essential (see also Figure 3.4):

- a regeneration heat source;
- desiccant material;
- cooling unit (or evaporative humidifier).

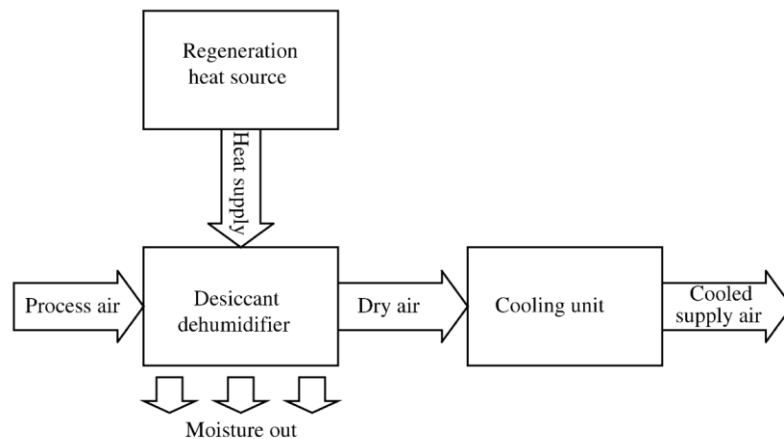


Figure 3.4 Principle of desiccant cooling [70]

Desiccant cooling systems can be feasible if there is waste heat available with sufficient temperature or alternatively solar thermal energy can be used.

Mavroudaki et al. [71] carried out a simulation based feasibility study for a desiccant cooling system for seven European cities (Table 3.3). In the study it was assumed that the cooling system is driven by a combination of a gas boiler and solar collectors. The team found the moisture content of outdoor air influences the desiccant cooling system more than the availability of solar energy. Solar energy covered from 25 % of heating energy requirements in London to 93 % of heating energy requirements in Oslo.

Table 3.3

Comparison of energy analysis for different European cities [71]

City	Max. dry Bulb temp. (°C)	Min. dry Bulb temp. (°C)	Latent Gain (W/m <sup>2</sup> )	Solar water temp. (°C)	Gas Saved (%)
Oslo	25.4	13.6	5.86	50	93.0
London	26.9	17.6	10.92	55	25.1
Budapest	30.4	17.8	8.99	60	33.9
Lyon	28.8	17.1	7.91	55	39.7
Lisbon	35.1	21.8	9.60	70	38.5
Athens	36.6	26.4	9.72	70	46.5
Sofia	35.1	21.8	9.96	70	29.1

### 3.6 Passive geothermal cooling

It is well known that at natural thermal equilibrium conditions the ground temperature at around 3 m depth can be considered constant and is equal to the mean temperature on its surface [72]. In 1992 Mihalakakou et al. [73] proposed a model for calculation of the ground temperature that was based on 74 years of temperature measurements in National Observatory of Athens. According to this model the ground surface temperature can be estimated with following Equation (Equation (3.11)).

$$t_{surf} = t_m - A_S \cdot \cos\left(\frac{2\pi \cdot tm}{365}\right), \quad (3.11)$$

where  $t_{surf}$  – surface temperature, °C;

$t_m$  – average annual earth temperature, °C;

$A_S$  – the temperature amplitude, °C;

$tm$  – time, day of the year.

Assuming the soil is homogeneous and with constant thermal diffusivity, the temperature at any depth  $z$  can be found by the Equation (3.12).

$$t(z, tm) = tm_m - A_S e^{-z\left(\frac{n}{365a}\right)^{0.5}} \cdot \cos\left(\frac{2\pi}{365}\left(t - \frac{z}{2}\left(\frac{365a_{lag}}{\pi}\right)^{0.5}\right)\right), \quad (3.12)$$

where  $t(z, tm)$  – temperature in soil at time  $tm$  and depth  $z$ , °C;

$z$  – depth, m;

$a_{lag}$  – lag coefficient.

Since then many energy balance based models have been proposed [74–76].

Geothermal cooling technologies can be divided in two main categories: earth to air heat exchangers (EATHE) and earth to liquid heat exchangers. Both technologies are fairly common and extensively researched in the past.

### **3.7 Earth to air heat exchangers**

Earth to air heat exchangers have been extensively used and studied. The performance of a EATHE system is related to heat exchange surface (the length and diameter), the air flow rate and other characteristics such as depth, outdoor air conditions and soil properties [77–79].

For moderate climates the seasonal passive cooling capacity for most systems is around 8-10 kWh/m<sup>2</sup> ground heat exchange area a year and peak cooling capacity for 32 °C outdoor air temperature is around 45 W/m<sup>2</sup> of heat exchange area [58,80]. Different case studies have reported various performance of the system:

- 20 % - 30 % decrease in discomfort hours in Belgium [81];
- energy savings of 13.1 to 23.8 kWh/m<sup>2</sup> per year in Germany [82];
- coverage of 1/3 of cooling requirements in Switzerland [80];
- 33 kWh/m<sup>2</sup> of cooling energy savings a year for a building in Greece [83].

### **3.8 Earth to liquid heat exchangers**

Earth to liquid heat exchanger typically consists of horizontal hydronic circuits or hydronic circuits located inside concrete pile (energy piles) or boreholes. These heat exchangers are usually used for both heat source (using geothermal heat pumps) and as a heat sink for passive and/or vapour compression driven cooling.

Ground around these hydronic circuits shall be viewed as an energy storage rather than energy source. If there is a seasonal energy disbalance delivered to the hydronic circuit the energy potential of the circuit can be depleted resulting in lower SCOP values for heating due to overcooled ground or inability for utilisation of free cooling due to overheated ground [84].

For effective use of earth to liquid heat exchangers they shall be utilized for both cooling and heating or regenerated using solar energy or other methods [85,86] however there have been reports that such application leads to a higher failure probability [87].

Properly sized earth to liquid heat exchanger with balanced energy extraction can fully sustain building cooling and heating requirements.

### **3.9 Conclusion**

This chapter of the literature review addresses existing passive cooling technologies that can be supported by latent thermal energy storage systems (including PCM cooling panels). These technologies rely on different principles and their performance and efficiency can vary case to case for different types of building and different climatic conditions; however, they hold the key for meeting future and present energy requirements in buildings.

Most passive cooling technologies (apart from geothermal cooling in some cases) cannot cover 100 % of building cooling requirements and have some limitations. Night cooling is highly dependent on outdoor temperature, radiant cooling is dependent on the sky cloud cover, adiabatic cooling as well as desiccant cooling lose efficiency during periods of high outdoor humidity and geothermal cooling must have annual energy balance otherwise cooling and heating potential of the ground can be depleted.

It is clear that to fully cover or at least extend the fraction of passive cooling in a building a combination of passive cooling technologies and a suitable thermal energy storage must be used. This is further discussed in chapters 4 and 5.

## 4 REVIEW OF PHASE CHANGE MATERIALS

Latent thermal storage systems in principle consist of two components – latent thermal storage medium and heat exchanger in case of active application or a method where and how it is incorporated in the case of passive application. Therefore the research in PCM field can be divided into two categories [88] (see also Figure 4.1):

- material research that deals with development of the PCM itself;
- development of heat exchangers.

The development of heat exchangers is perceived as methods for delivering or extracting the thermal energy from PCMs for different application. This thesis is mainly concentrated on the energy delivery/extraction methods; however, it is essential to understand the characteristics of PCMs available and the fundamental principles of these materials. This chapter focuses on the PCM itself. The heat exchange methods of energy delivery/extraction from the latent thermal storage is described in chapter 5.

First studies employing PCM for heating and cooling applications were conducted almost five decades ago by Telkes [89] and Barkmann and Wessling [90]. Since then this technology has been researched extensively and new commercial and non-commercial materials have been developed.

PCM technologies rarely possess the ability to provide desired thermal comfort in buildings on their own. Thus, generally they are used in combination with other passive (evaporative cooling, nocturnal cooling, night cooling) or non-passive cooling technologies such as vapour compression cooling. PCM in combination with passive technologies are recognized as attractive solutions for Passive houses, NZEBs, net zero-energy buildings or even carbon negative buildings. PCM technologies in combination with more traditional cooling equipment are usually used for increasing energy efficiency, down-sizing equipment by cooling power peak-shaving or utilizing lower energy prices during off-peak hours.

PCM is an effective thermal energy storage due to its ability to store energy not only due to temperature change (sensible thermal energy storage) but also due to melting and solidifying (latent thermal energy storage) that takes place at a narrow temperature range. This principle allows storing 5 to 14 times more thermal energy than sensible thermal storage with the same weight and volume.

The heat storage in a solid-liquid PCM can be described as with Equation (4.1) [91].

$$Q = m \cdot a_m \cdot h_m + \int_{T_i}^{T_m} m \cdot c_{PCM} dT + \int_{T_m}^{T_2} m \cdot c_{PCM} dT = m(a_m \cdot h_m + \bar{c}_{PCM_s}(T_m - T_i) + \bar{c}_{PCM_l}(T_2 - T_m)), \quad (4.1)$$

where  $Q$  – energy stored/released, J;  
 $m$  – mass, kg;  
 $a_m$  – fraction melted;  
 $h_m$  – heat of fusion, J/kg;  
 $T_i$  – Initial temperature, K;

- $T_m$  – melting/solidification temperature, K;  
 $T_2$  – final temperature, K;  
 $\bar{c}_{PCM_s}$  – average specific heat of the capacity PCM between  $T_i$  and  $T_m$ , J/kg·K;  
 $\bar{c}_{PCM_l}$  – average specific heat of the capacity PCM between  $T_m$  and  $T_2$ , J/kg·K.

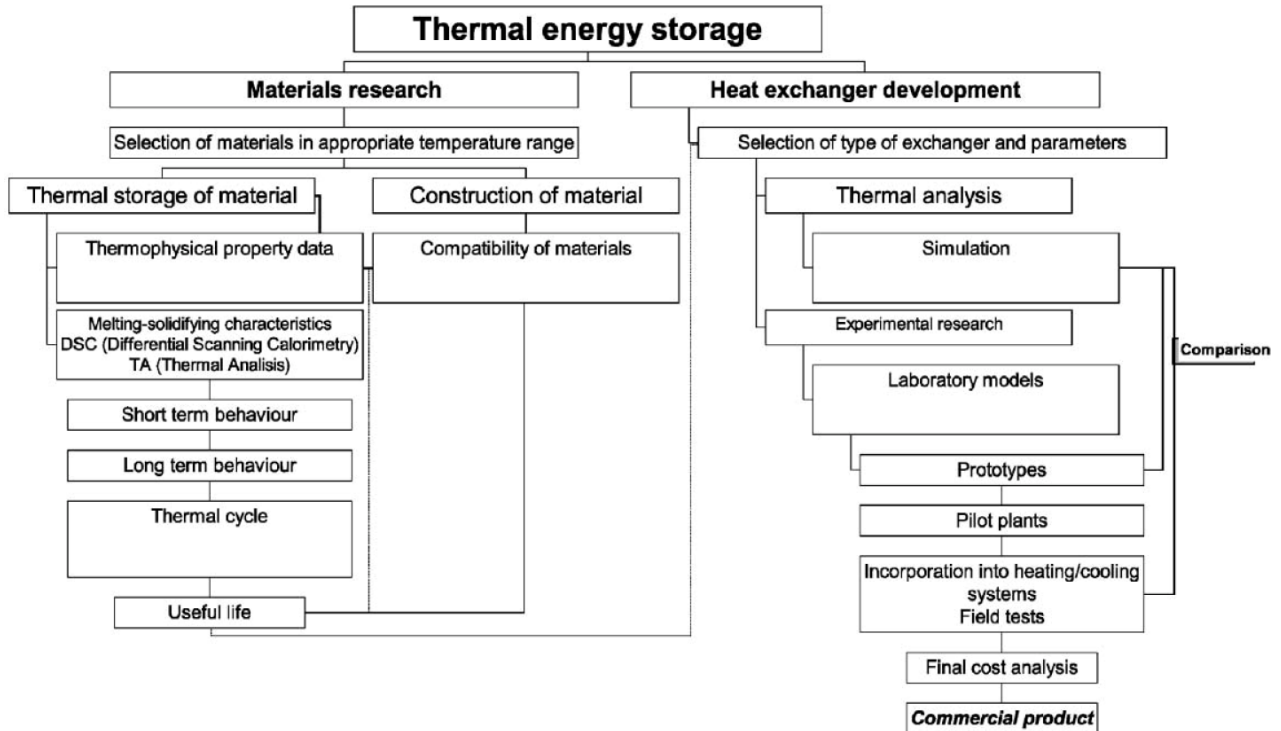


Figure 4.1 Aspects studied in PCM research field [88]

## 4.1 Different types of PCM materials

In 1983 Abhat [92] classified materials that can be used for thermal energy storage (Figure 4.2). As described in the classification latent or phase change thermal storage can utilise phase change of gas-liquid, solid-gas, solid-liquid and solid-solid.

A solid-solid PCM [93] utilises the phase change in solid from crystalline to another form. These materials are an alternative option that does not require encapsulation since it is a solid. Also these materials have small volumetric changes during phase transition. Clearly these benefits come with a disadvantage of lower latent heat [94]. A good example of solid-solid phase change material is pentaerythritol, pentaglycerine and neopentyl glycol [91].

Another form of PCMs are solid-gas and liquid-gas physically these materials have the highest latent heat storage capacity but their practical application is very limited due to technical limitations. These materials require large volumes making their application impractical. One of few feasible examples is steam accumulators.

The most common PCM materials are solid-liquid that are further discussed in the next chapter.

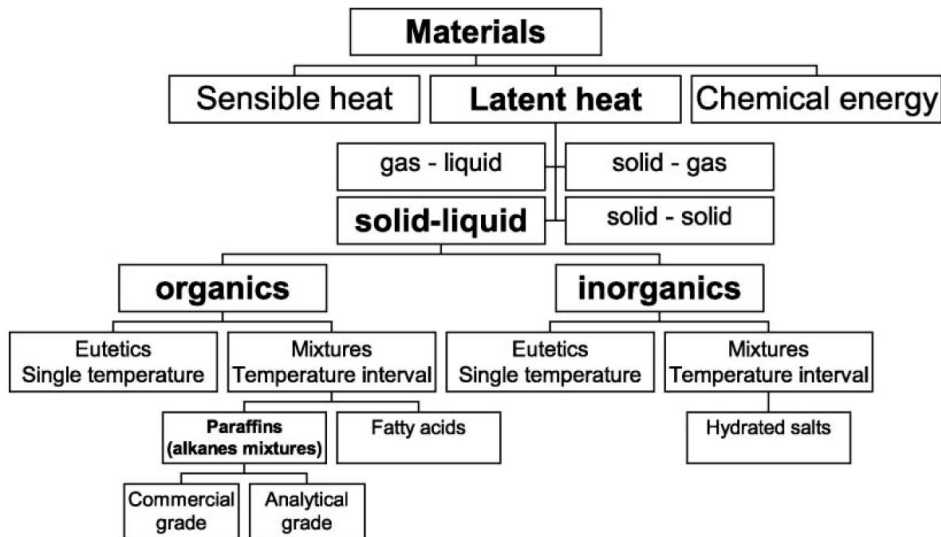


Figure 4.2 Classification of energy storage materials (information from [92], figure from [88])

### Solid-liquid PCMs

Solid-liquid PCMs have smaller latent energy storage potential if compared with solid-gas or liquid-gas PCMs nevertheless other favourable characteristics such as small volume change during phase change makes them more feasible and common for thermal storage application. This type of PCM is the most studied, commercially produced and industry ready.

In 1983 Abhat [92] conducted a major study in the field of latent thermal storage substances and produced a classification tree of PCM materials according to their chemical composition (Figure 4.3). According to Abath [92] there are three main categories of PCMs: organic compounds, inorganic compounds and eutectics.

Another classification of PCMs according to phase-change enthalpy and melting temperatures was provided by Dieckmann and Heinrich [95] (Figure 4.4).

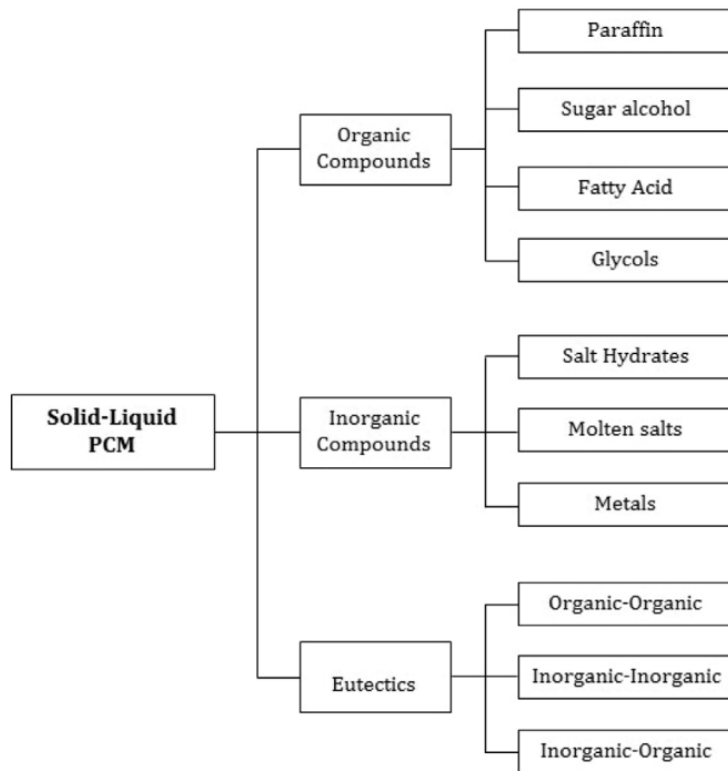


Figure 4.3 Classification of solid-liquid PCMs according to their chemical composition (information from [92], figure form [93])

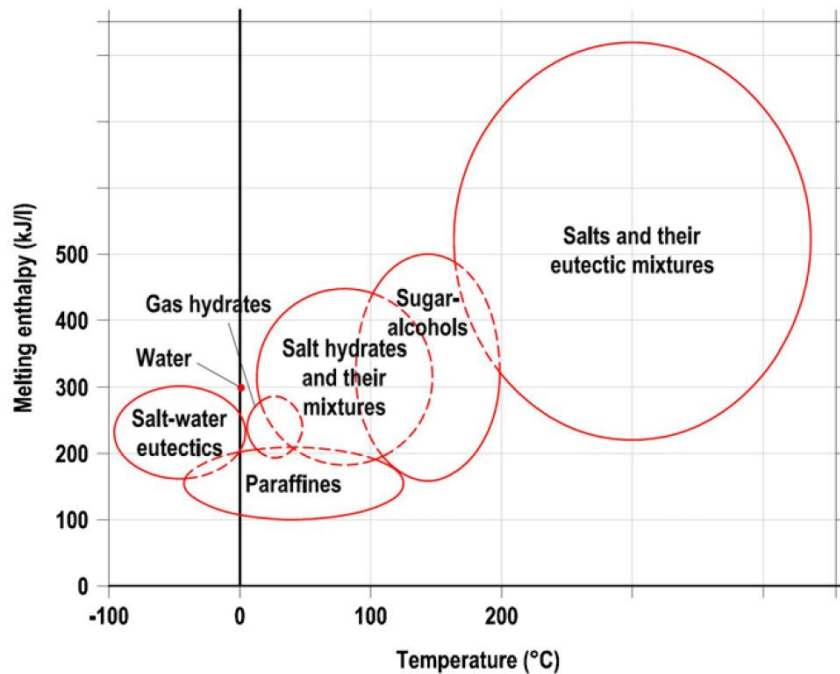


Figure 4.4 Temperature and latent enthalpy ranges for different types of solid-liquid PCMs

## Paraffin based PCMs

Most common organic PCMs include fatty acids and paraffins. Paraffins generally have more attractive characteristics that make them more suitable for practical applications. The main advantages of paraffin based PCMs according to Whiffen and Riffat [96] are:

- wide and variable melting point range;
- relatively high heat of fusion (around 120-200 kJ/kg for most materials);
- no super-cooling;
- chemically stable and recyclable;
- good compatibility with other materials (for mixtures) that allows to adjust their melting range.

However, there are also a few disadvantages, for example, their low thermal conductivity ( $\sim 0.2 \text{ W/m}\cdot\text{K}$ ), high volume change during phase transition and flammability.

The thermal conductivity can be enhanced by introducing additional heat conducting mechanisms like aluminium fins [97], carbon micro-fibres [98] or incorporating paraffins in composite materials like paraffin/expanded graphite composite [99]. The flammability of paraffins can be overcome with addition of fire-retardants [100].

Other positive commercially available paraffin properties pointed out by Beatens et al. [101] include non-corrosivity, non-toxicity, the fact that they do not undergo phase segregation.

In 2019 Navarro et al. [102] performed a study on the stability of thermophysical properties of the most common paraffin based PCMs when they undergo 10; 100; 1000 and 10 000 phase change cycles. The measurements were conducted using differential scanning calorimetry. The team found that for most materials there is a 6-26 % latent enthalpy drop after first 10 melting and solidifying cycles. Between 10 and 10 000 cycles the properties remain relatively stable for most materials with latent enthalpy drop of 10-27 %. However, there are materials that experience no performance decay at all or even an increase of performance. Unfortunately, some materials also lose approximately 60 % of their phase change enthalpy after 10 000 cycles (see Table 4.1). The same team [102] found that also melting and solidification temperatures of PCMs can drift when the material is being cycled however for all materials these temperatures did not change by more than  $\sim 2 \text{ }^\circ\text{C}$  (Table 4.1).

Table 4.1

Phase change enthalpy and temperature of the PCM before and after 10, 100, 1000 and 10 000 cycles [102].

Material		$H_m^{(1)}$ (kJ/kg)	Property loss (%)	$H_s^{(2)}$ (kJ/kg)	Property loss (%)	$t_m^{(3)}$ (°C)	Property loss (%)	$t_s^{(4)}$ (°C)	Property loss (%)
Bulk PCM									
<i>RT21 HC</i>	Not-cycled	137.02	0.00	126.03	0.00	22.21	0.00	21.47	0.00
	Cycled (10)	127.94	6.63	114.12	9.45	22.69	-2.15	21.87	-1.86
	Cycled (100)	124.88	8.86	113.77	9.73	22.76	-2.46	21.91	-2.08
	Cycled (1000)	141.22	-3.07	139.37	-10.58	22.11	0.47	21.15	1.46
	Cycled (10 000)	109.47	21.74	110.71	12.16	21.32	4.03	20.73	3.45
<i>RT22 HC</i>	Not-cycled	141.17	0.00	144.74	0.00	23.06	0.00	22.27	0.00
	Cycled (10)	137.01	3.04	127.91	13.16	22.94	0.55	22.21	0.30
	Cycled (100)	130.49	8.18	130.47	10.94	22.07	4.52	21.18	5.16
	Cycled (1000)	130.58	8.11	125.97	14.90	23.16	-0.43	22.41	-0.62
	Cycled (10 000)	128.20	10.11	124.28	16.46	21.96	5.01	21.19	5.11
<i>RT25 HC</i>	Not-cycled	177.29	0.00	186.03	0.00	25.27	0.00	n.a.	n.a.
	Cycled (10)	128.86	27.32	129.09	30.61	26.66	-0.75	25.40	n.a.
	Cycled (100)	125.34	29.30	121.99	34.42	24.54	0.39	23.77	n.a.
	Cycled (1000)	126.88	28.43	130.7	29.74	26.56	-0.69	25.85	n.a.
	Cycled (10 000)	129.10	27.18	130.79	29.69	26.58	-0.70	25.94	n.a.
<i>RT27 HC</i>	Not-cycled	164.43	0.00	151.54	0.00	26.46	0.00	26.45	0.00
	Cycled (10)	120.93	26.45	122.88	18.91	26.84	-1.44	25.49	3.65
	Cycled (100)	112.02	31.88	100.54	33.66	25.14	4.96	24.61	6.97
	Cycled (1000)	111.315	32.30	110.33	27.20	27.31	-3.23	26.76	-1.16
	Cycled (10 000)	69.28	57.87	69.16	54.37	27.07	-2.30	26.49	-0.12
<i>Pure Temp 23</i>	Not-cycled	215.02	0.00	215.79	0.00	24.17	0.00	20.66	0.00

	Cycled (10)	172.75	19.66	181.06	16.10	22.97	4.96	17.69	14.36
	Cycled (100)	183.88	14.48	193.77	10.21	23.39	3.23	19.29	6.63
	Cycled (1000)	166.30	22.66	175.58	18.64	22.84	5.52	17.77	13.99
	Cycled (10 000)	170.71	20.61	170.23	21.11	22.23	8.04	18.51	10.42
Macro-encapsulated PCM									
<i>MacroPCM24</i>	Not-cycled	86.81	0.00	86.25	0.00	23.61	0.00	19.28	0.00
	Cycled (10)	82.94	4.46	99.63	-15.51	23.71	-0.42	18.87	2.13
	Cycled (100)	82.65	4.79	86.74	-0.56	23.49	0.49	18.94	1.75
	Cycled (1000)	83.75	3.52	99.18	-14.99	23.56	0.18	18.58	3.63
	Cycled (10 000)	59.81	31.10	59.06	31.53	23.91	-1.28	18.94	1.75
<i>MacroPCM28</i>	Not-cycled	128.59	0.00	138.65	0.00	28.82	0.00	21.82	0.00
	Cycled (10)	130.68	-1.63	139.07	-0.30	28.99	-0.58	21.64	0.81
	Cycled (100)	130.06	-1.15	134.58	2.93	29.19	-1.28	21.58	1.08
	Cycled (1000)	129.97	-1.07	134.79	2.78	28.70	0.43	22.07	-1.18
	Cycled (10 000)	132.37	-2.94	136.39	1.63	28.96	-0.49	21.40	1.93
Micro-encapsulated PCM									
<i>MC DS5040X</i>	Not-cycled	111.99	0.00	100.15	0.00	22.97	0.00	20.87	0.00
	Cycled (10)	99.23	11.39	69.18	30.92	22.63	1.48	20.59	1.34
	Cycled (100)	73.98	33.94	68.62	31.49	22.61	1.55	20.59	1.37
	Cycled (1000)	73.56	34.32	61.64	38.45	22.64	1.44	20.60	1.31
	Cycled (10 000)	73.30	34.55	50.57	49.51	22.67	1.31	20.49	1.82
<i>MC DS5008X</i>	Not-cycled	109.04	0.00	102.27	0.00	24.63	0.00	23.19	0.00
	Cycled (10)	88.78	18.58	94.31	7.78	24.62	0.05	23.18	0.03
	Cycled (100)	88.24	19.08	90.03	11.97	24.64	-0.03	23.18	0.04
	Cycled (1000)	85.67	21.43	92.19	9.85	24.65	-0.07	23.17	0.09

	Cycled (10 000)	83.50	23.42	92.69	9.37	24.60	0.12	23.17	0.09
<i>MC DS5038X</i>	Not-cycled	84.28	0.00	78.64	0.00	25.07	-1.80	21.54	7.12
	Cycled (10)	83.22	0.97	77.30	1.31	25.03	-1.64	21.68	6.50
	Cycled (100)	82.81	1.35	77.38	1.23	25.02	-1.60	21.67	6.55
	Cycled (1000)	83.20	0.99	77.55	1.06	25.02	-1.60	21.71	6.40
	Cycled (10 000)	80.22	3.72	75.44	3.13	25.10	-1.89	21.74	6.27
<i>MPCPM24D</i>	Not-cycled	99.69	0.00	88.65	0.00	23.14	0.00	20.43	0.00
	Cycled (10)	88.20	11.53	83.13	6.23	22.66	2.10	20.23	1.01
	Cycled (100)	89.02	10.70	84.08	5.16	22.71	1.88	19.36	5.27
	Cycled (1000)	84.09	15.64	79.36	10.48	22.81	1.44	20.21	1.08
	Cycled (10 000)	82.94	16.80	73.04	17.61	22.66	2.09	20.25	0.90

$H_m^{(1)}$  - melting enthalpy, kJ/kg;

$H_s^{(2)}$  - solidification enthalpy, kJ/kg;

$t_m^{(3)}$  - melting temperature, °C;

$t_s^{(4)}$  - solidification temperature, °C.

### Fatty acid based PCMs

According to Beatens et al. [101] the most popular non-paraffin organic PCMs are fatty acids or palmitoleic acids ( $CH_3(CH_2)_nCOOH$ ). These substances have high latent phase-change heat, small volumetric changes during phase transition and narrow range of phase change temperature. The most common fatty acids can be divided into six categories: caprylic, capric, lauric, myristic, palmitic and stearic. The carbon atom count per molecule in these substances range from 8 to 18. The melting-freezing temperatures range from 16 to 65 °C, heat of fusion is between 155 kJ/kg and 180 kJ/kg. However, the cost of fatty acid based PCMs is approximately three times higher than paraffin based. One drawback for fatty acid based PCMs is that there are not many materials with phase transition around 21 °C that can be utilized in passive cooling systems.

### Inorganic solid-liquid PCMs

Inorganic PCMs generally include salt hydrates, metallic alloys and molten salts however the most common inorganic PCMs are hydrated salts. These substances have relatively good thermal conductivity of around 0.5 W/m·K (more than two times higher than paraffins), high energy storage density of around 240 kJ/kg. Most of inorganic PCMs are corrosive to many

metals and they undergo super-cooling. Hydrated salts are generally significantly cheaper than paraffin based PCMs but slightly toxic.

Hydrated salts are the most investigated PCMs. These PCMs take the form of inorganic salt and water mixtures creating a crystalline solid of general formula  $A \cdot nH_2O$  where A represents the salt component. Phase change temperature can be adjusted by varying the chemical composition of salts. The solid-liquid phase transition of salt hydrate is hydration or dehydration of a salt. During melting the hydrate salt either melts to salt hydrate and fewer molecules of water or to anhydrous salt and water [93].

Incongruent melting is the main drawback faced when applying salt hydrates for energy storage. The hydrate or anhydrous salt usually remains at the bottom of the container due to density difference and reduces the opportunity of recombination during the next cycle. This problem can be addressed with mechanical stirring and addition of thickening agents [93].

A good example of hydrated salt PCM is *Glaubers's salt* ( $Na_2SO_4 \cdot H_2O$ ) with melting temperature between 32 °C and 35 °C and latent heat of 254 kJ/kg. This is one of the cheapest materials that can be used for thermal storage but it suffers from phase segregation [101,103]. Additionally the energy storage capacity will deteriorate over time due to formation of lower salts that are unable to recombine with water.

Molten salts have high heat of fusion but also high melting temperature, thus they can be utilized for solar energy storage.

### Eutectic PCMs

Eutectic PCMs usually are a mixture of two or more substances that solidify and melt congruently. An advantage of these PCMs is that their phase change range is very sharp and can be easily manipulated by changing the ratio of substances in the mixture. However, there is a lack of data regarding the thermal properties of these mixtures. Examples of some common eutectic PCMs are shown in Table 4.2 [93].

Table 4.2

Eutectic PCMs with phase change temperature between 19 and 30 °C (table form [93], data from [100,104–106])

PCM Compound	Melting temp. (°C)	Heat of fusion (kJ/kg)
65.5% Capric + 34.5% Lauric acid	18-19.5	140.8
61.5% Capric acid + 38.5% Lauric acid	19.1	132
45% Capric + 55% Lauric acid	21	143
75.2% Capric acid + 24.8% Palmitic acid	22.1	153
26.5% Myristic acid + 73.5% Capric acid	22.4	152
34% C <sub>14</sub> H <sub>28</sub> O <sub>2</sub> + 66% C <sub>10</sub> H <sub>20</sub> O <sub>2</sub>	24	147.7
50% CaCl <sub>2</sub> + 50% MgCl <sub>2</sub> · 6H <sub>2</sub> O	25	95
66.6% CaCl <sub>2</sub> · 6H <sub>2</sub> O + 33.3% MgCl <sub>2</sub> · 6H <sub>2</sub> O	25	127
Octadecane + docosane	25.5-27	203.8
Octadecane + heneicosane	25.8-26	173.93

13.4% Stearic acid + 86.6% Capric acid	26.8	160
48% CaCl <sub>2</sub> + 4.3% NaCl + 0.4% KCl + 47.3% H <sub>2</sub> O	26.8	188
50% CH <sub>3</sub> CONH <sub>2</sub> + 50% NH <sub>2</sub> CONH <sub>2</sub>	27	163
Triethylolethane + urea	29.8	218
47% Ca(NO <sub>3</sub> ) <sub>2</sub> ·4H <sub>2</sub> O + 53% Mg(NO <sub>3</sub> ) <sub>2</sub>	30	136
60% Na(CH <sub>3</sub> COO) ·3H <sub>2</sub> O + 40% CO(NH <sub>2</sub> ) <sub>2</sub>	30	200.5

## 4.2 Conclusion

Previous research in the field of PCMs indicates that fatty acid, and paraffin based PCMs can be utilized to support passive cooling technologies. Paraffin based PCMs have a good combination of cost and performance and many commercial products are available with a wide range of melting temperatures. These properties make paraffin based PCMs the best candidate for passive cooling applications in the scope of this thesis.

Moreover, an important factor for the selection of PCM thermal storage media is the property decay that is often not considered. Previous research on the property decay for PCMs indicates a wide range property stability for these materials ranging from ~60 % loss of phase change enthalpy to even a slight increase of phase change enthalpy after 10 000 cycles.

The next chapter focuses on the energy delivery/extraction methods for the PCM thermal storage. All of the described methods utilise different forms of paraffin based PCMs (bulk, microencapsulated, PCM-water slurry).

## **5 REVIEW OF THERMAL STORAGE SYSTEMS BASED ON PCM APPLICATION**

This chapter focuses on the previous research in thermal storage systems, that includes information on reported performance of these systems, the developed numerical models, simulation and experimental studies.

PCM thermal storage technologies can in principle be categorized into two categories: passive thermal storage systems and active thermal storage systems.

Passive thermal storage systems mainly rely on incorporation of PCM materials into building structures where they function as a “thermal mass” which stabilizes indoor temperature. These systems are usually combined with other passive cooling techniques, for example, night cooling (night ventilation).

Active thermal storage systems employ some mechanical/controlled means of supplying or extracting energy from PCM storage. Traditionally, these systems are PCM tanks, PCM thermal storage incorporated into hybrid ventilation systems, thermally activated heating and cooling panels with PCM storage or PCM slurry systems where PCM slurry is used as a heat transfer medium.

### **5.1 Passive PCM thermal storage systems**

The simplest form for integrating PCM into building structures is to mix encapsulated PCM into structural materials such as plasterboards, concrete etc. or immerse these structures into liquid PCM for the PCM to infiltrate into the pores of the material. This is a very simple form of PCM integration that requires little additional expenses. However, this method has drawback such as decomposing or a risk of PCM material leaking from structures [107–109]. This method is not very efficient: however, some energy savings can be gained. Hunger et al. [110] reported a 12 % of energy savings by mixing 5 % of microencapsulated PCM into concrete.

A more advanced method is an integration of encapsulated PCM into building structures. Variety of container types have been developed and tested, for instance, plastic bags, aluminium foil bags and plastic containers. The main advantage of passive TES is the lower cost and no energy transportation system required. In this case the PCM is recharged by using night ventilation; however, in most cases this approach does not reach the full potential of the thermal storage. Due to limited area of contact and limited heat transfer coefficients the PCM fails to solidify [108,111,112]. However there are also examples with impressive energy savings [26,113]. Passive TES applications in more detail are described in the following chapters.

### PCM integration into plasterboards

Integration of PCM into plasterboards is very common and many numerical and experimental studies evaluating the effectiveness have been conducted [114–117]. Kuznik et al. [114] performed a study to test PCM wallboard developed by Dupont de Nemours Society (Figure 5.1). The wallboard panel was composed of 60 % microencapsulated paraffin with melting temperature of around 22 °C and the density of the material was 1019 kg/m<sup>3</sup>.

The team used differential scanning calorimetry to measure the heat storage capacity in a temperature range from 0 °C to 34 °C with heating rate of 2 °C/min and guarded hot-plate apparatus to measure heat conductivity. As a result of numerical modelling the team concluded that the optimum thickness of the wallboard is around 10 mm that represents energy storage of the room for a daily temperature swing from 18 °C to 26 °C for a 24 hour period. The use of the 10 mm wallboard allowed doubling the thermal inertia of the room.

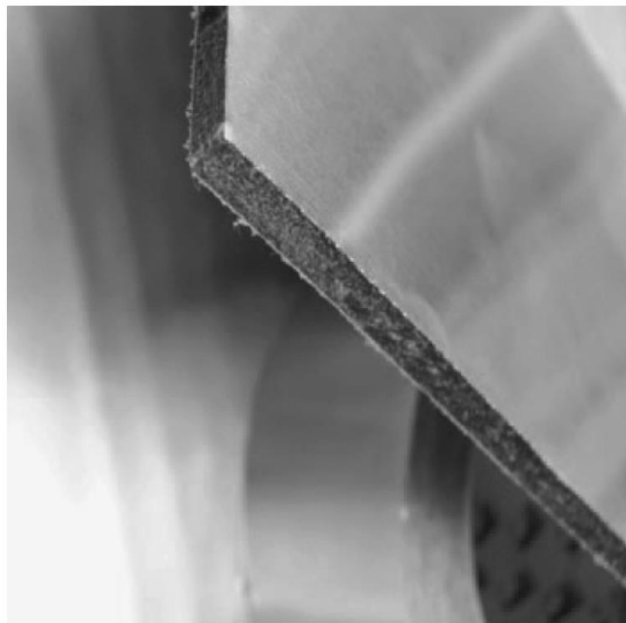


Figure 5.1 Wallboard developed by *DuPont de Nemours* Society (Figure from [114])

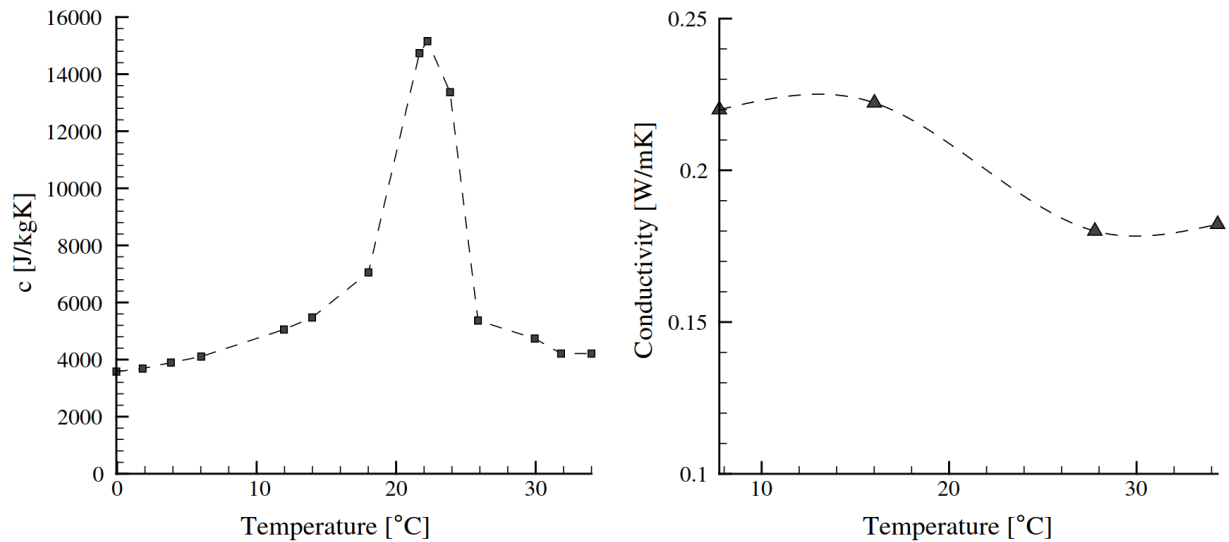


Figure 5.2 Measured specific heat and thermal conductivity of the wallboard developed by *DuPont de Nemours* (Figure from [114])

Another team Berzin et al. conducted a study with PCM wallboards for heating application [113] and night cooling application [26]. The study was performed experimentally with test cabins.

For heating application the team used an energy price based control system (Figure 5.3) in a combination with floor heating and gypsum board with paraffin based PCM encapsulated in the material. The results indicated 18.8 % energy savings and up to 28.7 % cost savings over a five day measurement period.

For cooling applications a combination of night ventilation, AC unit and energy price based control system (Figure 5.3) was used. The results indicated an impressive 73 % energy saving and 67 % cost saving over one week measurement period. However, in the same study it was indicated that if a proper control strategy is not used the same combination of systems can also lead to an increase in energy consumption.

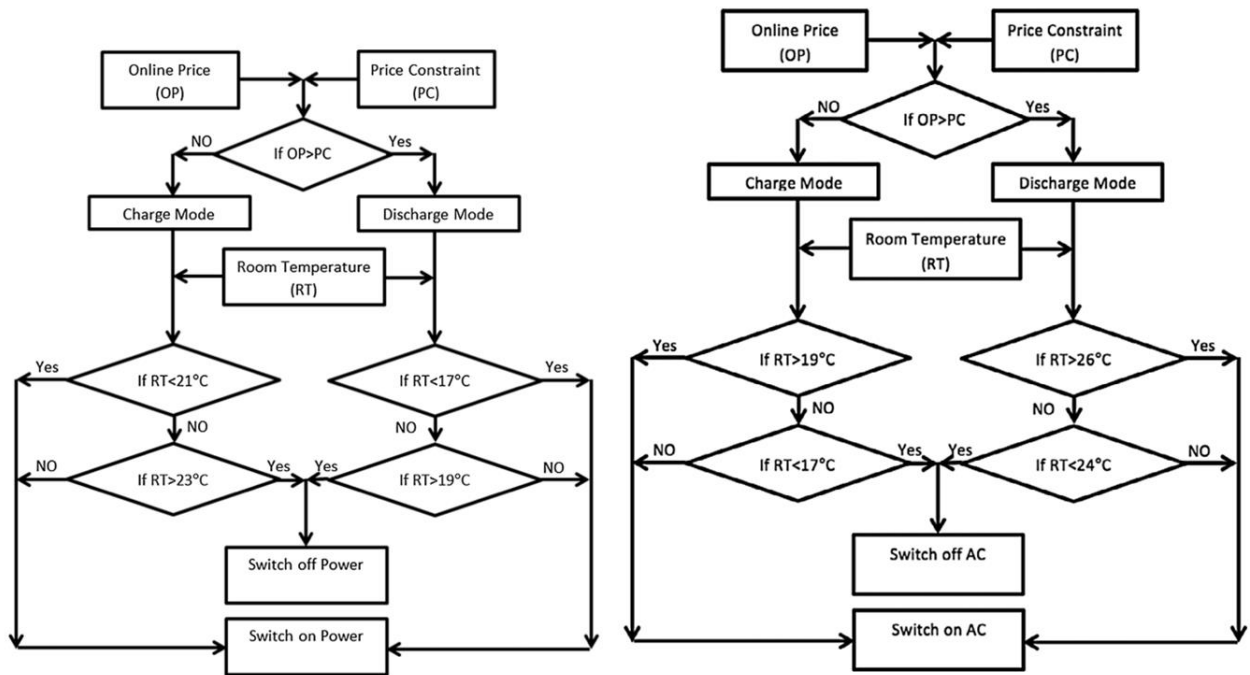


Figure 5.3 Energy price based control logic for study [113] on the left side and study [26] on the right side

### PCM integration into external envelope

PCM integration into external walls can help to lower heat flux from exterior to interior of a room. This is particularly important in lightweight wooden or metal frame walls. Incorporation of PCMs in wooden frame walls can be an interesting option in northern part of Europe where wooden frame panel buildings are popular. It is common for these buildings to suffer from overheating in early spring when there is high solar radiation and the elevation of sun is low exposing vertical glazing to increased solar radiation during all seasons [1].

Carbonari et al. [118] performed an experimental and numerical study on prefabricated sandwich panels with integrated PCM layer. The mathematical model showed good agreement with measured values. The team found that the incorporation of PCM materials in sandwich type external walls allows them to thermodynamically resemble high thermal mass walls while keeping the advantages of a sandwich wall (fast and easy installation and low weight).

Evers et al. [119] carried out a numerical study for lightweight frame wall with integrated PCMs. The team found that the peak heat flux was reduced by 9.2 % and the daily average heat flow reduced by 1.2 %.

An external wall with a composition of insulation-PCM-insulation (resistance-capacity-resistance) was numerically tested by Halford and Boehm [120]. The proposed wall model was intended for cooling peak load shifting. The models predicted a 11-25 % of peak load reduction over a scenario with only mass but no PCM inside the wall and 19-57 % of peak load reduction over a scenario with only insulation.

Alawadhi [121] performed numerical study on bricks with cavities filled with PCM. The author concluded that if three PCM cylinders are located in the middle part of the brick the heat flux can be reduced by approximately 18 %.

Alawadhi and Alqallaf [122] studied a roof with cone shaped PCM pockets in the roof slab (Figure 5.4) and concluded that the heat flux to indoor space can be reduced by approximately 39 %.

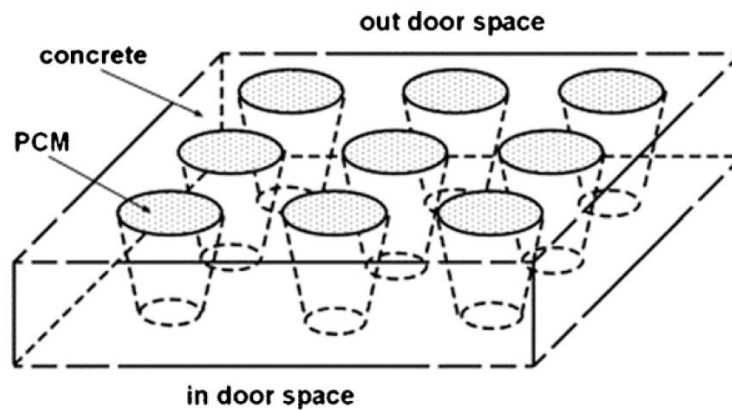


Figure 5.4 Roof slab studied by Alawadhi and Alqallaf [122]

Additionally, attempts have been carried out to integrate PCMs in external parts of facades to accumulate heating energy with Fresnel lens as a passive heating system for NZEBs, this is a promising approach but requires field studies [123].

## 5.2 Active PCM thermal storage systems

Active thermal storage systems typically include some active energy delivery or extraction mechanism that serves as a heat exchanger between the room and the PCM storage or between the PCM and a cooling or heating energy source. The energy source is usually of a passive nature. In further chapters active PCM storage applications are described.

### PCM to air heat exchangers

PCM to air heat exchangers are probably the most researched type of active PCM thermal storage systems. These types of systems allow to control the energy flow in and out of PCM storage as well as fully utilize the energy storage potential by selecting proper PCM layer thickness [124–126]. This allows to overcome low thermal conductivity and to access all stored energy. Cooling and heating energy delivery to conditioned spaces can also be controlled. On the other hand, these systems usually have significant space requirements and are rather intricate with complex control logic.

Hed and Bellander [127] described and validated an air to PCM heat exchanger model for utilization in indoor climate and energy simulation software using finite difference method.

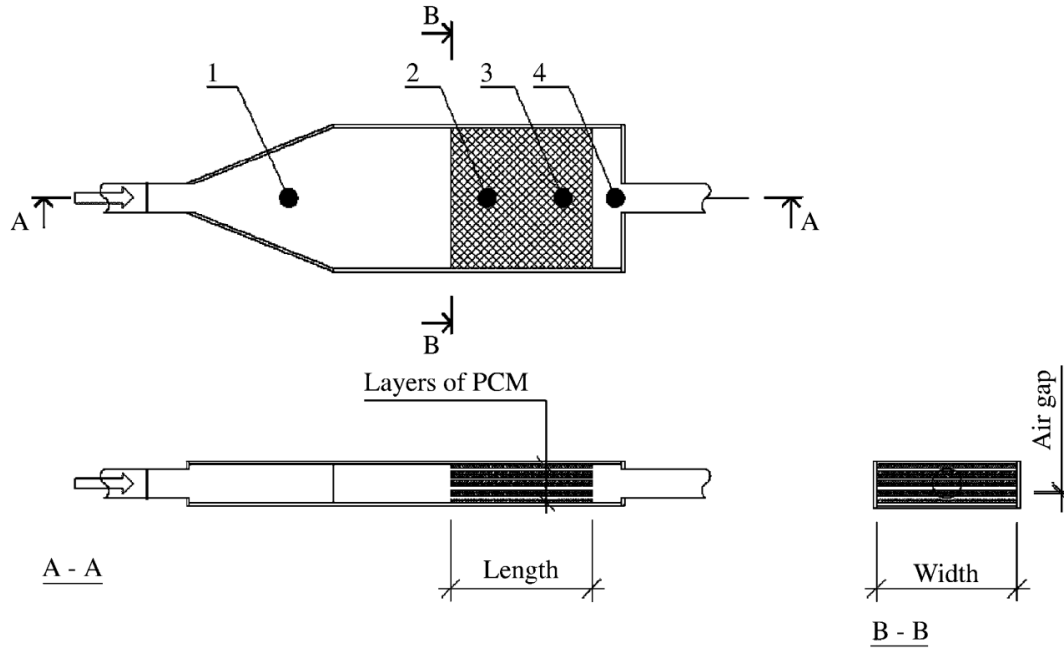


Figure 5.5 PCM to air heat exchanger proposed by Hed and Bellander [127]

In the model that Hed and Bellander proposed the heat exchanger is modelled as a duct with air flow where PCM has a constant temperature. Heat balance for an element  $dx$  (Figure 5.6; Equation (5.1)) is

$$u \cdot A \cdot \rho_{air} \cdot c_{air} \cdot (T(x) - T(x + dx)) + Per \cdot dx \cdot U_p \cdot (T_{PCM} - T(x)), \quad (5.1)$$

$$= 0$$

where  $u$  – air velocity, m/s;  
 $A$  – area cross section of the duct, m<sup>2</sup>;  
 $\rho_{air}$  – density of air, kg/m<sup>3</sup>;  
 $c_{air}$  – is heat capacity of air, J/kg·K;  
 $T(x)$  – temperature at coordinate  $x$ , K;  
 $T(x + dx)$  – temperature at coordinate  $x + dx$ , K;  
 $Per$  – perimeter of the heat exchanger, m;  
 $U_p$  – heat transfer coefficient between the middle of the PCM and air, W/m<sup>2</sup>K;  
 $T_{PCM}$  – temperature in PCM, K.

The solution of the governing equation is (Equation (5.2)).

$$T(x) = T_{PCM} + (T_0 - T_{PCM}) \cdot e^{-\frac{P \cdot U_p}{u \cdot A \cdot \rho_{air} \cdot c_{air}} \cdot x}, \quad (5.2)$$

where  $T_0$  – air inlet temperature, K;  
 $e$  – mathematical constant, 2.71828;  
 $x$  – length coordinate, m.

The power of the heat exchanger can be written as (Equation (5.3)).

$$P_c = u \cdot A \cdot \rho_{air} \cdot c_{air} \cdot (T_0 - T(x)), \quad (5.3)$$

where  $P_c$  – cooling power, W.

Combining Equation (5.1), Equation (5.2) and Equation (5.3)  $P$  can be expressed as Equation (5.4).

$$P = h_p \cdot Per \cdot L \cdot (T_0 - T_{PCM}), \quad (5.4)$$

where  $L$  – length of the heat exchanger, m;

$h_p$  – fictive convective heat transfer coefficient  $W/m^2 \cdot K$ .

$h_p$  is a fictive convective heat transfer coefficient and can be described with Equation (5.5).

$$h_p = \frac{u \cdot A \cdot \rho_{air} \cdot c_{air} \cdot (1 - e^{-\frac{P \cdot U_P}{u \cdot A \cdot \rho_{air} \cdot c_{air}} \cdot L})}{Per \cdot L}, \quad (5.5)$$

$h_p$  can be compared with the surface heat transfer coefficient.  $h_p$  is dependent of the geometry of the unit, the air flow and the perimeter of exposed material.

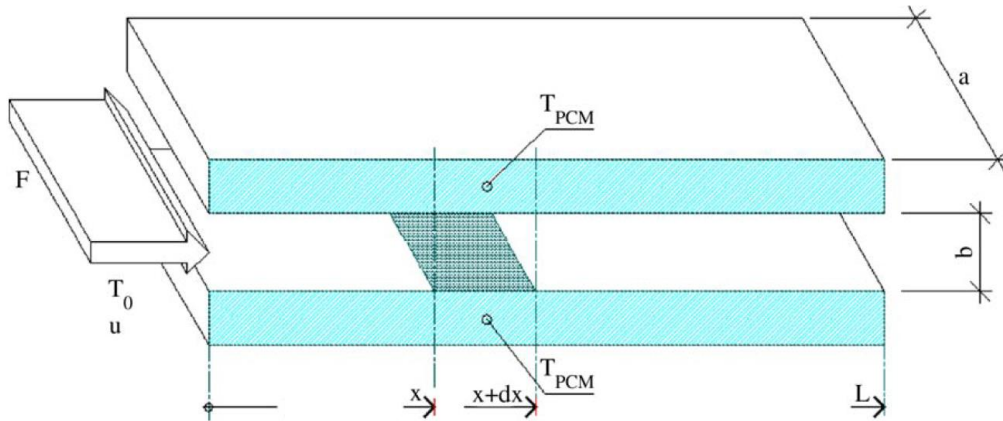


Figure 5.6 Model for establishing the governing differential equation of the heat exchanger

The heat transfer coefficients must be calculated for both smooth (laminar and turbulent flow) and rough (turbulent flow) surfaces. The transition from laminar to turbulent flow in the model is assumed to take place at Reynolds number of 2300. For smooth surface the heat transfer coefficient  $h_{cS}$  is calculated with Equation (5.6) and for turbulent flow the heat transfer coefficient  $h_{cR}$  is approximated with Equation (5.7) using Reynolds-Colburn analogy.

$$h_{cS} = \frac{Nu \cdot \lambda}{d_h}, \quad (5.6)$$

where  $h_{cs}$  – convective heat transfer coefficient for smooth surfaces,  $W/m^2 \cdot K$ ;  
 $Nu$  – Nusselt number;  
 $\lambda$  – thermal conductivity,  $W/m \cdot K$ ;  
 $d_h$  – hydraulic diameter, m.

$$h_{cR} = \frac{f \cdot \rho_{air} \cdot c_{air} \cdot u}{2 \cdot Pr^{2/3}}, \quad (5.7)$$

where  $f$  – friction coefficient;  
 $Pr$  – Prandtl number (assumed to be 0.7).

The agreement between the simulation model predictions and measured values in a prototype model was compared using mean squared temperature difference and the correlation was  $0.3 \text{ }^\circ\text{C}$  for rough surface and  $0.1 \text{ }^\circ\text{C}$  for smooth surface.

Jaworski et al. [128,129] performed an experimentally validated numerical study of a ceiling mounted PCM to air heat storage integrated into a ventilation system. The heat exchanger was constructed of a micro-encapsulated PCM and gypsum composite (Figure 5.7). The thermal storage was designed to withstand an 8 hour  $30 \text{ }^\circ\text{C}$  heat wave of outdoor air flow through the heat exchanger after a 16 hour recharging period with outdoor air temperature of  $16 \text{ }^\circ\text{C}$ . During the heat wave period the supply air temperature did not exceed  $24 \text{ }^\circ\text{C}$  and the melting temperature of the used PCM was  $22.8 \text{ }^\circ\text{C}$ .

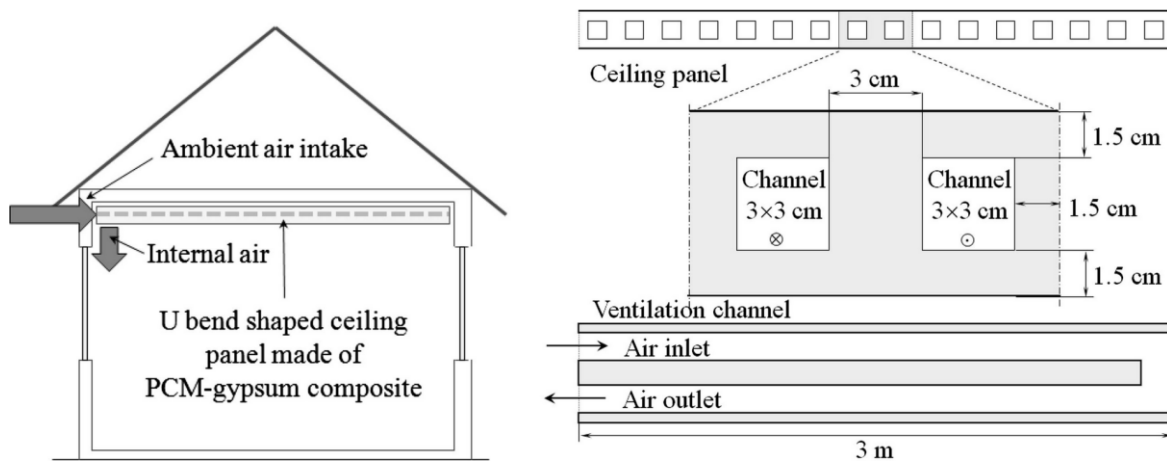


Figure 5.7 Ceiling mounted PCM storage proposed by Jaworski et al. [128,129]

Borderon et al. [130] performed an exhaustive simulation study for a  $100 \text{ m}^2$  residence cooled with ventilation air from a PCM to air heat exchanger storage system. The simulation study was performed for four locations in France: Lyon, Nice, Trappes, Carpentras. The team found that with a  $700 \text{ kg}$  PCM thermal storage it is possible to limit the overheating in the residence to under  $8 \%$  if  $26 \text{ }^\circ\text{C}$  is considered the limit. The main issues the team reported was

the inability to fully recharge the PCM storage during warm nights that resulted in increased fan energy.

### **PCM storage tanks**

PCM Storage in tanks or other similar enclosures is widely commercialised, the most popular being ice storages. These methods are mainly used for peak load shifting or utilization of off-peak energy prices.

There are also PCM storage tank proposals for solar energy storage that utilize paraffin based PCM and offers chemical stability and is non-corrosive [131].

### **Cooling panels with integrated PCM thermal storage**

Another commonly researched method is to use thermally activated building structures (TABS) or cooling units with integrated PCMs such as ceiling panels with PCM layers or slabs with capsulated PCMs, however this system is not widely commercialized. Aforementioned units generally are thermally activated with a hydronic circuit and cooling energy is supplied from a central cooling plant with a passive or active cooling energy generator.

There has also been an effort by Wang et al. [132] to use a PCM slurry as a heat transfer media that is pumped through a cooling panel for utilisation together with evaporative cooling tower in a hybrid system (Figure 5.8). In this case the slurry consists of water and microencapsulated hexadecane ( $C_{13}H_{34}$ ) particles with melting temperature of  $18.1\text{ }^{\circ}\text{C}$  and latent heat of melting  $224\text{ kJ/kg}$  and Amino plastics as the shell material. The core to shell ratio was around 7:1 by weight. The diameter of the particles was approximately  $10\text{ }\mu\text{m}$ . The slurry contained around 30 % of microencapsulated PCM by weight (Figure 5.9). Properties of the materials used in the study are described in Table 5.1. The characteristics for some of the slurries was already previously investigated by Wang et al. [133]. The team performed a simulation study for this type of system for five Chinese cities (Hong Kong, Shanghai, Beijing, Lanzhou and Urumqi). The highest energy saving estimates of approximately 80 % was for Urumqi and the lowest estimate of around 15 % was for Hong Kong. The potential energy saving is dependent of the heat exchange area in the room and external conditions, for example, air wet bulb temperature.



The most common application is to use a hydronic circuit which is located near or immersed in the PCM layers of a cooling panel or a slab.

Tzivanidis et al. [137] performed a numerical study for a system where cooling circuit is embedded in a concrete slab and a PCM layer is located between the thermally activated concrete layer and room. The studied slab contained PCM material that is consistent with *Rubitherm RT25* [138] PCM with a phase change temperature of around 25 °C and heat storage capacity of 230 kJ/kg in the temperature range from 16 °C to 31 °C [138] The team concluded that the proposed system allows:

- to perform night cooling utilizing the lower night-time temperatures;
- to utilize lower night-time energy price rates;
- improve indoor thermal comfort due to lower temperature fluctuations indoors;
- more even temperature distribution in the ceiling slab.

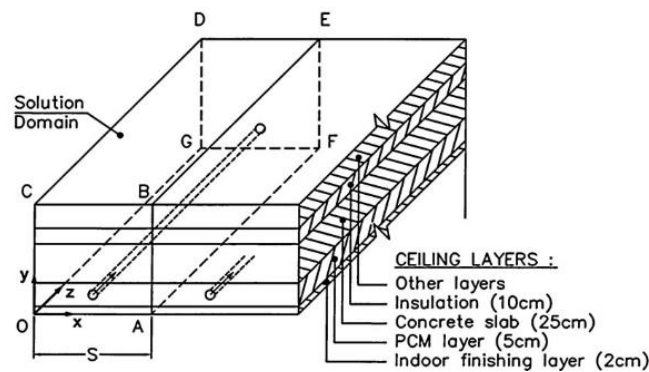


Figure 5.10 PCM storage investigated by Tzivanidis et al. [137]

Koschenz and Lehmann [97] developed a thermally activated ceiling panel for cooling (Figure 5.11 and Figure 5.12) and also did numerical analyses in *TRANSYS*. The developed panel had a thermal storage capacity of 0.3 kWh/m<sup>2</sup> and was composed of microencapsulated PCM (Heptadecane-based paraffin with phase change temperature of approximately 22 °C) and gypsum composite. Gypsum was chosen due to its internal water content that performs as a fire retardant for fire safety precautions. To enhance the thermal conductivity of the panel it was supplemented with aluminium fins. The measured average heat conductivity of the panel was 1.1-1.2 W/m·K, the density was 1030 kg/m<sup>3</sup> and the amount of microencapsulated PCM was 13.3 kg/m<sup>2</sup>. According to the test results the panel withstood a 40 W/m<sup>2</sup> heat flux for 7.5 hours before the PCM transitioned to a liquid state.

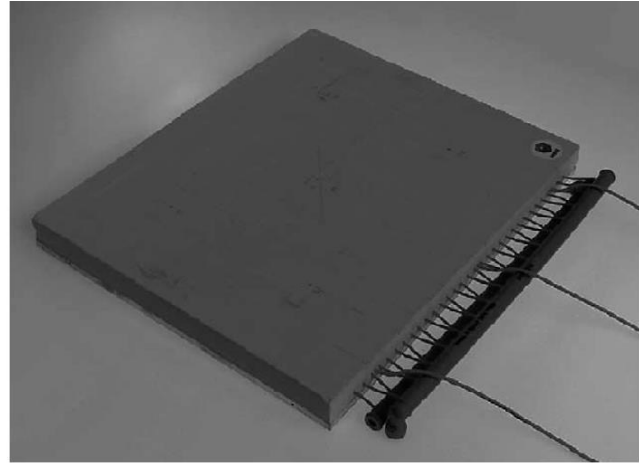
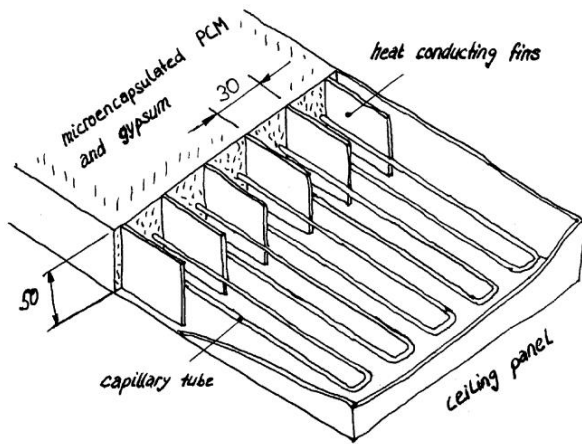


Figure 5.11 PCM cooling panel developed by Koschenz and Lehmann [97]

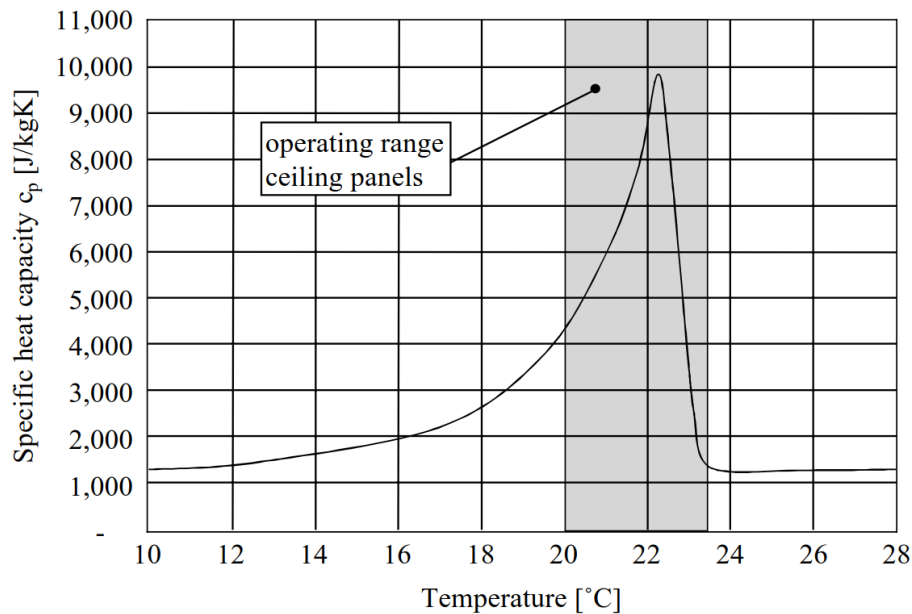


Figure 5.12 Specific heat capacity of the gypsum and micro-encapsulated heptadecane PCM developed by Koschenz and Lehmann [97]

Koschenz and Lehmann [97] also formulated the general finite difference model for the cooling panel with Equation (5.8) (See also Figure 5.13). For full formulation details of the model refer to [97].

$$t_i^{n+1} = t_i^n + M_i^n \left( (1 - tm_p)(t_{i+1}^n - 2t_i^n + t_{i-1}^n) + tm_p(t_{i+1}^{n+1} - 2t_i^{n+1} + t_{i-1}^{n+1}) \right), \quad (5.8)$$

where  $t_i^{n+1}$  – temperature in node at time step  $n + 1$  and location  $i$ , °C;  
 $t_i^n$  – temperature in node at time step  $n$  and location  $i$ , °C;  
 $M_i^n$  – modulus in node at time step  $n$  and location  $i$ ;  
 $tm_p$  – parameter of time;  
 $t_{i+1}^n$  – temperature in node at time step  $n$  and location  $i + 1$ , °C;

- $t_{i-1}^n$  – temperature in node at time step  $n$  and location  $i - 1$ , °C;
- $t_{i+1}^{n+1}$  – temperature in node at time step  $n + 1$  and location  $i + 1$ , °C;
- $t_i^{n+1}$  – temperature in node at time step  $n + 1$  and location  $i$ , °C;
- $t_{i-1}^{n+1}$  – temperature in node at time step  $n + 1$  and location  $i - 1$ , °C.

Modulus  $M$  can be expressed with Equation (5.9).

$$M_i^n = \alpha(t_i^n) \frac{\Delta tm}{\Delta x^2}, \quad (5.9)$$

- where  $\alpha$  – thermal diffusivity,  $m^2/s$ ;
- $tm$  – time, s;
- $x$  – space coordinate, m.

The thermal diffusivity  $a$  can be expressed with Equation (5.10).

$$a(t) = \frac{1}{\rho} \frac{\lambda(t)}{c(t)}, \quad (5.10)$$

- where  $\lambda$  – thermal conductivity,  $W/m \cdot K$
- $\rho$  – density of the material,  $kg/m^3$ ;
- $c$  – specific heat capacity,  $J/kg \cdot K$ .

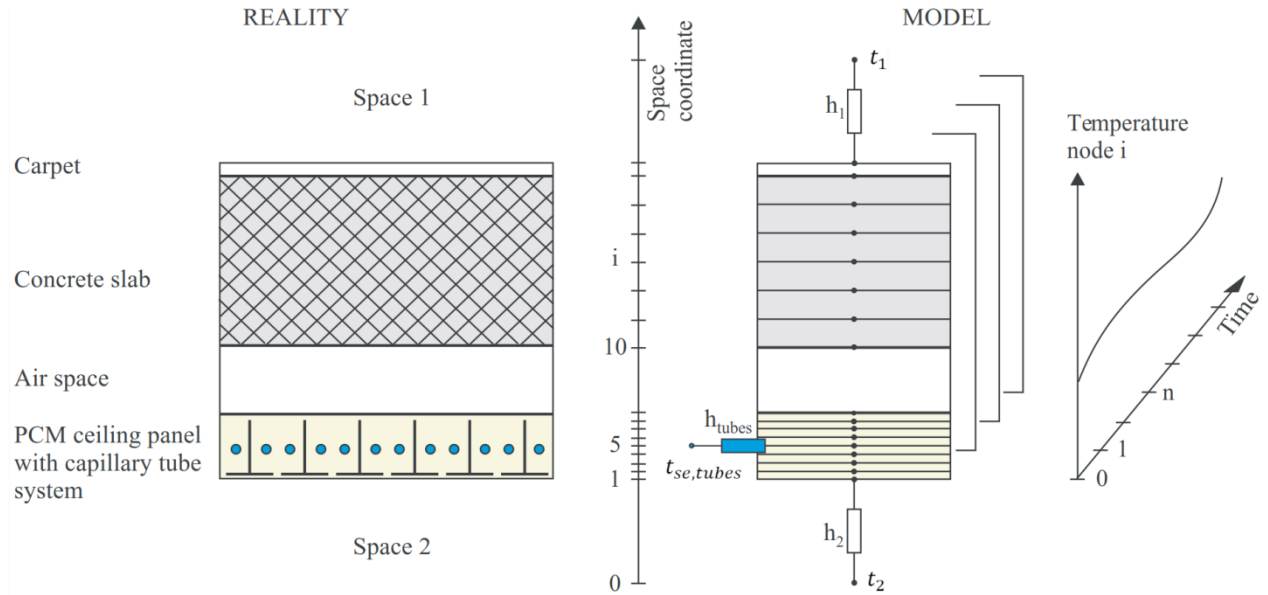


Figure 5.13 Computation model developed by Koschenz and Lehmann [93]

Weinlander et al. [139] developed and tested two types of ceiling panels (Figure 5.14) with microencapsulated PCM layer above the hydronic circuit – the first type of cooling panel; and below the hydronic circuit – the second type of cooling panel. The measured passive cooling powers were from 8 W to 17 W per square meter of ceiling area for globe temperatures from 24 °C to 27 °C. Passive cooling power for 26 °C globe temperature was

between 10-15 W/m<sup>2</sup> depending on the heat load. The phase change temperature for the investigated PCM was between 22 °C and 24 °C.

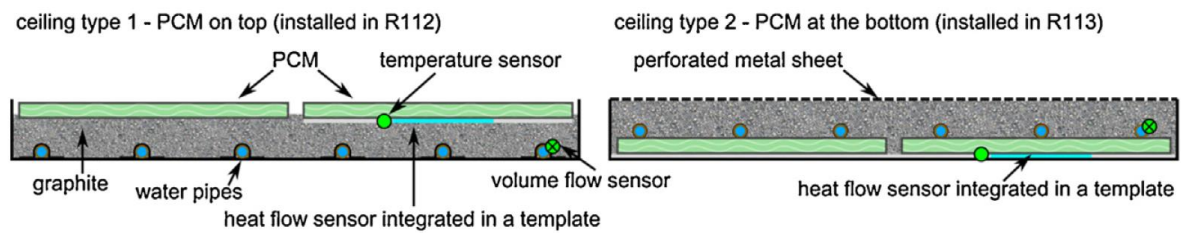


Figure 5.14 Cooling panels developed by Weinlander et al. [139]

Similar approach was tried by a Latvian researcher team Rucevskis et al. [140–142] that performed an extensive numerical analysis using CFD modelling for steel panel with liquid PCM. This type of PCM panel is also investigated in the experimental part of this thesis where results generated by an experimentally calibrated numerical model developed in *IDA ICE* were compared to CFD modelling results reported by Rucevskis et al. [141,142] (see chapter 7 and 8 of this thesis).

The estimated thermal storage capacity for the panel was 0.59 kWh/m<sup>2</sup> panel area and the phase change temperature was around 23 °C. The team modelled a room for three scenarios:

- room without PCM panels;
- room with passive PCM panels;
- room with active PCM panels.

The team modelled PCM panels with 25 mm thickness and 100 % coverage of the ceiling for an eight day period. The maximum room temperature for the analysed period is nearly 7 °C lower if thermally active PCM panels are used and only 2 °C lower if passive PCM panels are used. It was also concluded that in the case of thermally active panels only 66 % of the thermal storage capacity was used but in the case of passive PCM panels after 85 hours the PCM storage had been completely depleted and did not solidify during the following simulation period (see Figure 5.15).

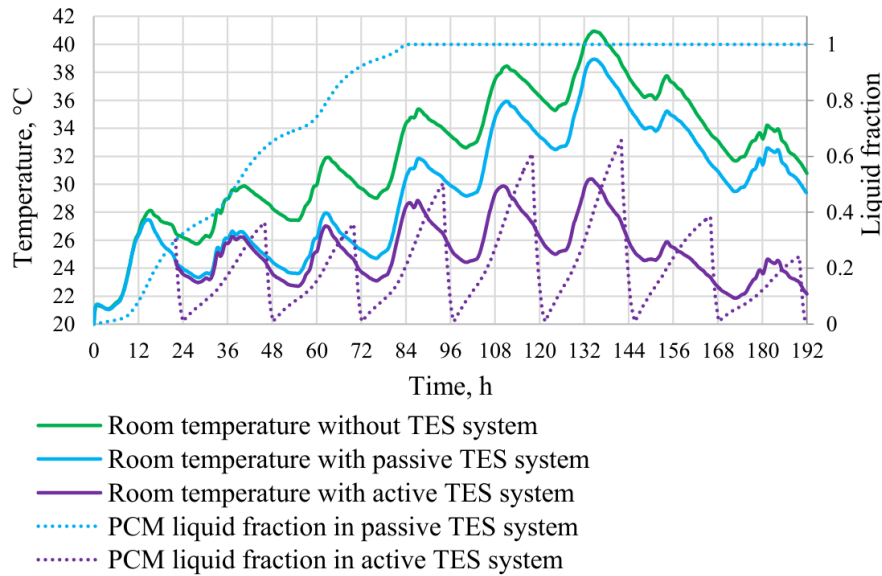


Figure 5.15 Temperature and PCM liquid fraction for PCM storage simulated by Rucevskis et al. [140–142]

### 5.3 Conclusion

This chapter of the literature review addresses previous research on latent thermal storage systems. These systems are important in order to accumulate cooling energy and fully utilize the existing passive cooling technologies as in most cases passive cooling technologies cannot cover all cooling requirements in a building.

PCM based TES in general can be divided into two types: active and passive. Passive applications have smaller capital investment but generally tend to be less effective; however there are also a few examples with significant energy savings. The most promising active applications are PCM to air heat exchangers incorporated in ventilation systems and ceiling based cooling panels with integrated latent thermal storage. The control of PCM to air heat exchanger in a ventilation system requires complex control logic. On the other hand ceiling based cooling panels with integrated latent thermal storage are simpler to integrate in buildings and existing technologies.

Application of this type of system requires in-depth understanding of heat transfer fundamentals in order to understand the governing processes and develop calculation methods and simulation models for these components. The next chapter is dedicated to the fundamentals of heat transfer in relation to HVAC systems (including PCM cooling panels).

## 6 REVIEW OF THE HEAT TRANSFER THEORY

In every thermodynamic system where there is a temperature difference inevitably irreversible heat transfer will happen due to the second law of thermodynamics. Therefore heat transfer is the fundament for all HVAC and other technologies. There are three fundamental types of heat transfer in HVAC systems – conduction, convection and radiation. These three types of heat transfer are described following chapters.

### 6.1 Conduction

Conduction takes place in solids, liquids, stationary gases and vapour boundary layers through the collisions of molecules and atoms. Conduction can be described with Fourier's Law of Heat Conduction that was formulated in 1822 and can be represented with Equation (6.1) for one-dimensional steady-state case with constant specific heat conductivity.

$$q_x = -\lambda \frac{dT}{dx} = \frac{Q_x}{A}, \quad (6.1)$$

where  $q_x$  – the specific heat transfer due to conduction in direction  $x$ , W/m<sup>2</sup>;  
 $\lambda$  – thermal conductivity, W/m·K;  
 $\frac{dT}{dx}$  – the temperature gradient, K/m;  
 $Q_x$  – total heat flow in direction  $x$  over area  $A$  (See Figure 6.1), W;  
 $A$  – area, m<sup>2</sup>.

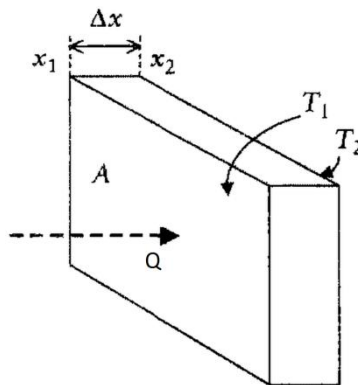


Figure 6.1 One dimensional heat flow [143]

Integration of Equation (6.1) gives Equation (6.2).

$$Q \int_{x_2}^{x_1} dx = -\lambda A \int_{T_2}^{T_1} dT \rightarrow Q = -\lambda A \frac{\Delta T}{\Delta x}, \quad (6.2)$$

where  $Q$  – heat flow, W;  
 $x_1$  – coordinate of surface 1, m;

- $x_2$  – coordinate of surface 2, m;
- $T_1$  – temperature of pane 1, m;
- $T_2$  – temperature of pane 2, m;
- $\Delta T$  – temperature difference across the layer, m;
- $\Delta x$  – thickness of the layer, m.

Goodfellow and Tahti [143] described general heat conduction for a control volume  $V = \delta x \delta y \delta z$  (see Figure 6.2) with heat generation in a homogeneous and isotropic material where internal heat generation is  $P_g''(T)$  and thermal conductivity  $\lambda(T)$  is a function of temperature.

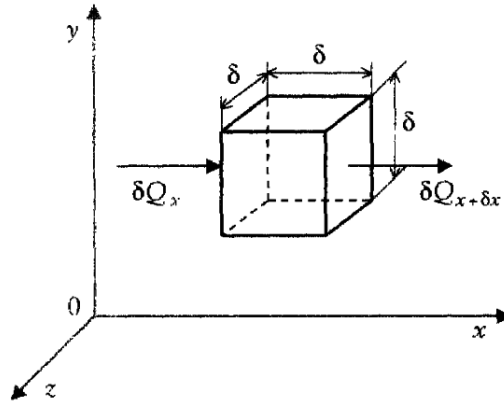


Figure 6.2 Control volume for general heat conduction [143]

The heat flow to the control volume through area  $\delta y \delta z$  at direction  $x$  is (Equation (6.3)).

$$\delta Q_x = -\delta y \delta z \lambda(T) \left( \frac{dT}{dx} \right) \delta t m, \quad (6.3)$$

- where  $\delta Q_x$  – heat flow through a surface of the control volume at direction  $x$ , W;
- $\delta t m$  – time period, s;
- $\delta y \delta z$  – area at coordinate,  $m^2$ ;
- $\lambda(T)$  – thermal conductivity as a function of temperature,  $W/m \cdot K$ .

The outgoing heat flow at the point  $x + \delta x$  is (Equation (6.4)).

$$\delta Q_{x+\delta x} = -\delta y \delta z \left( \lambda(T) \frac{dT}{dx} + \frac{d}{dx} \left( \lambda(T) \frac{dT}{dx} \delta x \right) \right) \delta t m, \quad (6.4)$$

- where  $\delta Q_{x+\delta x}$  – heat flow through a surface at coordinate  $x + \delta x$ , W;
- $\delta x$  – length of the control volume at direction  $x$ , m.

Similar equations can be derived for directions  $y$  and  $z$ . The change of internal energy  $\delta H$  inside the control volume during time period  $\delta t$  is (Equation (6.5)).

$$\delta H = \rho c_p \delta x \delta y \delta z \frac{dT}{dt m} \delta t m, \quad (6.5)$$

where  $\delta H$  – change of internal energy, J;  
 $\rho$  – density of the material, kg/m<sup>3</sup>;  
 $c_p$  – specific heat capacity, J/kg·K;  
 $\delta x \delta y \delta z$  – volume, m<sup>3</sup>;  
 $\delta tm$  – time period, s.

The heat generation inside the control volume is (Equation (6.6)).

$$\delta P_g = P_g'''(T) \delta x \delta y \delta z, \quad (6.6)$$

where  $\delta P_g$  – heat generation inside the control volume, W;  
 $P_g'''(T)$  – specific heat generation inside the control volume as a function of temperature, W/m<sup>3</sup>.

When applying the first law of thermodynamics (the sum of incoming heat flow and the heat generated inside the volume is equal to the sum of outgoing heat flow and the increase of energy inside the volume) Equation (6.7) is formulated.

$$\delta Q_x + \delta Q_y + \delta Q_z + \delta P_g = \delta Q_{x+\delta x} + \delta Q_{y+\delta y} + \delta Q_{z+\delta z} + \delta H, \quad (6.7)$$

where  $\delta Q_x$  – heat flow at direction  $x$  at point  $x$ , W;  
 $\delta Q_y$  – heat flow at direction  $y$  at point  $y$ , W;  
 $\delta Q_z$  – heat flow at direction  $z$  at point  $z$ , W;  
 $\delta Q_{x+\delta x}$  – heat flow at direction  $x$  at point  $x + \delta x$ , W;  
 $\delta Q_{y+\delta y}$  – heat flow at direction  $y$  at point  $y + \delta y$ , W;  
 $\delta Q_{z+\delta z}$  – heat flow at direction  $z$  at point  $z + \delta z$ , W.

When substituting Equation (6.4) and similar equations for other directions into Equation (6.7) Equation (6.8) is formulated:

$$\frac{d}{dx} \left( \lambda(T) \frac{dT}{dx} \right) + \frac{d}{dy} \left( \lambda(T) \frac{dT}{dy} \right) + \frac{d}{dz} \left( \lambda(T) \frac{dT}{dz} \right) + P_g'''(T) = \rho c_p \frac{dT}{dt}, \quad (6.8)$$

Assuming that the thermal conductivity is temperature independent Equation (6.9) is formulated.

$$\frac{d^2 T}{dx^2} + \frac{d^2 T}{dy^2} + \frac{d^2 T}{dz^2} + \frac{P_g'''}{\lambda} = \frac{dT}{\alpha dtm}, \quad (6.9)$$

where  $\alpha$  – thermal diffusivity ( $\alpha = \lambda / \rho c_p$ ), m<sup>2</sup>/s  
 $\frac{dT}{dtm}$  – the derivative of temperature as a function of time (in steady-state case it is zero).

## 6.2 Convection

Convection occurs between a surface and a moving liquid. Although the heat transfer in the boundary takes place in the form of conduction the energy transfer with matter governs the process.

Convection can be divided into two types: natural and forced. Natural convection is self-induced because the density of a liquid is temperature dependent and cooler parts of the liquid with higher density are pulled down by the gravity and parts with lower density are displaced up. Forced convection is caused by an external force that causes the liquid to move near a convective surface.

Convection between a surface and a fluid can be described with Newton's Law of Cooling (Equation (6.10)).

$$q_{conv} = h_{conv}\Delta T, \quad (6.10)$$

where  $q_{conv}$  – specific heat flow between a fluid and a surface, W/m<sup>2</sup>;

$h_{conv}$  – convective heat transfer coefficient, W/m<sup>2</sup>·K;

$\Delta T$  – is temperature between the surface and the liquid over a long distance (average temperature of the liquid flow), K.

Because the heat transfer occurs through a boundary layer of the liquid the heat transfer coefficient can be approximated with Equation (6.11).

$$h_{conv} \sim \frac{\lambda}{\delta}, \quad (6.11)$$

where  $\lambda$  – thermal conductivity of the layer, W/m·K;

$\delta$  – thickness of the layer, m.

However, in practical applications the determination of the convective heat transfer coefficient and convection in general is very complex and it is practically impossible to theoretically describe it. In order to practically estimate convective heat transfer empirical formulas must be used.

Convective heat transfer coefficients for practical applications can vary in orders of magnitude depending on liquids used and properties of the system, typical values are illustrated in Table 6.1.

Table 6.1

Typical convective heat transfer coefficients

Type of convection, W/m <sup>2</sup> ·K	Literature source		
	ASHRAE Fundamentals [39]	Goodfellow and Tahti [143]	Stoecker and Jones [144]
Free convection, gases	2 to 25	3.5 to 50	5 to 25 (air)
Free convection, liquids	10 to 1000	-	50 to 100 (water)

Forced convection, gases	50 to 20 000	10 to 500 (air)	10 to 200 (air)
Forced convection, liquids	2500 to 100 000	100 – 5000	50 to 100 000 (water)

In order to approximate the convective heat transfer in a thermodynamic system Nusselt number  $Nu$  is introduced. The relation of the Nusselt number and convective heat transfer coefficient can be expressed with Equation (6.12).

$$Nu = \frac{h_{conv}L}{\lambda} \rightarrow h_{conv} = \frac{Nu\lambda}{L}, \quad (6.12)$$

where  $Nu$  – Nusselt number;

$L$  – characteristic length (pipe diameter or hydraulic diameter  $d_h = 4A/P$  where  $A$  is the cross section area and  $P$  is the whetted perimeter), m.

For forced convection Nusselt number is a function of Reynolds number and Prandtl number ( $Nu = f(Re, Pr)$ ) and for free convection Nusselt number is a function of Grashof number and Prandtl number ( $Nu = f(Gr, Pr)$ ).  $Pr$  is the Prandtl number (Equation (6.13)) and  $Gr$  is the Grashof number (Equation (6.14)) and  $Re$  is the Reynolds number (Equation (6.15)).

$$Pr = \frac{v\rho c_p}{\lambda}, \quad (6.13)$$

where  $Pr$  – Prandtl number;

$v$  – kinematic viscosity,  $m^2/s$ ;

$\rho$  – density of the fluid,  $kg/m^3$ ;

$c_p$  – heat capacity of the liquid,  $J/kg \cdot K$ .

$$Gr = \frac{g\beta\Delta TL^3}{v^2}, \quad (6.14)$$

where  $Gr$  – Grashof number;

$g$  – is the acceleration due to the earth's gravity,  $9.80665 m/s^2$ ;

$\beta$  – coefficient of thermal expansion,  $1/K$ .

$$Re = \frac{uL}{v}, \quad (6.15)$$

where  $Re$  – Reynolds number;

$u$  – velocity of the flow,  $m/s$ .

For practical calculations there are numerous empirical correlations for  $Nu = f(Re, Pr)$  and  $Nu = f(Gr, Pr)$  functions for generalized cases that can be found in literature. Typical examples can be found in Table 6.2 and Table 6.3.

Table 6.2

Correlations for Reynolds number, Nusselt number and Grashof number for natural convection [143]

Flow up a vertical wall:
$Nu = (0.825 + \frac{0.387(Gr Pr)^{\frac{1}{6}}}{\left(1 + \left(\frac{0.492}{Pr}\right)^{\frac{9}{16}}\right)^{\frac{8}{27}}})^2$ <p>Valid for <math>Gr Pr &lt; 10^{12}</math>  <math>T_{st} = 0.5(T_{\infty} + T_p)</math></p>
Flow upward on a horizontal plane:
$Nu = 0.70(Gr Pr)^{\frac{1}{4}} \quad Gr Pr < 4 \cdot 10^7$ $Nu = 0.155(Gr Pr)^{\frac{1}{3}} \quad Gr Pr > 4 \cdot 10^7$ $T_{st} = 0.5(T_{\infty} + T_p)$

Table 6.3

Correlations for Reynolds number, Nusselt number and Prandtl number for forced convection [143]

Geometry	Conditions	Correlation
Flat plate	Laminar, local, $T_{av}$ $Pr \geq 0.6, Re_x < 10^5$	$Nu = 0.332 \cdot Re_x^{1/2} Pr^{1/3}$
	Laminar, average, $T_{av}$ $Pr \geq 0.6, Re_x < 10^5$	$Nu = 0.664 \cdot Re_x^{1/2} Pr^{1/3}$
	Turbulent, local, $T_{av}$ $60 \geq Pr \geq 0.6, Re_x \leq 10^8$	$Nu = 0.0296 \cdot Re_x^{1/2} Pr^{1/3}$
	Mixed, average, $T_{av}$ $60 > Pr > 0.6, Re_x \leq 10^8$	$Nu = (0.037 \cdot Re_x^{\frac{4}{5}} - 871) Pr^{\frac{1}{3}}$
	Fully turbulent, average, $T_{av}$ $5 \cdot 10^5 < Re_x \leq 10^8$	$Nu = 0.037 \cdot Re_x^{4/5} Pr^{1/3}$
Cylinder	Average, $T_{\infty}, Pr > 0.7$ $0.4 < Re_d < 4 \cdot 10^5$	$Nu = C \cdot Re_d^m Pr^{\frac{1}{3}}$ $C$ and $m$ can be found in [143]
	Average, $T_{\infty}, 500 > Pr > 0.7$ $1 < Re_d < 10^6$	$Nu = C \cdot Re_d^m Pr^n \left(\frac{Pr_{\infty}}{Pr_s}\right)$ $C$ and $m$ can be found in [143]
	Average, $T_{av}, Re_d Pr > 0.2$	$Nu = 0.3 + \frac{0.62 Re_d^{1/2} Pr^{1/3}}{\left(1 + \left(\frac{0.4}{Pr}\right)^{\frac{2}{3}}\right)^{1/4}} \cdot \left(1 + \left(\frac{Re_d}{28200}\right)^{\frac{5}{8}}\right)^{4/5}$
Sphere	Average, $T_{\infty}, 380 > Pr > 0.71$ $3.5 < Re_d < 7.6 \cdot 10^4$ $1 < \frac{\mu_{\infty}}{\mu_s} < 3.2$	$Nu = 2 + (0.4 Re_d^{\frac{1}{2}} + 0.06 Re_d^{\frac{2}{3}}) \cdot Pr^{0.4} \left(\frac{\mu_{\infty}}{\mu_s}\right)^{1/4}$

Falling drop	Average, $T_\infty$	$Nu = 2 + 0.6Re_d^{\frac{1}{2}} \cdot Pr^{1/3} (25(\frac{x}{d})^{-0.7})^{1/4}$
Note: $T_{av} = 0.5(T_\infty + T_s)$ , where $T_\infty$ is the free stream temperature and $T_s$ is the surface temperature		

### 6.3 Radiation

Radiation energy transfer is governed by:

- Planck’s law of Radiation that describes radiation energy distribution in a spectrum;
- Stefan-Boltzmann law that describes the energy emitted by a black body;
- Wien’s law that describes the product of maximum wavelength (or at which wavelength radiation energy peaks for different temperatures).

However, Stefan-Boltzmann law and Wien’s law can be derived from the more fundamental Planck’s law of Radiation.

In more simple terms Planck’s law of Radiation describes the location of each point on the distribution lines in Figure 6.3, Stefan-Boltzmann law describes the area each spectral line forms with abscissa axis in Figure 6.3 (that also is the total energy emitted) and Wiens’s law describes the extrema (peak) of each spectral line of Figure 6.3.

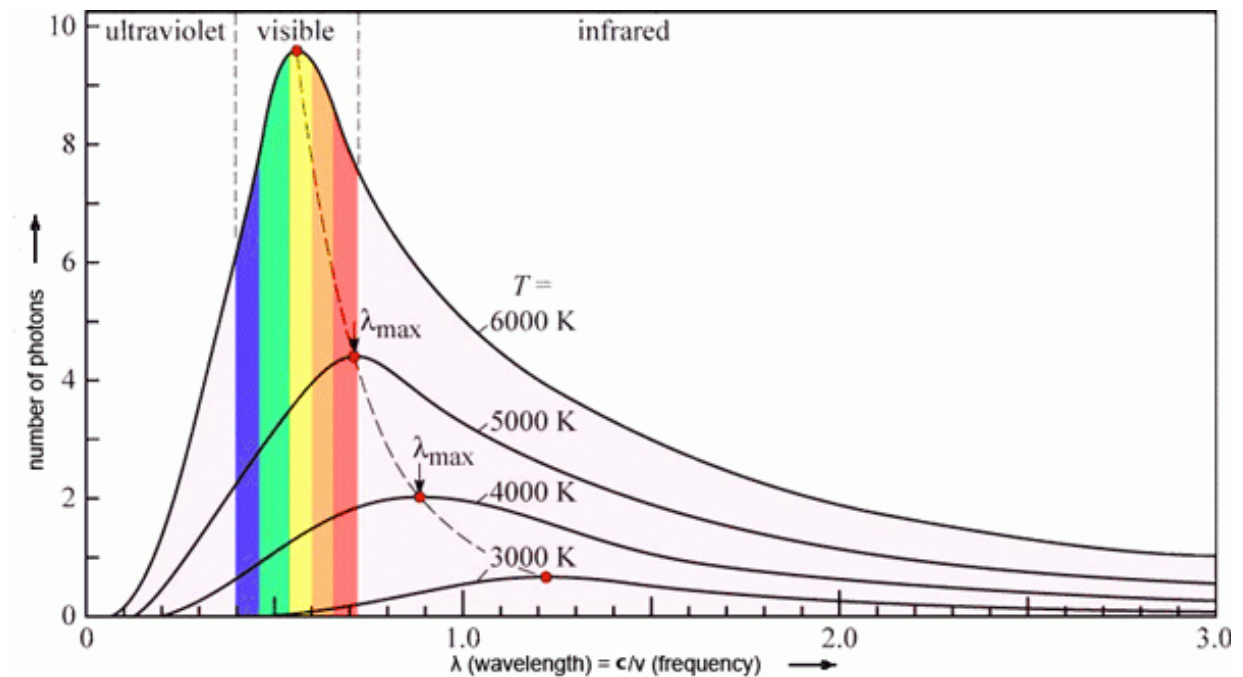


Figure 6.3 The spectral distribution of black body radiation (Figure from [145])

Planck’s law of Radiation describes radiation energy distribution in a spectrum and can be expressed with Equation (6.16) in a form of wavelength.

$$U_B(\lambda, T) = \frac{2hc^2}{\lambda^5 e^{\frac{hc}{\lambda k_B T}} - 1}, \quad (6.16)$$

where  $U_B(\lambda, T)$  – spectral radiance of the black body radiator (function of absolute temperature and wavelength) , W;

- $h$  – Planck’s constant,  $6.62607015 \cdot 10^{-34}$  J·s;
- $c$  – speed of light in vacuum,  $2.99792 \cdot 10^8$  m/s;
- $\lambda$  – wavelength, m;
- $k_B$  – Boltzmann constant,  $1.380649 \cdot 10^{-23}$  J/K;
- $T$  – absolute temperature of the black body, K;
- $e$  – mathematical constant, 2.71828.

Stefan-Boltzmann law that describes the energy emitted by a black body is described with Equation (6.17).

$$P_{rad} = A \cdot \sigma \cdot \varepsilon_{rad} \cdot T^4, \quad (6.17)$$

- where  $P_{rad}$  – is the power of radiation emitted by a black body, W;
- $A$  – area of a black body, m<sup>2</sup>;
  - $\sigma$  – Stefan Boltzmann constant,  $5.670374419 \cdot 10^{-8}$  W·m<sup>-2</sup>·K<sup>-4</sup>;
  - $\varepsilon_{rad}$  – the total emissivity of a surface (in case of a black body  $\varepsilon_r=1$ ).

Wien’s law is expressed with Equation (6.18).

$$\lambda_{max} = \frac{b}{T}, \quad (6.18)$$

- where  $\lambda_{max}$  – the product of maximum wavelength, m;
- $b$  – Wien’s displacement constant,  $2.897771955 \cdot 10^{-3}$  m·K.

Stefan-Boltzmann law for engineering calculations must be used while keeping in mind that the law describes the total energy radiation and the emissivities given in the literature are the total values over the whole spectrum. Many materials have different emissivities for different wavelengths, for example, white paper is highly reflective for visible wavelengths and highly emissive for longer infra-red wavelengths.

This principle is used for the daytime radiative cooling technology. This technology utilizes materials that are reflective over most of wavelengths, but highly emissive between 8  $\mu\text{m}$  and 13  $\mu\text{m}$ . In this wavelength range Earth’s atmosphere is highly transparent.

## 6.4 Conclusion

This chapter of the literature review addresses the heat transfer fundamentals in HVAC systems. These fundamentals are needed to develop new latent thermal storage systems and to apply existing systems. Moreover, they are essential for developing mathematical representations or simulation models of physical components to predict the behaviour of these components for the specific case of interest.

The simplest form of heat transfer that is quite accurately described by Fourier's Law is conduction. Conduction takes place mainly in solids and can be relatively easily modelled, also heat conductivity of most materials can be found in literature.

Radiation can be more difficult to theoretically describe. Nevertheless, Stefan-Boltzmann law of radiation of a black body relatively well describes the total energy transfer for materials that resemble the characteristics of a black body. Planck's law of radiation describes radiation distribution in a spectrum and must be applied for cases where spectral energy distribution is important, for example daytime radiative cooling. However, data for emissivities in different wavelengths for various materials are not common.

The most complex form of heat transfer is convection that is described with empirical equations. Forced convection for surfaces with common shape can be described quite well using these equations; however, natural or free convection for non-ideal cases is very challenging to model. Therefore, a combined convective and radiant heat transfer coefficient is used to describe the cooling panel studied in this thesis.

## 7 METHODOLOGY

The experimental part of this thesis focuses on the development and experimental verification of an equation based simulation model for a PCM cooling panel - a stainless steel container filled with PCM and an integrated hydronic circuit. This PCM panel was previously developed in the scope of a research project *No.1.1.1.1/16/A/007 “A New Concept for Sustainable and Nearly Zero-Energy Buildings”*.

The developed model may further be used for faster, simpler, more accurate energy modelling and sizing of heating, ventilation and air conditioning systems.

There are four main objectives of this study:

- To indirectly measure the heat loss coefficient of the experimental chamber at thermal equilibrium conditions using the temperature measurements inside the chamber, temperature measurements of the surrounding environment and measurements of the thermal energy supplied inside the chamber;
- To perform a series of experiments with PCM panels in a test chamber using variable internal heat gains for a case without a cooling panel and a case with a cooling panel that is connected to a cooling water flow;
- To validate the developed PCM cooling panel simulation model using *IDA ICE 4.8* [146,147] simulation software and measurements from the test chamber;
- To perform a comparative simulation study using the validated simulation model of the PCM panel and compare it with the results obtained in a previous CFD simulation study carried out by Rucevskis et al. [141,142].

### 7.1 Experimental set-up

#### Experimental test chamber

To carry out laboratory tests, an experimental chamber was constructed for this experiment (Figure 7.1). The internal dimensions of the chamber are 1.93 m × 0.79 m × 1.52 m (length × width × height). The envelope composition of the chamber is described in Table 7.1.

However, the envelope of the chamber is not homogenous and contains thermal bridges; thus, the heat loss coefficient could not be calculated with reasonable precision and had to be measured.

The heat loss coefficient was indirectly measured by inserting a heat source with a heating capacity of 90.1 W inside the chamber. The temperatures inside and outside of the chamber were measured. When a thermal equilibrium was reached (Figure 7.2) the heat loss coefficient (W/K) of the chamber was calculated using the temperature difference between the inside and outside of the chamber and the power of the heat source (refer to Equation (7.1)). The calculated heat loss coefficient of the chamber was  $H_t = 8.06$  W/K.

$$H_t = \frac{P_h}{(T_c - T_s)}, \quad (7.1)$$

where  $H_t$  – heat loss coefficient (EN ISO 13790 [148]), W/K;  
 $P_h$  – power of the heat source, W;  
 $T_c$  – temperature inside the chamber, K;  
 $T_s$  – temperature of the surrounding environment, K.

The chamber was equipped with eight temperature/humidity (see Figure 7.1) probes at various locations of the chamber:

- T1—Surface temperature sensor on the upper face of the panel;
- T2—Surface temperature sensor on the lower face of the panel;
- TH3—Air temperature and humidity sensor outside the chamber;
- T4—Surface temperature sensor for the supply pipe of the panel;
- T5—Surface temperature sensor for the return pipe of the panel;
- TH6—Air temperature and humidity sensor in the middle part of the chamber;
- TH7—Air temperature and humidity sensor in the lower part of the chamber;
- TH8—Air temperature and humidity sensor in the upper part of the chamber.

The accuracy for temperature sensors was  $\pm 0.5$  °C in range from  $-30$  °C to  $90$  °C, the accuracy for humidity sensors were  $\pm 2$  % ranging from  $5$  % to  $95$  %.

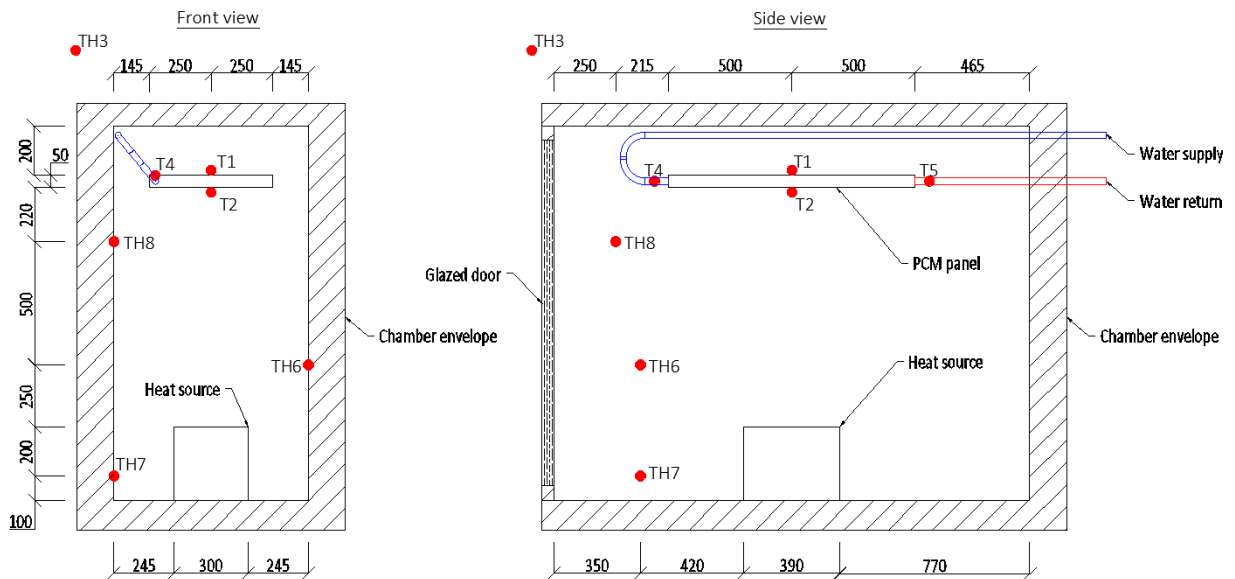


Figure 7.1 Test chamber used for the study

Table 7.1

## Envelope composition of the test chamber

Material	Thickness, mm	Density, kg/m <sup>3</sup>	Specific heat capacity, kJ/kg	Heat conductivity, W/m·K
Side walls of the chamber (arranged from inside to outside)				
Wood chip board	12	700	1700	0.180
Wooden studs with mineral wool insulation;	100	92	2010	0.085
Plywood board	12	1000	1300	0.250
Front and back walls of the chamber (arranged from inside to outside)				
Plywood board	12	1000	1300	0.250
Wooden studs with mineral wool insulation;	100	92	2010	0.085
Plywood board	12	1000	1300	0.250
Roof of the chamber (arranged from inside to outside):				
Plywood board	12	1000	1300	0.250
Expanded polystyrene insulation	50	20	1200	0.041
Gypsum board	13	970	1090	0.220
Floor of the chamber (arranged from inside to outside):				
Gypsum board	13	970	1090	0.220
Expanded polystyrene insulation	50	20	1200	0.041
Plywood board	12	1000	1300	0.250
Glazed door				
Glazing	-	-	-	1.100
Frame (37 % of door area)	-	-	-	3.000

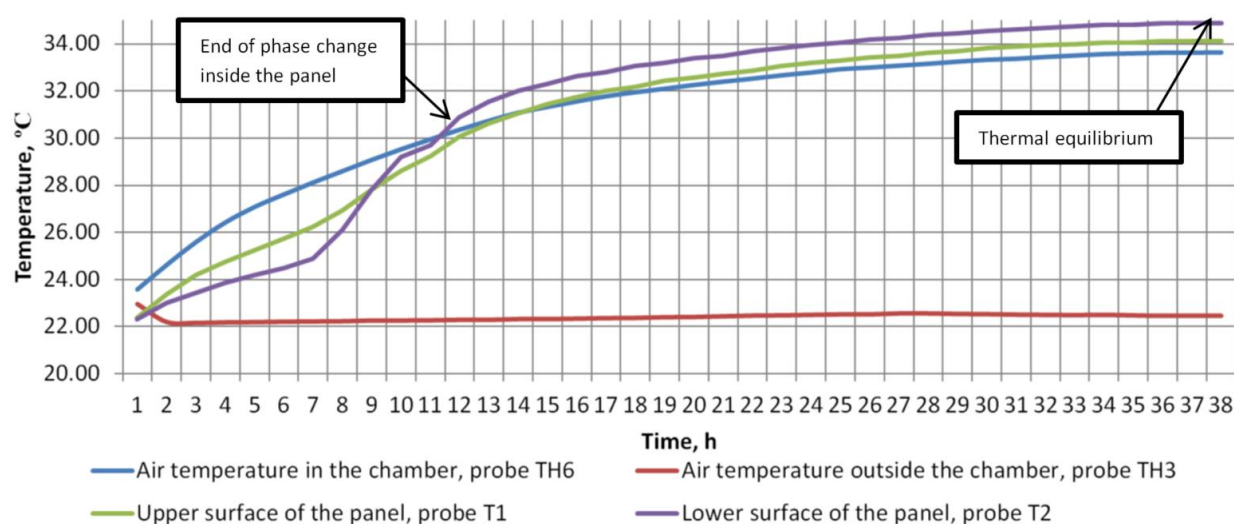


Figure 7.2 Temperatures inside the chamber when heated with 90.1 W heat source

The test chamber was located inside a laboratory room, but, unfortunately, due to technical limitations the indoor temperature of the room could not be controlled. The room temperature changed over time due to solar radiation and other factors. However, the room

temperature was measured during the experiments and later accounted for in the simulation model.

### **The cooling panel**

The cooling panel consists of a stainless-steel container with internal hydronic circuit (Figure 7.3). 80 % of panel volume was filled with *RUBITHERM*® *RT22HC* [149] phase change material. According to the technical properties provided by the manufacturer, the heat storage capacity of the PCM is 190 kJ/kg in the temperature range from 14 to 29 °C, which in theory would provide the panel a heat storage capacity of approximately 1.48 kWh/m<sup>2</sup> panel area. However, the operational temperature range of the panel typically ranges from 19 to 24 °C. That ensures a useful heat storage capacity of the PCM only 140 kJ/kg and the heat storage capacity of 1.09 kWh/m<sup>2</sup> panel area. At the beginning of each experiment, the PCM can be considered at a solid state (below the temperature of a peak partial phase-change enthalpy).

Since the commercial PCM brand used is a mixture of different paraffin based phase change materials, the phase change does not happen at one constant temperature but rather at a certain temperature range.

Moreover, according to the manufacturer's data [149] there is an inconsistency because the total phase change enthalpy over the phase change range (14 to 29 °C) is different for melting (208 kJ/kg·K) and solidification (197 kJ/kg·K). The partial enthalpies used for the simulation model were slightly adjusted for numerical reasons to have the same phase change enthalpy for both melting and solidification. The measured data provided by the manufacturer and the corrected data used for the simulation model can be observed in Figure 7.4.

It is important to note that, during the measurement of  $H_t$  value, the upper and lower surfaces had a different temperature trend (Figure 7.2). It can be explained by the fact that the panel is only 80 % filled with PCM. In the lower surface, the PCM has a direct contact with the panel wall; however, in the upper part of the panel there is an air gap between the steel wall and the PCM that reduces heat transfer. The small temperature differences between chamber temperature, upper surface, and lower surface temperatures after thermal equilibrium is reached, can be attributed to a measurement error, thermal stratification, radiative heat transfer and local effects due to the sensor placement.

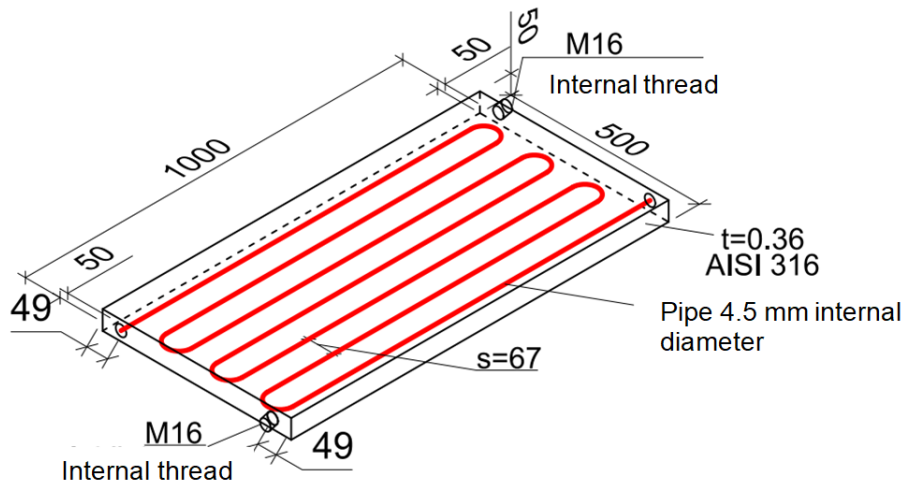


Figure 7.3 Cooling panel (dimensions in mm)

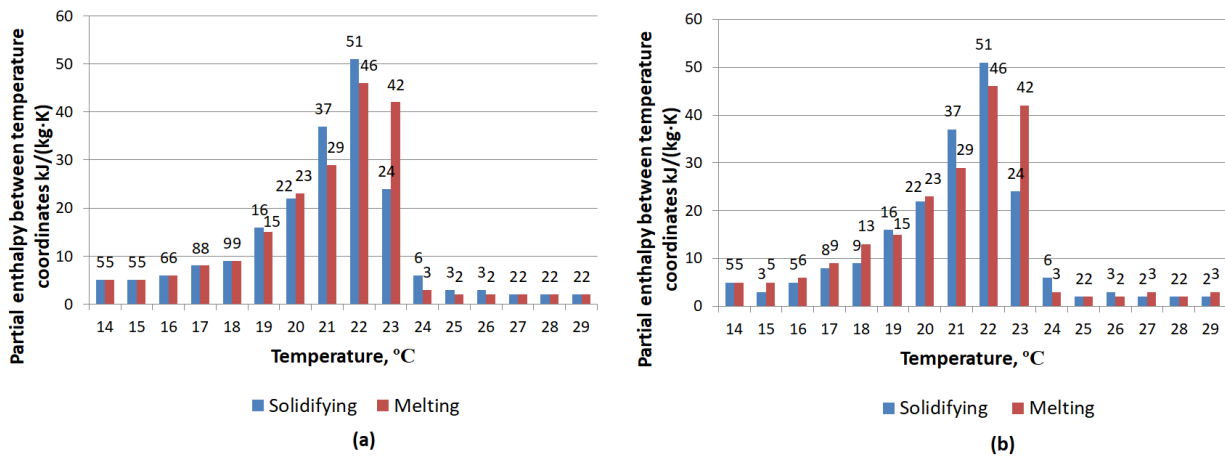


Figure 7.4 Adjusted (a) and measured (b) partial enthalpy model of the PCM

The cooling panel has an internal hydronic circuit that consisted of stainless steel pipes with 4.5 mm internal diameter and 67 mm gap between pipes. The hydronic circuit was connected to an external cooling source and the water flow was set to 0.80 l/min. The feed-water temperature changed over time and the temperature was measured with surface temperature sensors (T4 and T5) and was accounted for in the simulation.

### Simulated heat gains

A heat source was introduced to simulate the performance of the cooling panel. The heat source that consisted of five light bulbs with different heating capacities was turned on and off in different combinations with timers for 15 minute steps to approximate a typical heat gain distribution for a 24 hour cycle. The hourly average heat gains are visualized in Figure 7.5.

To avoid a direct short wave radiant heat transfer from the heat sources to the cooling panel, the heat source was covered with a cardboard box (Figure 7.6). In order to estimate the ratio of a long wave radiation to a convective heat exchange between the heat source and the chamber the temperature of internal surfaces and the surfaces of the heat source were

measured. Using the Stefan–Boltzmann law for net radiation heat loss (see Equation (3.3)) it was estimated that approximately 20 % of heat exchange is radiant. It was assumed that the remaining 80 % is the convective heat exchange - this was later accounted for in the simulation model.

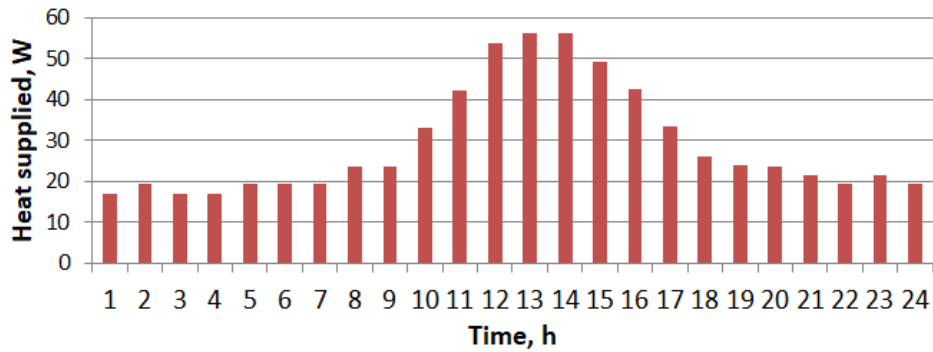


Figure 7.5 Heat supply schedule



Figure 7.6 Heat source

### Simulation model for validation

A simulation model of the experimental system (test chamber and the surrounding room) was developed in *IDA ICE 4.8*.

*IDA ICE* is a commercial dynamic equation based simulation tool that has been validated according to the majority of the industry standards:

- *ANSI/ASHRAE* Standard 140-2004 [150];
- *CEN* Standards EN 15255-2007 [151] and EN 15265-2007 [152];
- *CEN* Standard EN 13791 [153];
- *International Energy Agency* SHC Task 34 [154];
- *Technical Memorandum* 33 [155].

*IDA ICE* is used to create multi-zone equation based simulators using models written in *Modelica* [147,156] and *NMF* [157]. *IDA ICE* uses a variable timestep solver that automatically adjusts simulation timesteps, optimizing accuracy and speed [147].

The geometrical dimensions and envelope parameters in the simulation were modelled as close as reasonably possible to the actual chamber. The measured heat loss coefficient  $H_t$  was used to fine-tune envelope U-values of the simulated test chamber. During the simulation runs, the temperature of the surrounding environment in the simulation model was kept the same as the measured surrounding room temperature during the experiments. Only the radiant heat exchange between the surroundings and the chamber could not be precisely modelled because the surface temperatures and the short and long wave radiation sources (windows) were not measured during the experiments. Similarly, the cooling water temperature was also controlled according to the values measured with probes T4 and T5.

The cooling panel was modelled as a hydronic circuit thermally connected to PCM layers and container wall which was then exposed to the simulated zone with combined radiant and convective heat transfer coefficients. Graphical representation of the PCM panel simulation model can be observed in Figure 7.7.

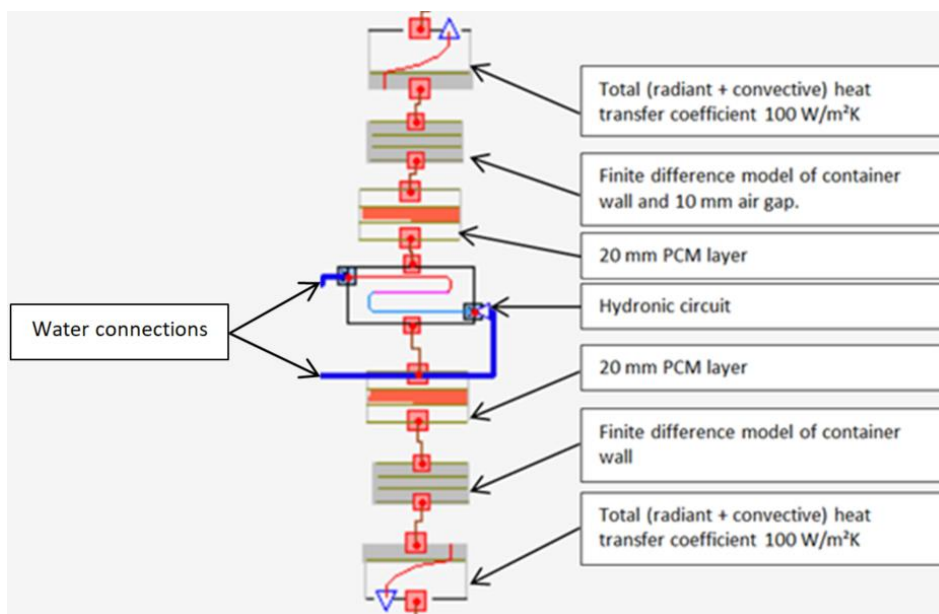


Figure 7.7 *IDA ICE* model of the PCM cooling panel

### Total heat transfer coefficients

Total or combined radiant and convective heat transfer coefficients were adjusted during the model validation to  $100 \text{ W/m}^2\cdot\text{K}$  (a relatively high value for natural convection). However, these coefficients did not significantly influence the heat transfer from the hydronic circuit as it is mostly dependent on the relatively low heat conductivity of the PCM material ( $\lambda = 0.2 \text{ W/m}\cdot\text{K}$  as claimed by the PCM manufacturer [149]). Furthermore, the area of the lower face of the panel was increased from  $0.5 \text{ m}^2$  to  $0.65 \text{ m}^2$  in order to account for the full surface area of the panel including the small side walls.

The combined radiant and convective heat transfer is modelled using Equation (7.2).

$$0 = Q + A_{surf} \cdot h_{surf} \cdot (T_{Air} - T_{surf}), \quad (7.2)$$

where  $Q$  – is the heat transfer (heat flow), W;

$A_{surf}$  – area of the exposed surface, m<sup>2</sup>;

$h_{surf}$  – total (radiant + convective) heat transfer coefficient, W/m<sup>2</sup>·K;

$T_{Air}$  – air temperature inside the chamber, K;

$T_{surf}$  – temperature of the heat exchange surface, K.

### Container walls and fixed air gap

Lower and upper wall with the fixed air layer of the container was modelled with a finite difference model [157,158] of multi-layer components with four cells for each layer. The principle of the model applied is illustrated in Figure 7.8.

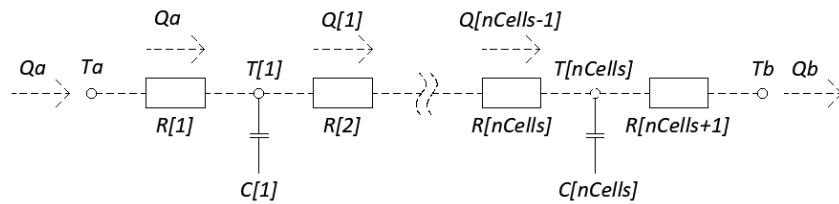


Figure 7.8 Finite difference model

The boundary heat flux is calculated with Equation (7.3) and Equation (7.4).

$$Q_a = A \cdot (T_a - T[1])/R[1], \quad (7.3)$$

where  $Q_a$  – heat flux at surface “a”, W;

$A$  – surface area, m<sup>2</sup>;

$T_a$  – temperature at surface “a”, K;

$T[1]$  – temperature between the first and second cell, K;

$R[1]$  – thermal resistance of the first cell, m<sup>2</sup>·K/W.

$$Q_b = A \cdot (T[nCells] - T_b)/R[nCells + 1], \quad (7.4)$$

where  $Q_b$  –heat flux at surface “b”, W;

$T[nCells]$  – the temperature between the last two cells, K;

$T_b$  – temperature at surface “b”, K;

$R[nCells + 1]$ – is the thermal resistance of the last cell in the network, m<sup>2</sup>·K/W.

Heat flux between boundaries is calculated with Equation (7.5).

$$Q[i] = A \cdot (T[i] - T[i + 1])/R[i + 1], \quad (7.5)$$

where  $Q[i]$  – heat flux between two cells  $i$  and  $i + 1$ , W;  
 $T[i]$  – temperature between cells  $i$  and  $i + 1$ , K;  
 $T[i + 1]$  – temperature between cells  $i + 1$  and  $i + 2$ , K;  
 $R[i + 1]$  – thermal resistance of cell  $i + 1$ ,  $m^2 \cdot K/W$ .

### PCM layer

The PCM layer was modelled by applying a mathematical model of different temperature - enthalpy relations during melting and solidification to consider the effect of hysteresis (the principle is illustrated in Figure 7.9). The model consists of 16 partial material enthalpies between temperature coordinates for a temperature range from 14 to 29 °C, which is consistent with thermal properties of *RUBITHERM© RT22HC* [149] phase change material.

If the layer temperature is below or above the phase transition temperature range then specific heat capacity of the PCM is used. In this range the panel acts as sensible heat storage. If the temperature is within the phase transition range partial enthalpies between temperature coordinates is used by the solver. Inside the phase transition temperature range also hysteresis is applied, thus the partial enthalpy is different for each temperature coordinate depending on the direction of temperature change in time. If the layer temperature is inside the hysteresis loop and the process switches from solidification to melting and vice versa specific heat capacity is applied.

Partial enthalpy measurement data given by the manufacturer [149] has a measurement inconsistency because the total phase change enthalpy over the phase change range (14 to 29 °C) is different for melting (208 kJ/kg·K) and solidification (197 kJ/kg·K). The partial enthalpies used for the simulation model were slightly adjusted to have the same phase change enthalpy for both melting and solidification. The measured data provided by the manufacturer and the corrected data used for the simulation model can be observed in Figure 7.4.

The heat conductivity of the PCM material was assumed to be constant (according to the manufacturer's data  $\lambda = 0.2$  W/m·K) for both liquid and solid state. Potential internal buoyancy flows in the liquid PCM as well as volumetric changes during phase transition were not modelled or accounted for.

The principle of PCM model is illustrated in Figure 7.10.

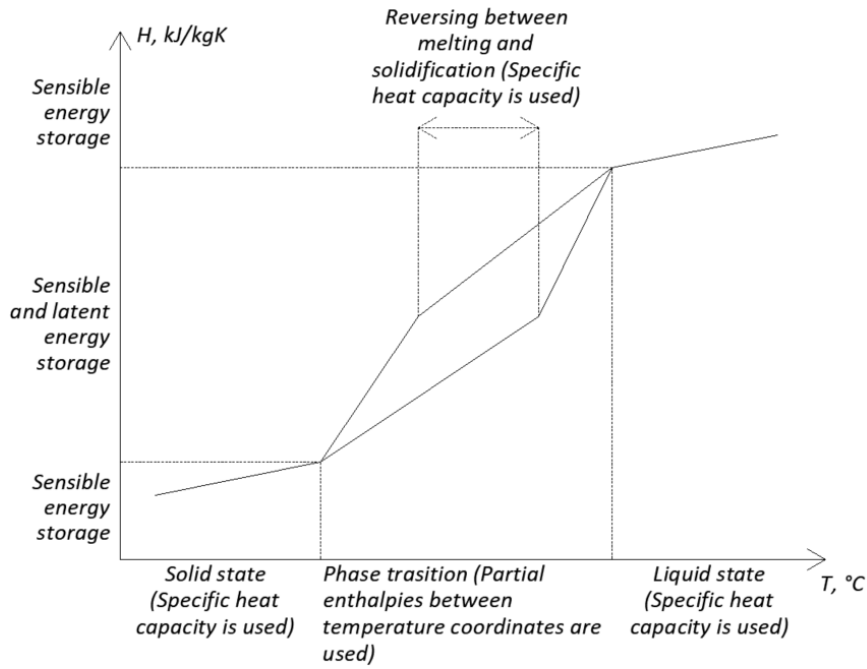


Figure 7.9 Principle of PCM phase transition hysteresis modelled

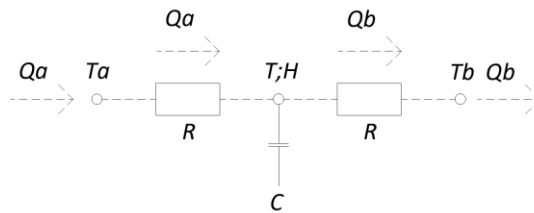


Figure 7.10 Illustration of PCM mathematical model

The total heat flux to or from PCM layer is calculated with Equation (7.6).

$$Q = Q_a + Q_b, \quad (7.6)$$

where  $Q$  – the total heat flux to or from PCM layer, W;

$Q_a$  – heat flux at surface “a”, W;

$Q_b$  – heat flux at surface “b”, W.

The change of enthalpy over time is calculated with Equation (7.7).

$$H' = \frac{Q}{m}, \quad (7.7)$$

where  $H'$  – increase of enthalpy over time, J/kg;

$m$  – mass of the layer, kg.

The heat fluxes at surfaces “a” and “b” are calculated with Equations (7.8) and (7.9).

$$Q_a = A \cdot \frac{T_{pa} - T}{R}, \quad (7.8)$$

where  $Q_a$  – heat flux to surface “a”, W;  
 $A$  – layer area, m<sup>2</sup>;  
 $T_{pa}$  – temperature at surface “a”, K;  
 $T$  – layer temperature (at the centre node), K;  
 $R$  – thermal resistance from surface to node, m<sup>2</sup>·K/W.

$$Q_b = A \cdot \frac{T_{pb} - T}{R}, \quad (7.9)$$

where  $Q_b$  – heat flux to surface “b”, W;  
 $T_{pb}$  – temperature at surface “b”, K.

Temperature of the PCM layer for solid and liquid state is calculated with Equations (7.10) and (7.11).

$$T = \frac{H - H_{m[1]}}{c} + T_{h[1]}, \quad (7.10)$$

where  $H$  – enthalpy of the PCM substance, J/kg;  
 $H_{m[1]}$  – enthalpy coordinate at the first point defined in the partial enthalpy-temperature coordinate model, J/kg;  
 $c$  – specific heat capacity, J/kg·K;  
 $T_{h[1]}$  – temperature coordinate at the first point defined in the partial enthalpy-temperature coordinate model, K.

$$T = \frac{H - H_{m[N]}}{c} + T_{h[N]}, \quad (7.11)$$

where  $H_{m[N]}$  – enthalpy coordinate at the last point defined in the partial enthalpy-temperature coordinate model, J/kg;  
 $T_{h[N]}$  – temperature coordinate at the last point defined in the partial enthalpy-temperature coordinate model, K.

During melting and solidification of the PCM layer, temperature  $T$  is computed by the solver using temperature coordinates and change of enthalpy over time.

### Hydronic circuit

The hydronic circuit in the model was approximated as a layer that delivers cooling energy to PCM material based on a heat transfer coefficient and temperature difference. Heat transfer coefficient fluid to PCM material was calculated with the *U-NORM 2012-2* software (developed by Gunnar Anderlind).

*U-NORM* is an interface for the *DAVID-32* program [159] that uses the finite difference model to calculate the heat flow and temperature distribution for two-dimensional and three-dimensional cases based on the energy balance.

The calculation procedure and the pipe circuit approximation to a layer was performed according to the methodology described in EN 15377-1 [160]. *U-NORM* software was used to calculate the extra thermal resistance between average water temperature inside the circuit and the average temperature of the heat conducting layer—the  $R_t$  value. The relative temperature distribution and calculation principle is visualised in Figure 7.11 where  $T_v$  is the average water temperature in a hydronic circuit,  $R_t$  is the additional thermal resistance for approximating piping circuit to a fictive surface,  $T_c$  is the average temperature for the heating or cooling layer,  $T_1$   $T_2$  and  $R_1$   $R_2$  are the surface temperatures and layer thermal resistances that are calculated by *IDA ICE* solver using the PCM mathematical model and finite difference models. The calculated heat transfer coefficient is  $1/R_t = 11.8 \text{ W/m}^2 \cdot \text{K}$ . Input data of the calculation can be found in Table 7.2.

Table 7.2

Input data used for the calculation of  $R_t$

Parameter	Description
Liquid inside the circuit	Pure water
Flow conditions inside the circuit	Turbulent
Convective heat transfer coefficient Water-pipe wall	500 $\text{W/m}^2 \cdot \text{K}$
Heat conductivity of pipe wall	50 $\text{W/m} \cdot \text{K}$
Heat conductivity PCM	0.2 $\text{W/m} \cdot \text{K}$

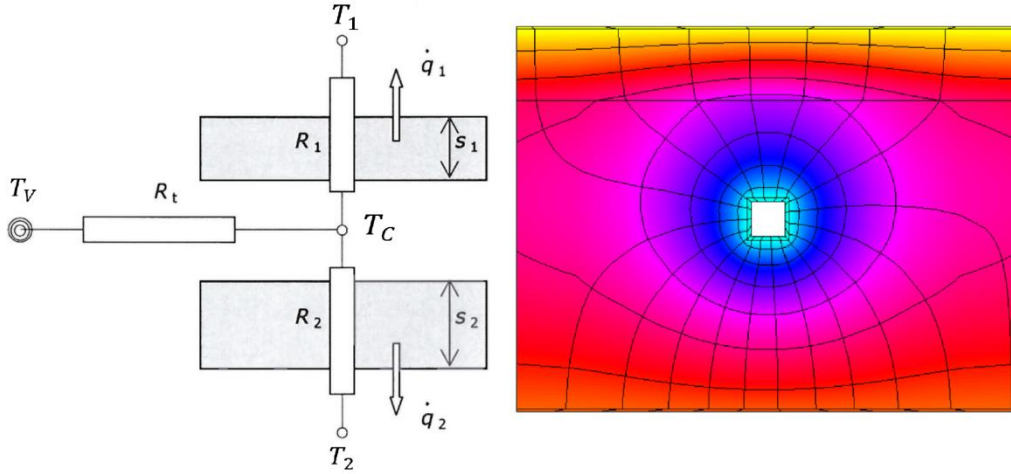


Figure 7.11 Resistance network in embedded water based surface heating and cooling systems [160] and relative temperature distribution in the PCM panel

Heat exchange between the hydronic circuit and other panel layers is governed with following equations. First mass flow coefficient  $M_{coef}$  is established (Equation (7.12)).

$$M_{coef} = \frac{1 \cdot A}{R_t \cdot c}, \quad (7.12)$$

where  $M_{coef}$  – mass flow coefficient, kg/s;

$A$  – area of the layer, m<sup>2</sup>;

$R_t$  – extra thermal resistance (according to nomenclature of EN 15377-1), m<sup>2</sup>·K/W;

$c$  – heat capacity of the heat transfer media (water), J/kg·K.

Circuit outlet water temperature  $T_{out}$  is calculated with Equation (7.13).

$$T_{out} = T_{Slab} + (T_{in} - T_{Slab}) \cdot e^{\left(\frac{M_{coef}}{M_{Liq}}\right)}, \quad (7.13)$$

where  $T_{out}$  – Circuit outlet water temperature, K;

$T_{Slab}$  – temperature of the heated or cooled layer, K;

$T_{in}$  – inlet water temperature, K;

$M_{Liq}$  – water mass flow in the circuit, kg/s.

The heat  $Q$  added to the layer is calculated with Equation (7.14).

$$Q = M_{Liq} \cdot c \cdot (T_{in} - T_{out}), \quad (7.14)$$

where  $Q$  – Heat added to the layer, W.

## 7.2 Simulation model for performance modelling

In order to model the PCM cooling panel performance for more realistic cooling application, it was decided to replicate a simulation model set-up from the previous study that was conducted by Rucevskis et al. [141,142].

This particular study was chosen because of a very similar type of the PCM cooling panel used and the same PCM material. Rucevskis et al. [141,142] performed the simulation using CFD (*Fluent*) and used a PCM panel with 25 mm thickness. The general simulation set-up used by Rucevskis et al. [141,142] is represented in Figure 7.12. As external boundary conditions the team used outdoor air temperature and solar radiation for a typical eight day summer period in Riga, Latvia. The input data for the outdoor air temperature and solar radiation is reflected in Figure 7.13. Envelope composition of the model simulated by Rucevskis et al. [141,142] is also demonstrated in Table 7.3.

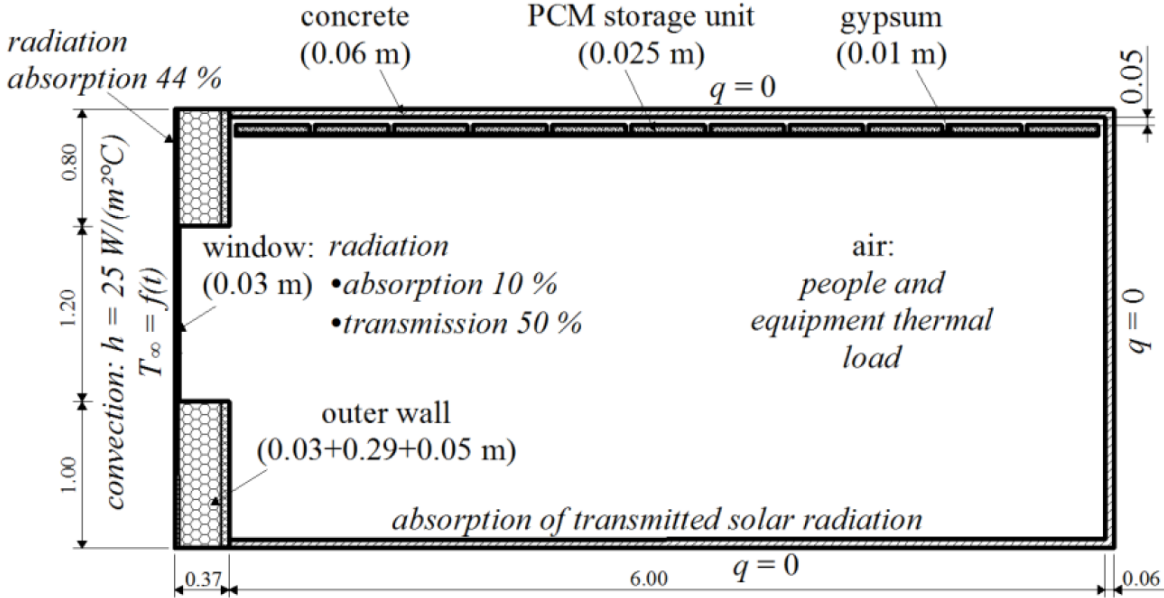


Figure 7.12 Simulation set-up used by Rucevskis et al. [141,142]

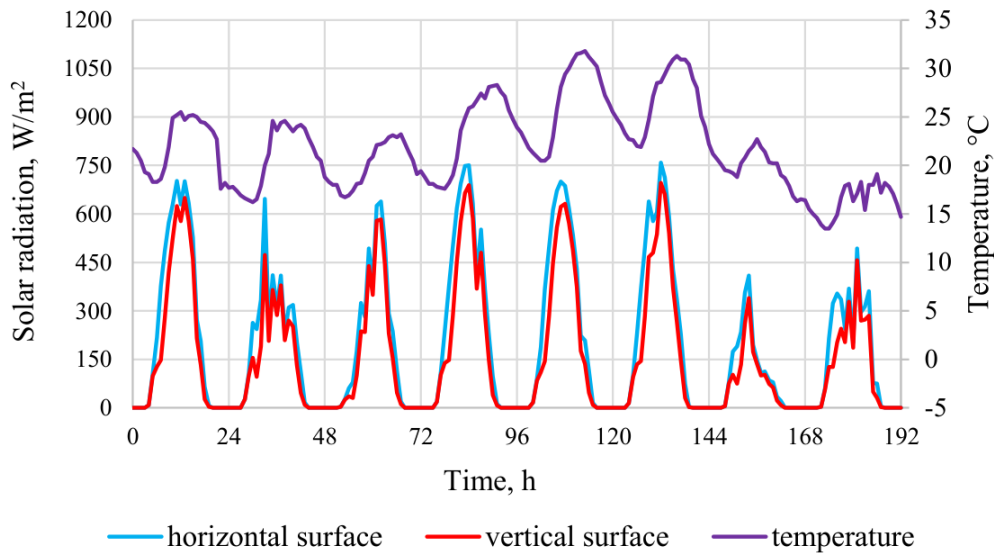


Figure 7.13 Outdoor air temperatures and solar radiation used by Rucevskis et al. [141,142]

Table 7.3

Envelope composition of the model simulated by Rucevskis et al. [141,142]

Structure	Material	Density, kg/m <sup>3</sup>	Specific Heat, J/(kg·°C)	Thermal Conductivity, W/(m·°C)
Inner wall and slabs	Concrete	2322	850	1.7
External wall	Outer layer (30 mm)	452.2	1650	0.112
	Middle layer (290 mm)	210.1	1250	0.062
	Inner layer (30 mm)	332.5	1450	0.077
Window	U-value = 1.9 W/m <sup>2</sup> K (g-value = 0.6)			
Finishing layer of the ceiling	Gypsum	800	950	0.15

A simulation model with equivalent input data was generated in *IDA ICE*. The PCM cooling panel thickness was decreased to 25 mm (the same as was used by Rucevskis et al. [141,142]).

The previous CFD study considered the simulation setup a two-dimensional problem and simulated it accordingly as a two-dimensional simulation model to reduce computational complexity. In this case the model does not consider the thermal properties of the walls on both sides. In theory this CFD model represents an infinitely long room.

In order to replicate this assumption in the *IDA ICE* model, the thermal effect (thermal mass) generated by the side walls had to be minimized. It was assumed that if the area of the side walls was made relatively small compared with the area of rest of the surfaces (external wall, window, back wall, ceiling, and floor) the effect generated by the presence of these walls in the simulation model would be negligible and a room with dimensions 6.00 m × 3.00 m × 60.00 m (width × height × length) was used for simulations in the *IDA ICE*.

## 8 RESULTS AND DISCUSSION

### 8.1 Verification of the simulation model

#### Statistical analyses of experimental results

In order to evaluate the agreement between measured values and results produced by the numerical model following metrics were used:

- maximum deviation between measured and simulated values;
- average deviation between measured and simulated values over the simulated time period;
- Pearson correlation coefficient;
- root mean square error (RMSE).

The maximum deviation between measured and simulated values was calculated with Equation (8.1).

$$D_{max} = |x_{Smax} - x_{Mmax}|, \quad (8.1)$$

where  $D_{max}$  – maximum deviation between measured and simulated values;

$x_{Smax}$  – simulated value at the point of the maximum deviation;

$x_{Mmax}$  – measured value at the point of the maximum deviation.

Average deviation between measured and simulated values over the simulated time period was calculated with Equation (8.2).

$$D_{avg} = \left| \frac{\Sigma x_S - \Sigma x_M}{n} \right|, \quad (8.2)$$

where  $D_{avg}$  – average deviation between measured and simulated values over the simulated time period;

$\Sigma x_S$  – sum of all hourly simulated values;

$\Sigma x_M$  – sum of all hourly measured values;

$n$  – number of measurements/simulated values.

Pearson correlation coefficient was calculated with Equation (8.3).

$$r = \frac{\Sigma(x_S - \bar{x}_S) \cdot (x_M - \bar{x}_M)}{\sqrt{\Sigma(x_S - \bar{x}_S)^2 \cdot \Sigma(x_M - \bar{x}_M)^2}} \quad (8.3)$$

where  $r$  – Pearson correlation coefficient;

$x_S$  – simulated value;

$\bar{x}_S$  – average of all simulated values;

$x_M$  – simulated value;  
 $\overline{x_M}$  – average of all measured values.

Root mean square error (RMSE) was calculated with Equation (8.4).

$$RMSE = \sqrt{\frac{\sum (x_M - x_S)^2}{n}}, \quad (8.4)$$

where  $RMSE$  – root mean square error.

### Simulation model without a PCM cooling panel

After adjusting the heat loss coefficient of the test chamber envelope according to the measured value a simulation was run for seven consecutive days and compared with the measurement data from the same time period. The simulated period was split into 453 timesteps by *IDA ICE* solver that on average provides a length of around 22 min for one timestep. In reality, the timestep is individually adjusted since *IDA ICE* uses a variable timestep solver. In total, 2334 iterations were required to find a solution for all timesteps.

The temperature in the surrounding room in the simulation was kept exactly the same as measured. The simulated temperature inside the chamber corresponded relatively well with the measurements - the maximum deviation between the measured value and the simulated value was less than 1 °C. It is nearly within the uncertainty on the measurement ( $\pm 0.5$  °C). One of the possible explanations for the discrepancy that arose can be the fact that the room where the experiment took place had significant glazing. Moreover, due to technical limitations the radiant temperature and the radiation from the glazed surfaces was not measured and, therefore, could not be accounted for in the simulation model. This would also explain why the first two days the measured and simulated data correspond almost perfectly, but the following days begin to drift apart as demonstrated in the Figure 8.2. This may be due to the fact that during the experiment the first two days were mostly cloudy and the following days were mostly sunny.

Measured and simulated values over the investigated period had a relatively high Pearson correlation coefficient of 0.98 and relatively low root mean square error (RMSE) of 0.53 °C. Additionally, it is visible in Figure 8.2 that the error produced by the *IDA ICE* model is slightly correlated with chamber temperature; however, the correlation is relatively weak ( $R^2 = 0.181$ ).

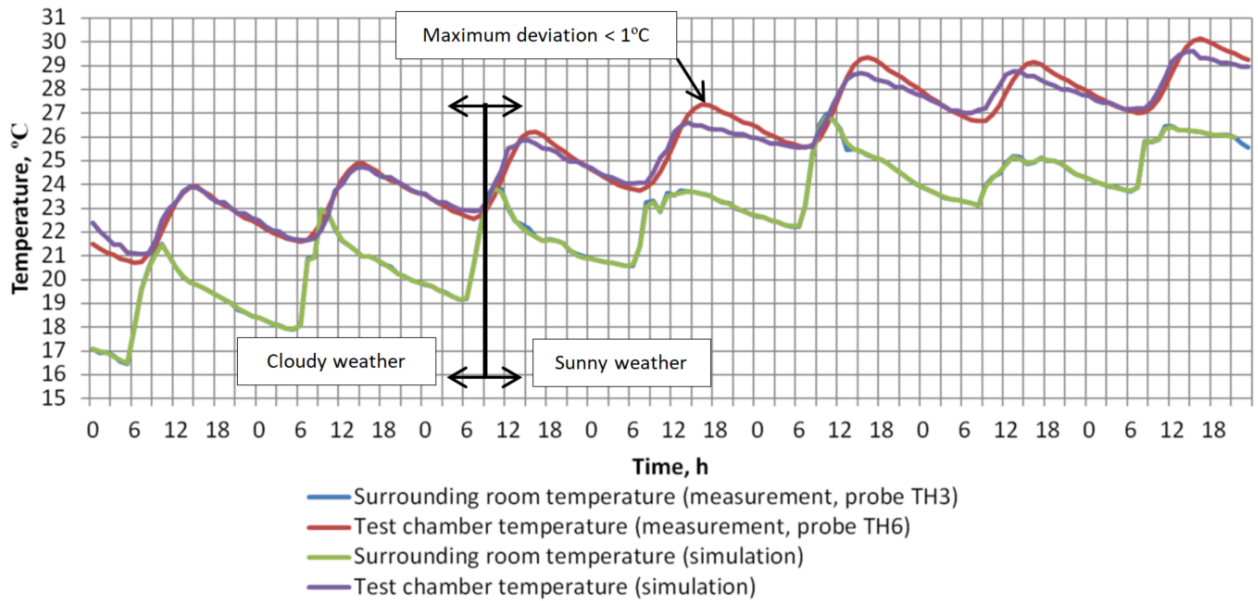


Figure 8.1 Measurements versus simulation-case without a PCM cooling panel

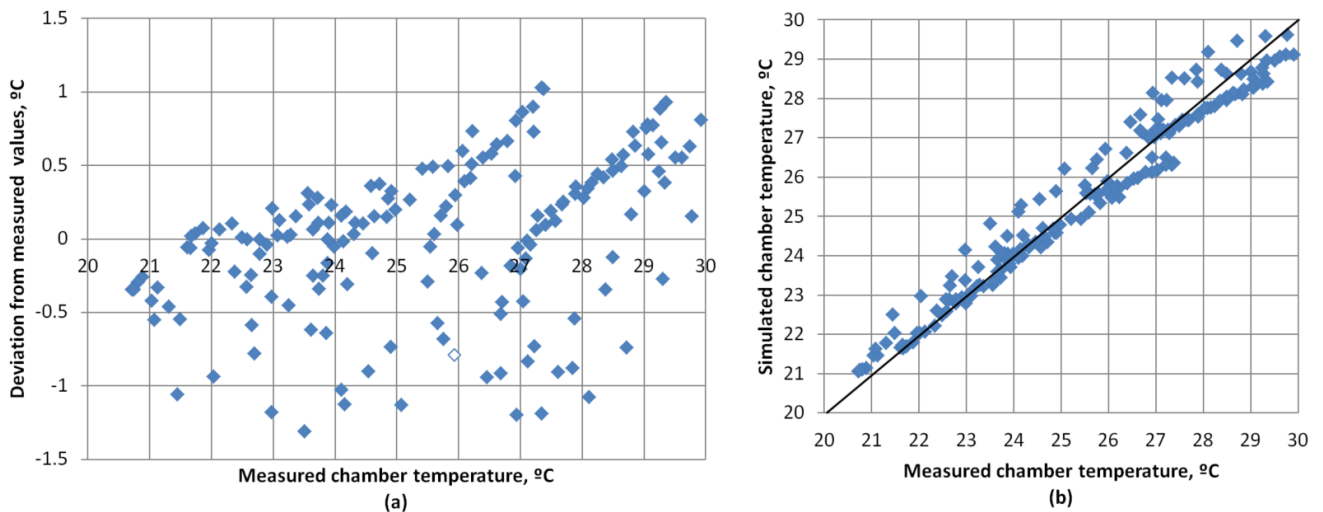


Figure 8.2 Scatter diagrams for measured chamber temperatures (probe TH6) vs. simulated value deviation from measured values (a) and measured chamber temperatures (probe TH6) vs. simulated chamber temperatures (b)

### Simulation model with a PCM cooling panel and a cooling water connection

After making sure that the test chamber envelope model had a reasonable agreement between the simulated and measured values by fine-tuning the chamber  $H_t$  value according to measurements, the PCM panel could be simulated. An 11-day period was chosen for the simulation (Figure 8.3 and Figure 8.4).

The simulated period was split into 687 timesteps by *IDA ICE* solver that on average provides a length of approximately 23 min for one timestep. In reality, the timestep is individually adjusted since *IDA ICE* uses a variable timestep solver. In total, 3323 iterations were required to find a solution for all timesteps. With the introduction of a PCM cooling

panel, the difference between the simulated and measured values increased to a maximum of 2 °C and the RMSE increased to 1.01 °C. This disagreement can partly be explained with the uncertainty of the temperature sensors and the fact that the radiant heat exchange between the test chamber and surrounding room was not properly modelled. However, the simulation model always calculates a higher temperature than actually measured in the test chamber - a phenomena reported also in the previous study performed by Nageler et al. [161]. Thus, in a practical application, the error would give an advantage rather than a disadvantage. However, when average temperatures over the 11-day period were compared the agreement between the measured and simulated data was better. The average temperature in the simulation was 26.4 °C versus 25.2 °C for the measured data, which results in a discrepancy of 1.2 °C.

Measured and simulated values over the investigated time period had a relatively high Pearson correlation coefficient of 0.95. Additionally, it is visible in Figure 8.5 that the error produced by the *IDA ICE* model is practically not correlated with the chamber temperature ( $R^2 = 0.046$ ).

The maximum panel surface temperature deviation from the measured values was approximately 1 °C (Figure 8.5). Nevertheless, the average temperatures over the simulated period had a much better agreement. The average simulated upper panel surface temperature was 25.2 °C and the measured lower panel surface temperature was 24.8 °C, giving a 0.4 °C difference. The average simulated lower panel surface temperature was 23.2 °C and the measured lower panel surface temperature was 23.3 °C, resulting in a 0.1 °C difference. It can be concluded that the simulation model can replicate temperature swings, but the accuracy increases if average temperatures over longer periods of time are compared.

In general, the agreement between simulated and measured values (maximum deviation of 2.0 °C and RMSE of 1.01 °C) is relatively good if compared to similar studies where simulation results of a dynamic simulation software are compared to measured values.

A team from Austria did a validation study [161] for four different dynamic simulation tools including *IDA ICE* and compared the results to measured values. The maximum deviation ranged from ~3.5 °C to ~4.7 °C and RMSE ranged from ~0.5 °C to ~2.5 °C for a yearly simulation carried out with several different simulation tools.

Furthermore, a team from Italy conducted a similar study using *IDA ICE* [162] with two test chambers and a passive PCM thermal storage. When the measured values were compared to simulated values for an eight-day period, the RMSE for the chamber with no PCM storage was 2.50 °C and the RMSE for a chamber with a PCM storage was 1.83 °C.

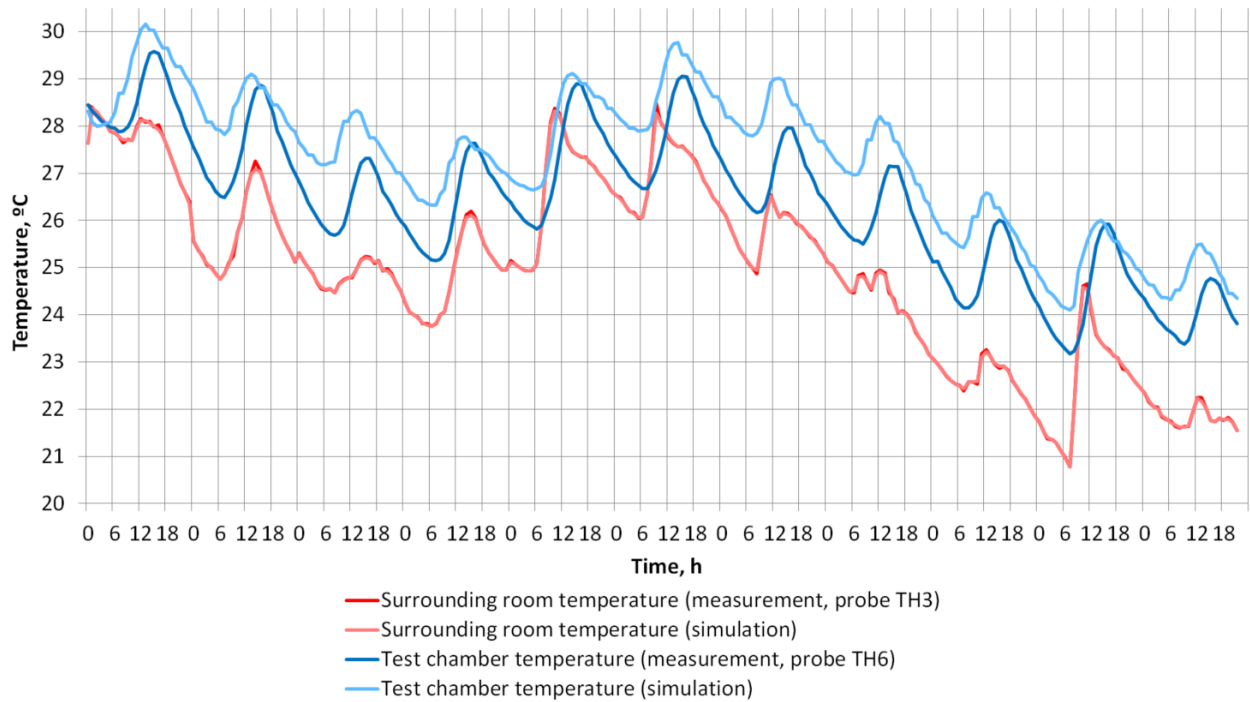


Figure 8.3 Air temperature measurements versus simulation—case with a PCM cooling panel

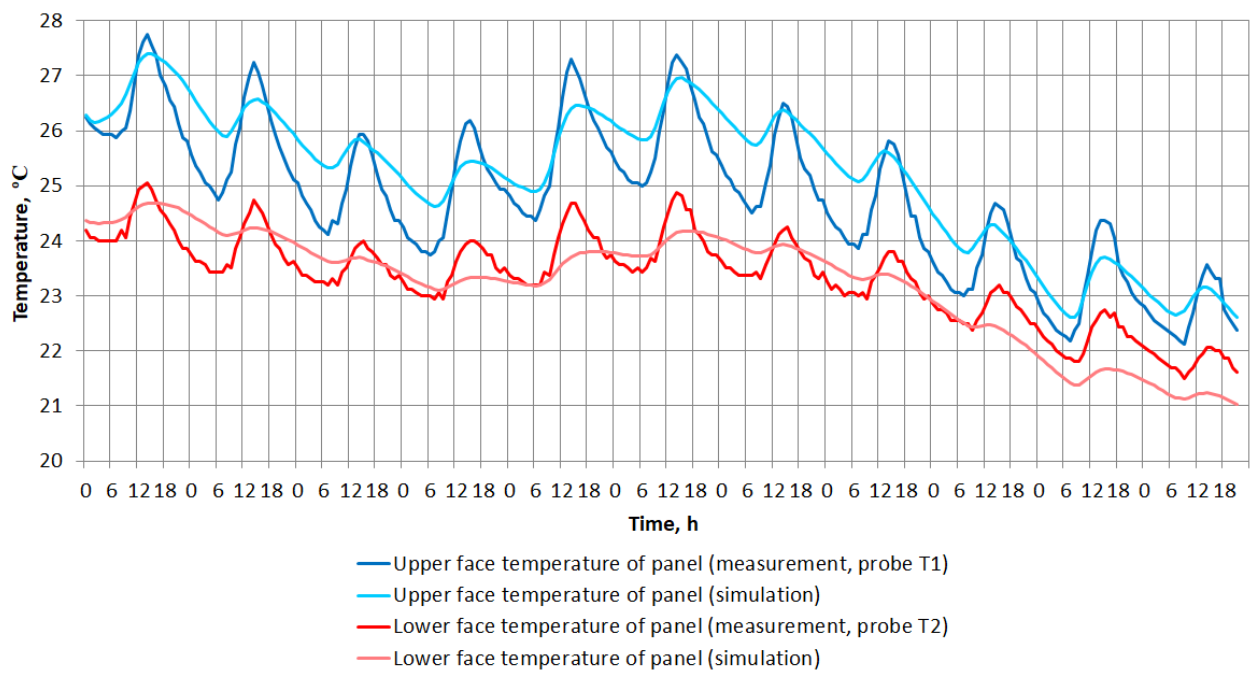


Figure 8.4 Surface temperature measurements versus simulation—case with a PCM cooling panel

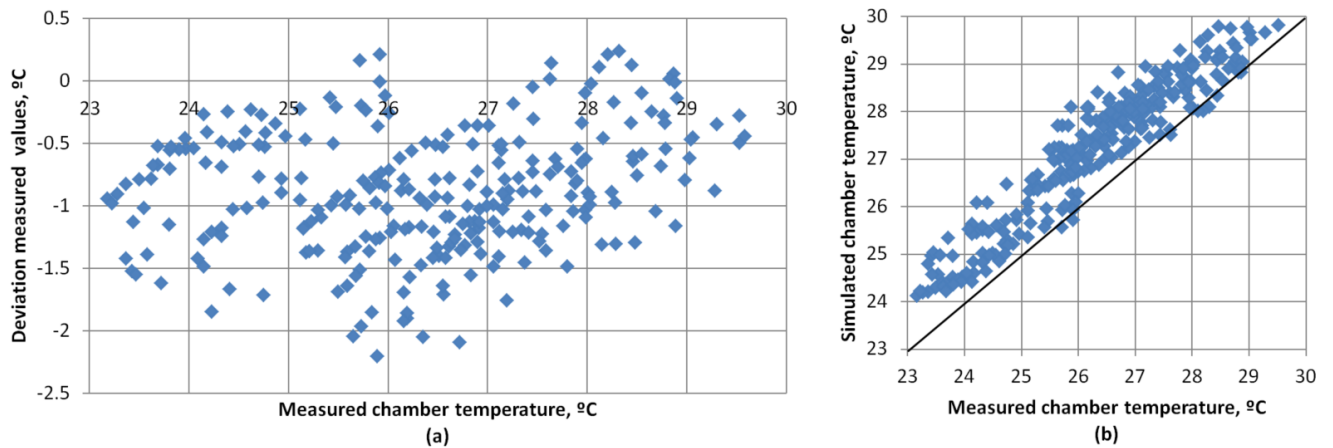


Figure 8.5 Scatter diagrams for measured chamber temperatures (probe TH6) vs. simulated value deviation from measured values (a) and measured chamber temperatures (probe TH6) vs. simulated chamber temperatures (b)

### Performance modelling - comparative Case

Results from both simulations provided very similar results (Figure 8.6). For the case with no cooling panels the maximum room temperature reached in the CFD simulation was 40.8 °C vs. 41.8 °C temperature in the *IDA ICE* simulation. In the case with thermally activated PCM panels, the maximum temperature reached was 30.4 °C in the CFD simulation whereas, in the *IDA ICE* it was 33.0 °C.

When comparing the average temperature over the simulated period the agreement between both studies was more significant. Average temperature for the case with no PCM cooling panels was 32.1 °C for the CFD simulation and 31.5 °C for *IDA ICE* simulation (0.6 °C difference). In the case with the active PCM cooling panels, the average temperature for the CFD simulation was 25.2 °C, and 24.5 °C for the *IDA ICE* simulation (0.7 °C difference). The RMSE when *IDA ICE* simulation was compared to CFD is 1.13 °C for the case with no PCM panel and 1.31 °C for the case with thermally active PCM panel.

Furthermore, in Figure 8.6 and Figure 8.7, it can be observed that, if compared with the CFD simulation, *IDA ICE* simulator overestimates the room temperature for higher temperature periods (daytime) and underestimates room temperature for cooler periods (nights). It can be concluded that *IDA ICE* and the CFD simulation demonstrate slightly different predictions regarding the magnitude of the temperature swings but provides better agreement regarding average temperatures.

Moreover, in a previous study [161] it was observed that overestimation of peak temperatures is a common phenomenon for various dynamic simulation tools. The reached agreement between CFD simulation and dynamic simulation in *IDA ICE* is similar as reported in other studies [161].

The difference of simulated results in *IDA ICE* and CFD for average temperatures is insignificant (less than 1 °C) and it can be considered negligible for annual energy simulations. However, the disagreement for peak values can reach approximately 2.5 °C, but

in this case the simulation model is slightly overestimating the peak temperature so the model can be used reliably also for the peak load calculations.

The developed simulation model is less accurate than the CFD simulation model; however, currently CFD simulations require significant computing power that limits their practical application for large scale simulation studies (cooling capacity and energy calculation for whole building) in construction industry. On the other hand, dynamic equation based simulation tools allow to perform these tasks relatively fast but with loss of accuracy. For comparison using a standard computer, the 192 hour long CFD simulation case performed by Rucevskis et al. [141,142] required around 150 hours to compute (even for a simplified two-dimensional case). However, the same simulation case with *IDA ICE* and similar computer took around 45 seconds.

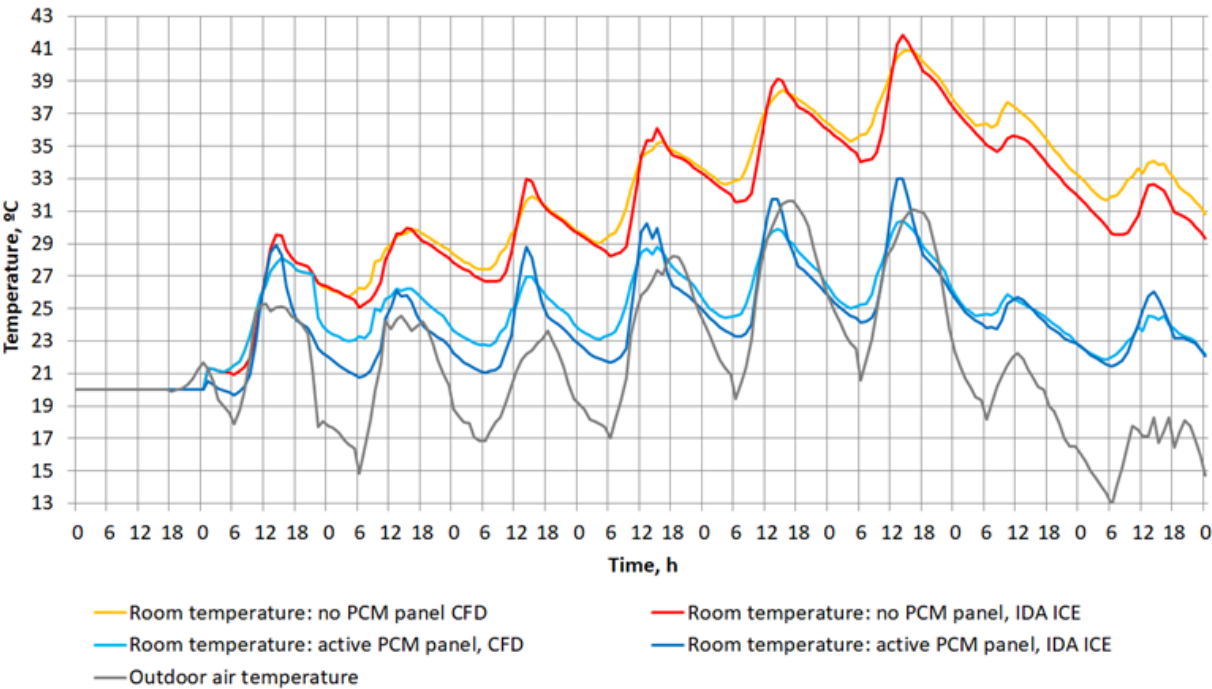


Figure 8.6 Comparison of predicted room temperatures in *IDA ICE* and CFD simulations

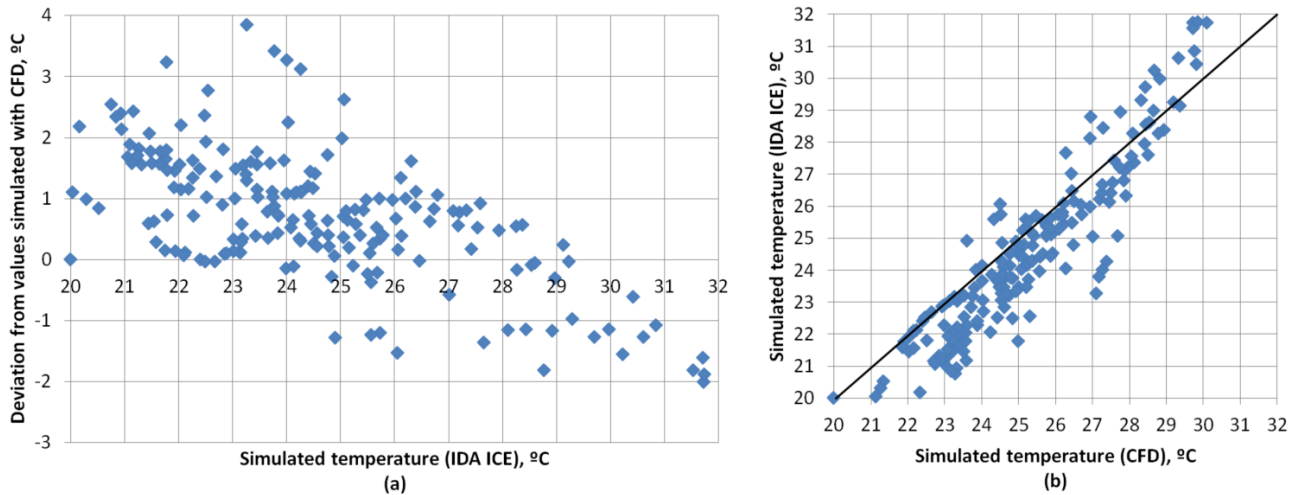


Figure 8.7 Scatter diagrams for room temperatures with active PCM panel simulated with *IDA ICE* vs. deviation from values simulated with CFD (a) and room temperatures simulated with *IDA ICE* vs. room temperatures simulated with CFD (b)

## 8.2 Summary of the results

Altogether four cases were simulated:

- simulated values against measurements – case without a PCM panel;
- simulated values against measurements – case with a PCM panel;
- simulation model against previous CFD study – case without a PCM panel;
- simulation model against previous CFD study – case with a PCM panel.

The first simulation of the test chamber without a PCM cooling panel was performed to confirm that in general the chamber in the simulation software is a valid representation of the actual set-up. During the simulation it was acknowledged that due to the technical limitations it was not possible to account for the long-wave and the short-wave radiation from windows in the laboratory room. Throughout the first two days when the weather was cloudy the measured and simulated values agreed nearly perfectly, but began to drift apart afterwards during the sunny weather.

The second simulation of the test chamber with a PCM cooling panel was performed in order to validate the results generated by the developed simulation model of the PCM cooling panel. With the introduction of the panel the maximum deviation and RMSE increased (see Table 8.1). However, these values were equal or better than reported in other similar studies.

The third and fourth simulation cases where the developed model was compared with the results from the CFD simulation study were performed to evaluate the performance for a more practical situation. The maximum deviation and RMSE in these cases was similar with the values acquired in the first and second case (see Table 8.1).

It can be concluded that the values acquired in the second and fourth case describe the actual accuracy of the developed model.

Table 8.1

## Summary of the statistical indicators of the simulation results

Statistical indicator	Value reached in this study	Values reached in other similar studies
Simulated values against measurements – case without a PCM panel		
$D_{max}$	less than 1 °C	-
$D_{avg}$	-	-
$r$	0.98	-
$RMSE$	0.53 °C	-
Simulated values against measurements – case with a PCM panel		
$D_{max}$	2.2 °C	Nageler et al. from ~3.5 °C to ~4.7 °C [161]; Cornaro et al. 2.5 °C [162]
$D_{avg}$	1.2 °C	-
$r$	0.95	-
$RMSE$	1.01 °C	Nageler et al. from ~0.5 °C to ~1.8 °C [161]; Cornaro et al. 1.83 °C [162]
Simulation model against previous CFD study – case without a PCM panel		
$D_{max}$	1 °C	-
$D_{avg}$	0.6 °C	-
$r$	0.98	-
$RMSE$	1.1 °C	-
Simulation model against previous CFD study – case with a PCM panel		
$D_{max}$	2.6 °C	-
$D_{avg}$	0.7 °C	-
$r$	0.93	-
$RMSE$	1.3 °C	-

### 8.3 Limitations of the developed model

#### Surface heat transfer coefficients

Since the developed model utilises a combined radiant and convective heat transfer coefficient and the estimated heat exchange in the experimental set-up is 80 % convective and 20 % radiant (conduction heat transfer is considered negligible) the model shall be applied for similar conditions.

The model shall not be used for highly convective applications or forced convection applications without adjusting the heat transfer coefficient.

The model shall not be used in situations with highly radiant heat exchange (panel directly exposed to solar radiation) without compensation for surface heat exchange coefficient.

The developed model should be used as a ceiling panel in rooms with heat gains typical for comfort cooling in non-industrial buildings.

### **PCM layer**

The panel was validated for 40 mm PCM thickness (20 mm above hydronic circuit and 20 mm below). Internal buoyancy and change of volume during phase transition is not modelled. The PCM layer is not modelled with finite difference model but as uniform layer with evenly distributed state of the PCM material and evenly distributed temperature. PCM thickness greater than 20 mm above the cooling circuit and 20 mm below the cooling circuit shall not be used when applying this model.

### **Hydronic circuit**

The hydronic circuit is modelled according to the EN 15377-1 [160] with fixed heat transfer that accounts for equivalent heat transfer from water to an imaginary layer located in the middle of the PCM. This heat transfer coefficient was calculated using finite difference method and is dependent on:

- The convective heat transfer coefficient between the liquid and wall of the pipe:
  - properties of the liquid;
  - flow rate of the liquid;
  - pipe diameter and roughness.
- Thermal conductivity of the pipe material and thickness;
- Thermal conductivity of the PCM material.

If the properties of the hydronic circuit and PCM significantly differ from the values used in this study (refer to table Table 7.2) the  $R_t$  value shall be recalculated to suit the properties of the modelled system. Particular attention shall be paid to the thermal conductivity of PCM and situations where the liquid inside the cooling circuit is not pure water (water with antifreeze additives) or the flow is not turbulent.

## 9 CONCLUSION

This thesis represents an original research that consists of a state of art literature review and an experimental study.

Chapter 2 describes the background for NZEB requirements in the EU member countries, description on how NZEB principles are incorporated on a national level and how overheating of buildings is addressed in the building codes. Most countries have acknowledged the current problem of overheating in modern buildings and incorporated measures to address this issue. In most cases there is a limitation of maximum temperature in rooms, defined as maximum temperature or a maximum degree-hour threshold above a certain room temperature. Unfortunately, some of the member countries, for example, Latvia has less developed building codes where in principle this issue is addressed: however, there is no further information on how to demonstrate compliance to these requirements. Such uncertainty in building codes can lead to wide range of interpretations. These requirements are the main driving force for the construction industry to apply passive cooling and thermal storage technology in order to meet required building energy performance.

Furthermore, chapter 3 outlines existing passive cooling technologies that can be supported by latent thermal energy storage systems (including PCM cooling panels). These technologies rely on different principles and their performance and efficiency can vary case to case for different types of buildings and different climatic conditions. Most passive cooling technologies (apart from geothermal cooling in some cases) cannot cover 100 % of building cooling requirements and have some limitations. Night cooling is highly dependent on outdoor temperature, radiant cooling is dependent on the sky cloud cover, whereas adiabatic cooling as well as desiccant cooling lose efficiency during periods of high outdoor humidity and geothermal cooling must have annual energy balance, otherwise cooling and heating potential of the ground can be depleted. It is clear that to fully cover or at least extend the fraction of passive cooling in a building a combination of passive cooling technologies and a suitable thermal energy storage must be used.

Chapters 4 and 5 address previous research on latent thermal storage systems. Research in the field indicates that fatty acid and paraffin based PCMs can be utilized to support passive cooling technologies. Paraffin based PCMs have a good balance between cost and performance and variety of commercial products are available with a wide range of melting temperatures. These properties make paraffin based PCMs the best candidate for passive cooling applications in the scope of this thesis.

PCM based TES in general can be divided into two types: active and passive. Passive applications have smaller capital investment but generally tend to be less effective; however, there are also a few examples with significant energy savings. The most promising active applications are PCM to air heat exchangers incorporated in ventilation systems and ceiling based cooling panels with integrated latent thermal storage. The control of PCM to air heat exchanger in a ventilation system requires complex control logic. On the other hand, ceiling

based cooling panels with integrated latent thermal storage are simpler to integrate in buildings and existing technologies.

Chapter 6 describes heat transfer fundamentals in HVAC systems. These fundamentals are required to develop new latent thermal storage systems and apply existing systems. Aforementioned fundamentals are essential for developing mathematical representations or simulation models of physical components to predict the behaviour of these components for the specific case of interest.

The experimental study (chapters 7 and 8) consists of a detailed description of the developed equation based simulation model and series of experiments to validate and evaluate the performance of the model. The developed simulation model is initially validated against experimental measurements in a test chamber. Afterwards a comparative study is performed to compare results generated by the developed model against a CFD simulation previously carried out by other authors. The main purpose of the experimental study is to acquire an industry ready simulation model for the previously developed cooling panel with integrated latent thermal storage system.

The main advantage of the equation based simulation model over the CFD simulation is the ability to perform practical full building scale cooling, thermal comfort and energy simulations. By using current technology it is impractical to perform such calculations with CFD simulation tools due to vast computational power that is required for these actions. This argument is confirmed by the fact that using a standard computer the CFD simulation case carried out by Rucevskis et al. [141,142] took approximately 150 hours to compute (a simplified two-dimensional case). On the other hand the same simulation case with *IDA ICE* took only 45 seconds. For larger simulation models and extended simulation time periods dynamic simulation models are the only practical tools to precisely predict the thermal behaviour of the researched cooling panel.

Statistical analyses are applied to evaluate the agreement between the results generated by the simulation model against experimental measurements and results generated in a previous CFD simulation study. The statistical indicators demonstrate that the reached accuracy of the developed model is adequate. The maximum deviation and RMSE is at least equal or better than achieved in similar previous studies. Studies carried out by Nageler et al. [161] and Cornaro et al. [162] were used to compare the accuracy of results acquired in this study. The maximum deviation for simulation results against measured results for the case with a PCM panel in this study is 2.2 °C. The reported maximum deviation is smaller than in both previous studies where it was up to ~4.7 °C (Nageler et al. [161]) and 2.5 °C (Cornaro et al. [162]). Similarly, the RMSE 1.01 °C is in line with both previous studies where it was up to ~1.8 °C (Nageler et al. [161]) and 1.83 °C (Cornaro et al. [162]).

Additionally, limitations of the developed model are emphasized in order to avoid inaccurate simulation cases. The simulation model must not be used for cases with high radiant heat gains, since the model is calibrated for 80 % convective and 20 % radiant heat source. The model must not be used for PCM layers with thickness more than 20 mm above and below the cooling circuit. This limitation is due to the fact that the PCM layer is modelled as a uniform layer. Moreover, the cooling circuit inside the panel is calculated according to

the EN 15377-1 [160], therefore, the  $R_t$  value must be recalculated if other type of pipe circuit is used or the thermal conductivity of the PCM is other than  $\sim 0.2 \text{ W/m}\cdot\text{K}$ .

The accuracy reached by the developed simulation model can be considered suitable for application in construction industry if the limitations of the developed model are respected. Therefore, the hypothesis stated before the completion of the research: *“Experimentally validated equation based numerical simulation model of a hydronic cooling panel with integrated latent thermal storage can produce simulation results with accuracy suitable for application in construction industry to support other passive cooling technologies”* is confirmed.

After completion of the research it can be concluded that:

1. Majority of the EU member countries have addressed the issue of overheating in NZEB and low energy buildings in their building codes;
2. Literature review indicates that there is a variety of reliable and industry-ready passive cooling technologies that can be supported by latent thermal storage systems;
3. Research of the field literature reveals that there are many PCM based thermal storage systems researched previously. PCM to air heat exchangers incorporated in ventilations systems and ceiling based PCM cooling panels can be perceived as the most promising systems;
4. According to the results it can be concluded that this type of numerical model indeed can produce simulation results with precision that is comparable with results acquired in a CFD study;
5. The accuracy of the results acquired from the developed model is similar or more accurate than reported in similar studies;
6. The developed numerical model can be applied for practical use in construction industry for a whole building scale thermal comfort, cooling capacity and annual energy simulations. The computational power required is orders of magnitude smaller than that of CFD simulations.

## 10 BIBLIOGRAPHY

1. Sergeev, V.V.; Petrichenko, M.R.; Nemova, D.V.; Kotov, E.V.; Tarasova, D.S.; Nefedova, A.V.; Borodinecs, A.B. The building extension with energy efficiency light-weight building walls. *Mag. Civ. Eng.* **2018**, *84*, 67–74, doi:10.18720/MCE.84.7.
2. Andy Overheating in dwellings Guidance Document The BRE Centre for Resilience. **2016**.
3. Aebischer, B.; Henderson, G.; Jakob, M.; Catenazzi, G. Impact of climate change on thermal comfort, heating and cooling energy demand in Europe. *ECEEE 2007 Summer Study* **2007**, 859–870.
4. Maivel, M.; Kurnitski, J.; Kalamees, T. Field survey of overheating problems in Estonian apartment buildings. *Archit. Sci. Rev.* **2015**, *58*, 1–10, doi:10.1080/00038628.2014.970610.
5. Gorshkov, A.S.; Vatin, N.I.; Rymkevich, P.P. Climate change and the thermal island effect in the million-plus city. *Строительство Уникальных Зданий И Сооружений* **2020**, *89*, 8902–8902, doi:10.18720/CUBS.89.2.
6. De Luca, F.; Dogan, T.; Kurnitski, J. Methodology for determining fenestration ranges for daylight and energy efficiency in Estonia. In *Proceedings of the Simulation Series*; 2018; Vol. 50, pp. 47–54.
7. Borodinecs, A.; Zemitis, J.; Geikins, A.; Bykova, I. V; Nefedova, A. V; Kupavykh, S. V Energy-efficient construction in the climatic conditions of Latvia TT - Энергоэффективное строительство в климатических условиях Латвии. *Stroit. Unikal'nyh Zdanij i Sooruz.* **2018**, *3*, 41–48, doi:http://dx.doi.org/10.18720/CUBS.66.4.
8. The Future of Cooling. *Futur. Cool.* **2018**, doi:10.1787/9789264301993-en.
9. Millers, R.; Korjakins, A.; Lešinskis, A.; Borodinecs, A. Cooling Panel with Integrated PCM Layer: A Verified Simulation Study. *Energies* **2020**, doi:10.3390/en13215715.
10. United Nations Kyoto Protocol reference manual on accounting of emissions and assigned amount Available online: [https://unfccc.int/resource/docs/publications/08\\_unfccc\\_kp\\_ref\\_manual.pdf](https://unfccc.int/resource/docs/publications/08_unfccc_kp_ref_manual.pdf).
11. United Nations Paris Agreement. *Int. Leg. Mater.* 2016, *55*, 740–755.
12. European Commission Proposal for a REGULATION OF THE EUROPEAN PARLIAMENT AND OF THE COUNCIL. *Eur. Union* 2020.
13. Eichhammer, W.; Fleiter, T.; Schlomann, B.; Faberi, S.; Fioretto, M.; Piccioni, N.; Lechtenbohmer, S.; Schuring, A.; Resch, G. *Study on the energy savings potentials in EU member states, candidate countries and EEA countries*; 2009;
14. Ovchinnikov, P.; Borodinecs, A.; Millers, R. Utilization potential of low temperature hydronic space heating systems in Russia. *J. Build. Eng.* **2017**, *13*, doi:10.1016/j.job.2017.07.003.
15. EPBD CA 2013 *Implementing the Energy Performance of Building Directive (EPBD)*; Porto, 2013;

16. ÖNORM B 8110-3 Wärmeschutz im Hochbau - Teil 3: Ermittlung der operativen Temperatur im Sommerfall (Parameter zur Vermeidung sommerlicher Überwärmung) 2020.
17. ÖSTERREICHISCHEN, R. DES; INSTITUTS FÜR BAUTECHNIK Oib richtlinie 2019.
18. EPBD CA 2016 *Implementing the Energy Performance of Building Directive (EPBD)*; 2016;
19. Christensen, J.E.; Schiønning, P.; Dethlefsen, E. Comparison of simplified and advanced building simulation tool with measured data. In *Proceedings of the Proceedings of BS 2013: 13th Conference of the International Building Performance Simulation Association*; 2013; pp. 2357–2364.
20. Vabariigi Valitsus Energiatõhususe miinimumnõuded 2015.
21. Majandus- ja kommunikatsiooniminister Hoonete tehnosüsteemidele esitatavad nõuded1 2015.
22. Latvijas republikas Ministru kabinets Noteikumi par ēku energosertifikāciju 2016.
23. Latvijas republikas Ministru kabinets Noteikumi par Latvijas būvnormatīvu LBN 002-19 “Ēku norobežojošo konstrukciju siltumtehnika” 2019.
24. Latvijas republikas Ministru kabinets Noteikumi par Latvijas būvnormatīvu LBN 231-15 “Dzīvojamo un publisko ēku apkure un ventilācija” 2015.
25. Stetiu, C.; Feustel, H.E. Phase-change wallboard and mechanical night ventilation in commercial buildings. *Lawrence Berkeley Natl. Lab.* **1998**.
26. Barzin, R.; Chen, J.J.J.; Young, B.R.; Farid, M.M. Application of PCM energy storage in combination with night ventilation for space cooling. *Appl. Energy* **2015**, *158*, 412–421, doi:10.1016/j.apenergy.2015.08.088.
27. Solgi, E.; Fayaz, R.; Kari, B.M. Cooling load reduction in office buildings of hot-arid climate, combining phase change materials and night purge ventilation. *Renew. Energy* **2016**, doi:10.1016/j.renene.2015.07.028.
28. Saffari, M.; de Gracia, A.; Ushak, S.; Cabeza, L.F. Passive cooling of buildings with phase change materials using whole-building energy simulation tools: A review. *Renew. Sustain. Energy Rev.* 2017.
29. Givoni, B. Evaporative Cooling Systems. *Passiv. Low Energy Cool. Build.* **1994**.
30. Givoni, B. Comfort, climate analysis and building design guidelines. *Energy Build.* **1992**, doi:10.1016/0378-7788(92)90047-K.
31. Givoni, B. Performance and applicability of passive and low-energy cooling systems. *Energy Build.* **1991**, doi:10.1016/0378-7788(91)90106-D.
32. SUSAN, R.; PHILIP, H.; ORR, J. Climate change and passive cooling in Europe. *Environ. FRfENDLY C. ES, Proce<idings PLEA '98* **1998**, 463–466.
33. Artmann, N.; Manz, H.; Heiselberg, P. Climatic potential for passive cooling of buildings by night-time ventilation in Europe. *Appl. Energy* **2007**, *84*, 187–201, doi:10.1016/j.apenergy.2006.05.004.
34. Meteoronorm Global meteorological database for engineers, planners and education 2005.

35. Prozuments, A.; Vanags, I.; Borodinecs, A.; Millers, R.; Tumanova, K. A study of the passive cooling potential in simulated building in Latvian climate conditions. In Proceedings of the IOP Conference Series: Materials Science and Engineering; 2017; Vol. 251.
36. Meir, M.G.; Rekstad, J.B.; LØvvik, O.M. A study of a polymer-based radiative cooling system. *Sol. Energy* **2002**, doi:10.1016/S0038-092X(03)00019-7.
37. Eicker, U.; Dalibard, A. Photovoltaic-thermal collectors for night radiative cooling of buildings. *Sol. Energy* **2011**, doi:10.1016/j.solener.2011.03.015.
38. Péan, T.; Gennari, L.; Olesen, B.W.; Kazanci, O.B. Nighttime radiative cooling potential of unglazed and PV / T solar collectors: parametric and experimental analyses. In Proceedings of the Proceedings of the 8th Mediterranean Congress of Heating, Ventilation and Air-conditioning (climamed 2015); 2015.
39. ASHRAE *ASHRAE Fundamentals*; 2017;
40. Maghrabi, A.H.; Al-Mostafa, Z.A.; Kordi, M.N.; Clay, R.W. Preliminary test of physically based models to estimate clear sky emissivity in Tabouk, Saudi Arabia. *J. Assoc. Arab Univ. Basic Appl. Sci.* **2010**, doi:10.1016/j.jaubas.2010.12.003.
41. Evangelisti, L.; Guattari, C.; Asdrubali, F. On the sky temperature models and their influence on buildings energy performance: A critical review. *Energy Build.* **2019**, doi:10.1016/j.enbuild.2018.11.037.
42. Catalanotti, S.; Cuomo, V.; Piro, G.; Ruggi, D.; Silvestrini, V.; Troise, G. The radiative cooling of selective surfaces. *Sol. Energy* **1975**, doi:10.1016/0038-092X(75)90062-6.
43. Granqvist, C.G.; Hjortsberg, A. Surfaces for radiative cooling: Silicon monoxide films on aluminum. *Appl. Phys. Lett.* **1980**, doi:10.1063/1.91406.
44. Granqvist, C.G.; Hjortsberg, A. Radiative cooling to low temperatures: General considerations and application to selectively emitting SiO films. *J. Appl. Phys.* **1981**, doi:10.1063/1.329270.
45. Hossain, M.M.; Gu, M. Radiative cooling: Principles, progress, and potentials. *Adv. Sci.* 2016.
46. Berk, A.; Anderson, G.P.; Acharya, P.K.; Bernstein, L.S.; Muratov, L.; Lee, J.; Fox, M.; Adler-Golden, S.M.; Chetwynd, J.H.; Hoke, M.L.; et al. MODTRAN (TM) 5: 2006 update - art. no. 62331F. In *Algorithms and Technologies for Multispectral, Hyperspectral, and Ultraspectral Imagery XII Pts 1 and 2*; 2006 ISBN 0277-786Xr0-8194-6289-6.
47. Raman, A.P.; Anoma, M.A.; Zhu, L.; Rephaeli, E.; Fan, S. Passive radiative cooling below ambient air temperature under direct sunlight. *Nature* **2014**, doi:10.1038/nature13883.
48. Bao, H.; Yan, C.; Wang, B.; Fang, X.; Zhao, C.Y.; Ruan, X. Double-layer nanoparticle-based coatings for efficient terrestrial radiative cooling. *Sol. Energy Mater. Sol. Cells* **2017**, doi:10.1016/j.solmat.2017.04.020.
49. Chen, Z.; Zhu, L.; Raman, A.; Fan, S. Radiative cooling to deep sub-freezing temperatures through a 24-h day-night cycle. *Nat. Commun.* **2016**, doi:10.1038/ncomms13729.

50. Jeong, S.Y.; Tso, C.Y.; Ha, J.; Wong, Y.M.; Chao, C.Y.H.; Huang, B.; Qiu, H. Field investigation of a photonic multi-layered TiO<sub>2</sub> passive radiative cooler in sub-tropical climate. *Renew. Energy* **2020**, doi:10.1016/j.renene.2019.06.119.
51. Kecebas, M.A.; Menguc, M.P.; Kosar, A.; Sendur, K. Passive radiative cooling design with broadband optical thin-film filters. *J. Quant. Spectrosc. Radiat. Transf.* **2017**, doi:10.1016/j.jqsrt.2017.03.046.
52. Kou, J. long; Jurado, Z.; Chen, Z.; Fan, S.; Minnich, A.J. Daytime Radiative Cooling Using Near-Black Infrared Emitters. *ACS Photonics* **2017**, doi:10.1021/acsp Photonics.6b00991.
53. Zhai, Y.; Ma, Y.; David, S.N.; Zhao, D.; Lou, R.; Tan, G.; Yang, R.; Yin, X. Scalable-manufactured randomized glass-polymer hybrid metamaterial for daytime radiative cooling. *Science (80-. )*. **2017**, doi:10.1126/science.aai7899.
54. Jeong, S.Y.; Tso, C.Y.; Wong, Y.M.; Chao, C.Y.H.; Huang, B. Daytime passive radiative cooling by ultra emissive bio-inspired polymeric surface. *Sol. Energy Mater. Sol. Cells* **2020**, doi:10.1016/j.solmat.2019.110296.
55. Millers, R.; Korjakins, A.; Lesinskis, A. Thermally activated concrete slabs with integrated PCM materials. In Proceedings of the E3S Web of Conferences; 2019; Vol. 111.
56. Zhiyin Duan a; Changhong Zhan b; Xingxing Zhang a; Mahmud Mustafa a; Xudong Zhao a, n; Behrang Alimohammadisagvand c; Ala Hasan Indirect evaporative cooling: Past, present and future potentials. *Renew. Sustain. Energy Rev.* **2012**.
57. Amer, E.H. Passive options for solar cooling of buildings in arid areas. *Energy* **2006**, doi:10.1016/j.energy.2005.06.002.
58. Santamouris, M.; Kolokotsa, D. Passive cooling dissipation techniques for buildings and other structures: The state of the art. *Energy Build.* **2013**.
59. Heidarinejad, G.; Bozorgmehr, M.; Delfani, S.; Esmaelian, J. Experimental investigation of two-stage indirect/direct evaporative cooling system in various climatic conditions. *Build. Environ.* **2009**, doi:10.1016/j.buildenv.2009.02.017.
60. Heidarinejad, G.; Farmahini Farahani, M.; Delfani, S. Investigation of a hybrid system of nocturnal radiative cooling and direct evaporative cooling. *Build. Environ.* **2010**, doi:10.1016/j.buildenv.2010.01.003.
61. Heidarinejad, G.; Khalajzadeh, V.; Delfani, S. Performance analysis of a ground-assisted direct evaporative cooling air conditioner. *Build. Environ.* **2010**, doi:10.1016/j.buildenv.2010.05.009.
62. Phillips, R. Using direct evaporative + chilled water cooling. *ASHRAE J.* **2009**.
63. Sheng, C.; Agwu Nnanna, A.G. Empirical correlation of cooling efficiency and transport phenomena of direct evaporative cooler. *Appl. Therm. Eng.* **2012**, doi:10.1016/j.applthermaleng.2012.01.052.
64. Kim, M.H.; Kim, J.H.; Kwon, O.H.; Choi, A.S.; Jeong, J.W. Energy conservation potential of an indirect and direct evaporative cooling assisted 100% outdoor air system. *Build. Serv. Eng. Res. Technol.* **2011**, doi:10.1177/0143624411402637.
65. Glanville, P.; Kozlov, A.; Maisotsenko, V. Dew point evaporative cooling: Technology review and fundamentals. In Proceedings of the ASHRAE Transactions; 2011.

66. Farmahini-Farahani, M.; Heidarinejad, G. Increasing effectiveness of evaporative cooling by pre-cooling using nocturnally stored water. *Appl. Therm. Eng.* **2012**, doi:10.1016/j.applthermaleng.2012.01.023.
67. Velasco Gómez, E.; Tejero González, A.; Rey Martínez, F.J. Experimental characterisation of an indirect evaporative cooling prototype in two operating modes. *Appl. Energy* **2012**, doi:10.1016/j.apenergy.2011.12.065.
68. Robinson, D.; Lomas, K.J.; Cook, M.J.; Eppel, H. Passive down-draught evaporative cooling: Thermal modelling of an office building. *Indoor Built Environ.* **2004**, doi:10.1177/1420326X04043816.
69. Nasr, M.M.; Hassan, M.S. Experimental and theoretical investigation of an innovative evaporative condenser for residential refrigerator. *Renew. Energy* **2009**, doi:10.1016/j.renene.2009.03.008.
70. Daou, K.; Wang, R.Z.; Xia, Z.Z. Desiccant cooling air conditioning: A review. *Renew. Sustain. Energy Rev.* 2006.
71. Mavroudaki, P.; Beggs, C.B.; Sleigh, P.A.; Halliday, S.P. The potential for solar powered single-stage desiccant cooling in southern Europe. *Appl. Therm. Eng.* **2002**, doi:10.1016/S1359-4311(02)00034-0.
72. Labs, K. *Passive Cooling*; Cook, Jeffrey, Eds.; The MIT Press: Cambridge, Massachusetts, 1989; ISBN 978-0-262-03147-9.
73. Mihalakakou, G.; Santamouris, M.; Asimakopoulos, D. Modelling the earth temperature using multiyear measurements. *Energy Build.* **1992**, doi:10.1016/0378-7788(92)90031-B.
74. Mihalakakou, G.; Santamouris, M.; Lewis, J.O.; Asimakopoulos, D.N. On the application of the energy balance equation to predict ground temperature profiles. *Sol. Energy* **1997**, doi:10.1016/S0038-092X(97)00012-1.
75. Staniec, M.; Nowak, H. The application of energy balance at the bare soil surface to predict annual soil temperature distribution. *Energy Build.* **2016**, doi:10.1016/j.enbuild.2016.05.047.
76. Badache, M.; Eslami-Nejad, P.; Ouzzane, M.; Aidoun, Z.; Lamarche, L. A new modeling approach for improved ground temperature profile determination. *Renew. Energy* **2016**, doi:10.1016/j.renene.2015.06.020.
77. Jacovides, C.P.; Mihalakakou, G.; Santamouris, M.; Lewis, J.O. On the ground temperature profile for passive cooling applications in buildings. *Sol. Energy* **1996**, doi:10.1016/S0038-092X(96)00072-2.
78. Mihalakakou, G.; Santamouris, M.; Asimakopoulos, D. On the cooling potential of earth to air heat exchangers. *Energy Convers. Manag.* **1994**, doi:10.1016/0196-8904(94)90098-1.
79. Mihalakakou, G.; Santamouris, M.; Asimakopoulos, D. Use of the ground for heat dissipation. *Energy* **1994**, doi:10.1016/0360-5442(94)90101-5.
80. International Energy Agency Low Energy Cooling 2000.
81. Breesch, H.; Bossaer, A.; Janssens, A. Passive cooling in a low-energy office building. In Proceedings of the Solar Energy; 2005.

82. Pfafferott, J. Evaluation of earth-to-air heat exchangers with a standardised method to calculate energy efficiency. *Energy Build.* **2003**, doi:10.1016/S0378-7788(03)00055-0.
83. International Energy Agency Energy Conservation in Buildings and Community Systems, Annex 36 Case studies overview- UK1. **2003**, 117–122.
84. Anis Akrouch, G.; Sánchez, M.; Briaud, J.L. Thermal performance and economic study of an energy piles system under cooling dominated conditions. *Renew. Energy* **2020**, doi:10.1016/j.renene.2018.11.101.
85. Fadejev, J.; Simson, R.; Kurnitski, J.; Kesti, J.; Mononen, T.; Lautso, P. Geothermal Heat Pump Plant Performance in a Nearly Zero-energy Building. In Proceedings of the Energy Procedia; 2016.
86. Fadejev, J.; Simson, R.; Kurnitski, J.; Kesti, J. Heat Recovery from Exhaust Air as a Thermal Storage Energy Source for Geothermal Energy Piles. In Proceedings of the Energy Procedia; 2016.
87. Hu, B.; Luo, Z. Life-cycle probabilistic geotechnical model for energy piles. *Renew. Energy* **2020**, doi:10.1016/j.renene.2019.09.022.
88. Zalba, B.; Marín, J.M.; Cabeza, L.F.; Mehling, H. Review on thermal energy storage with phase change: Materials, heat transfer analysis and applications. *Appl. Therm. Eng.* 2003.
89. Telkes, M. Thermal storage for solar heating and cooling. In Proceedings of the Workshop on Solar Energy Storage Subsystems for the Heating and Cooling of Buildings; Lembit U., L., James Taylor, B., Fulvio Anthony, I., Eds.; The Society: Charlottesville, 1975.
90. Barkmann, H.; Wessling, J. Use of buildings structural components for thermal storage. In Proceedings of the Workshop on Solar Energy Storage Subsystems for the Heating and Cooling of Buildings; Lembit U., L., James Taylor, B., Fulvio Anthony, I., Eds.; The Society: Charlottesville, 1975.
91. Lane GA. *Solar Heat Storage: Latent Heat Materials Volume 1: Background and Scientific Principles*; CRC Press: London, New York, 1983; ISBN 9781315897653.
92. Abhat, A. Low temperature latent heat thermal energy storage: Heat storage materials. *Sol. Energy* **1983**, doi:10.1016/0038-092X(83)90186-X.
93. Zeinelabdein, R.; Omer, S.; Gan, G. Critical review of latent heat storage systems for free cooling in buildings. *Renew. Sustain. Energy Rev.* **2018**, 82, 2843–2868, doi:10.1016/j.rser.2017.10.046.
94. Cárdenas, B.; León, N. High temperature latent heat thermal energy storage: Phase change materials, design considerations and performance enhancement techniques. *Renew. Sustain. Energy Rev.* 2013.
95. Dieckmann, J.H.; Heinrich, H. *Betonwerk und Fertigteil-Technik/Concrete Plant and Precast Technology*. 2008, pp. 10–17.
96. Whiffen, T.R.; Riffat, S.B. A review of PCM technology for thermal energy storage in the built environment: Part I. *Int. J. Low-Carbon Technol.* **2013**, doi:10.1093/ijlct/cts021.
97. Koschenz, M.; Lehmann, B. Development of a thermally activated ceiling panel with

- PCM for application in lightweight and retrofitted buildings. *Energy Build.* **2004**, doi:10.1016/j.enbuild.2004.01.029.
98. Frusteri, F.; Leonardi, V.; Vasta, S.; Restuccia, G. Thermal conductivity measurement of a PCM based storage system containing carbon fibers. *Appl. Therm. Eng.* **2005**, doi:10.1016/j.applthermaleng.2004.10.007.
  99. Sari, A.; Karaipekli, A. Thermal conductivity and latent heat thermal energy storage characteristics of paraffin/expanded graphite composite as phase change material. *Appl. Therm. Eng.* **2007**, doi:10.1016/j.applthermaleng.2006.11.004.
  100. Cabeza, L.F.; Castell, A.; Barreneche, C.; De Gracia, A.; Fernández, A.I. Materials used as PCM in thermal energy storage in buildings: A review. *Renew. Sustain. Energy Rev.* 2011.
  101. Baetens, R.; Jelle, B.P.; Gustavsen, A. Phase change materials for building applications: A state-of-the-art review. *Energy Build.* 2010.
  102. Navarro, L.; Solé, A.; Martín, M.; Barreneche, C.; Olivieri, L.; Tenorio, J.A.; Cabeza, L.F. Benchmarking of useful phase change materials for a building application. *Energy Build.* **2019**, 182, 45–50, doi:10.1016/j.enbuild.2018.10.005.
  103. Farid, M.M.; Khudhair, A.M.; Razack, S.A.K.; Al-Hallaj, S. A review on phase change energy storage: Materials and applications. *Energy Convers. Manag.* 2004.
  104. Zhang, Y.; Zhou, G.; Lin, K.; Zhang, Q.; Di, H. Application of latent heat thermal energy storage in buildings: State-of-the-art and outlook. *Build. Environ.* **2007**, doi:10.1016/j.buildenv.2006.07.023.
  105. Sharma, A.; Tyagi, V. V.; Chen, C.R.; Buddhi, D. Review on thermal energy storage with phase change materials and applications. *Renew. Sustain. Energy Rev.* 2009.
  106. Veerakumar, C.; Sreekumar, A. Phase change material based cold thermal energy storage: Materials, techniques and applications - A review. *Int. J. Refrig.* 2016.
  107. Hawes, D.W.; Feldman, D.; Banu, D. Latent heat storage in building materials. *Energy Build.* **1993**, doi:10.1016/0378-7788(93)90040-2.
  108. Voelker, C.; Kornadt, O.; Ostry, M. Temperature reduction due to the application of phase change materials. *Energy Build.* **2008**, doi:10.1016/j.enbuild.2007.07.008.
  109. Karaipekli, A.; Sari, A.; Biçer, A. Thermal regulating performance of gypsum/(C18–C24) composite phase change material (CPCM) for building energy storage applications. *Appl. Therm. Eng.* **2016**, doi:10.1016/j.applthermaleng.2016.06.160.
  110. Hunger, M.; Entrop, A.G.; Mandilaras, I.; Brouwers, H.J.H.; Founti, M. The behavior of self-compacting concrete containing micro-encapsulated Phase Change Materials. *Cem. Concr. Compos.* **2009**, doi:10.1016/j.cemconcomp.2009.08.002.
  111. Arce, P.; Castellón, C.; Castell, A.; Cabeza, L.F. Use of microencapsulated PCM in buildings and the effect of adding awnings. *Energy Build.* **2012**, 44, 88–93, doi:10.1016/j.enbuild.2011.10.028.
  112. Evola, G.; Marletta, L.; Sicurella, F. A methodology for investigating the effectiveness of PCM wallboards for summer thermal comfort in buildings. *Build. Environ.* **2013**, 59, 517–527, doi:10.1016/j.buildenv.2012.09.021.
  113. Barzin, R.; Chen, J.J.J.; Young, B.R.; Farid, M.M. Application of PCM underfloor

- heating in combination with PCM wallboards for space heating using price based control system. *Appl. Energy* **2015**, doi:10.1016/j.apenergy.2015.03.027.
114. Kuznik, F.; Virgone, J.; Noel, J. Optimization of a phase change material wallboard for building use. *Appl. Therm. Eng.* **2008**, doi:10.1016/j.applthermaleng.2007.10.012.
  115. Heim, D.; Clarke, J.A. Numerical modelling and thermal simulation of PCM-gypsum composites with ESP-r. In Proceedings of the Energy and Buildings; 2004.
  116. Zhang, Y.; Lin, K.; Jiang, Y.; Zhou, G. Thermal storage and nonlinear heat-transfer characteristics of PCM wallboard. *Energy Build.* **2008**, doi:10.1016/j.enbuild.2008.03.005.
  117. Stovall, T.K.; Tomlinson, J.J. What are the potential benefits of including latent storage in common wallboard? *J. Sol. Energy Eng. Trans. ASME* **1995**, doi:10.1115/1.2847868.
  118. Carbonari, A.; De Grassi, M.; Di Perna, C.; Principi, P. Numerical and experimental analyses of PCM containing sandwich panels for prefabricated walls. *Energy Build.* **2006**, doi:10.1016/j.enbuild.2005.08.007.
  119. Evers, A.C.; Medina, M.A.; Fang, Y. Evaluation of the thermal performance of frame walls enhanced with paraffin and hydrated salt phase change materials using a dynamic wall simulator. *Build. Environ.* **2010**, doi:10.1016/j.buildenv.2010.02.002.
  120. Halford, C.K.; Boehm, R.F. Modeling of phase change material peak load shifting. *Energy Build.* **2007**, doi:10.1016/j.enbuild.2006.07.005.
  121. Alawadhi, E.M. Thermal analysis of a building brick containing phase change material. *Energy Build.* **2008**, doi:10.1016/j.enbuild.2007.03.001.
  122. Alawadhi, E.M.; Alqallaf, H.J. Building roof with conical holes containing PCM to reduce the cooling load: Numerical study. *Energy Convers. Manag.* **2011**, doi:10.1016/j.enconman.2011.04.004.
  123. Vanaga, R.; Blumberga, A.; Freimanis, R.; Mols, T.; Blumberga, D. Solar facade module for nearly zero energy building. *Energy* **2018**, *157*, 1025–1034, doi:10.1016/j.energy.2018.04.167.
  124. Osterman, E.; Hagel, K.; Rathgeber, C.; Butala, V.; Stritih, U. Parametrical analysis of latent heat and cold storage for heating and cooling of rooms. *Appl. Therm. Eng.* **2015**, *84*, 138–149, doi:10.1016/j.applthermaleng.2015.02.081.
  125. Darzi, A.A.R.; Moosania, S.M.; Tan, F.L.; Farhadi, M. Numerical investigation of free-cooling system using plate type PCM storage. *Int. Commun. Heat Mass Transf.* **2013**, *48*, 155–163, doi:10.1016/j.icheatmasstransfer.2013.08.025.
  126. Borcuch, M.; Musiał, M.; Sztekler, K.; Kalawa, W.; Gumuła, S.; Stefański, S. The influence of flow modification on air and PCM temperatures in an accumulative heat exchanger. In Proceedings of the EPJ Web of Conferences; 2018; Vol. 180.
  127. Hed, G.; Bellander, R. Mathematical modelling of PCM air heat exchanger. *Energy Build.* **2006**, doi:10.1016/j.enbuild.2005.04.002.
  128. Jaworski, M.; Łapka, P.; Furmański, P. Numerical modelling and experimental studies of thermal behaviour of building integrated thermal energy storage unit in a form of a ceiling panel. *Appl. Energy* **2014**, doi:10.1016/j.apenergy.2013.07.068.

129. Jaworski, M. Thermal performance of building element containing phase change material (PCM) integrated with ventilation system - An experimental study. *Appl. Therm. Eng.* **2014**, doi:10.1016/j.applthermaleng.2014.05.093.
130. Borderon, J.; Virgone, J.; Cantin, R. Modeling and simulation of a phase change material system for improving summer comfort in domestic residence. *Appl. Energy* **2015**, *140*, 288–296, doi:10.1016/j.apenergy.2014.11.062.
131. Cassedy, S., E. *Prospects for Sustainable Energy*; Cambridge University Press: Cambridge, 2000; ISBN 0521631203.
132. Wang, X.; Niu, J.; van Paassen, A.H.C. Raising evaporative cooling potentials using combined cooled ceiling and MPCM slurry storage. *Energy Build.* **2008**, *40*, 1691–1698, doi:10.1016/j.enbuild.2008.02.028.
133. Wang, X.; Niu, J.; Li, Y.; Wang, X.; Chen, B.; Zeng, R.; Song, Q.; Zhang, Y. Flow and heat transfer behaviors of phase change material slurries in a horizontal circular tube. *Int. J. Heat Mass Transf.* **2007**, doi:10.1016/j.ijheatmasstransfer.2006.12.024.
134. Holmen, R.; Lamvik, M.; Melhus, O. Measurements of the Thermal Conductivities of Solid and Liquid Unbranched Alkanes in the C16-to-C19 Range During Phase Transition. *Int. J. Thermophys.* **2002**, doi:10.1023/A:1013988507251.
135. Yaws, C.L. *Yaws' Handbook of Thermodynamic and Physical Properties of Chemical Compounds*; McGraw-Hill: New York, 2003;
136. Dean, J.A. *Lange's handbook of chemistry*; McGraw-Hill: New York, 1999;
137. Tzivanidis, C.; Antonopoulos, K.A.; Kravvaritis, E.D. Parametric analysis of space cooling systems based on night ceiling cooling with PCM-embedded piping. *Int. J. Energy Res.* **2012**, doi:10.1002/er.1777.
138. Rubitherm GmbH Technical Data sheet for RT25HC 2020.
139. Weinsläder, H.; Klinker, F.; Yasin, M. PCM cooling ceilings in the Energy Efficiency Center - Passive cooling potential of two different system designs. *Energy Build.* **2016**, *119*, 93–100, doi:10.1016/j.enbuild.2016.03.031.
140. Ručevskis, S.; Akishin, P.; Korjakins, A. Parametric analysis and design optimisation of PCM thermal energy storage system for space cooling of buildings. *Energy Build.* **2020**, doi:10.1016/j.enbuild.2020.110288.
141. Rucevskis, S.; Akishin, P.; Korjakins, A. Performance Evaluation of an Active PCM Thermal Energy Storage System for Space Cooling in Residential Buildings. *Environ. Clim. Technol.* **2019**, doi:10.2478/rtuct-2019-0056.
142. Rucevskis, S.; Akishin, P.; Korjakins, A. Numerical Study of Application of PCM for a Passive Thermal Energy Storage System for Space Cooling in Residential Buildings. In *Proceedings of the IOP Conference Series: Materials Science and Engineering*; 2019.
143. Goodfellow, H.; Tahti, E. *Industrial Ventilation Design Guidebook*; Academic Press: Orlando, 2001; ISBN 0-12-289676-9.
144. Stoecker, W.F.; Jones, J.. *Refrigeration and Air Conditioning*; McGraw-Hill: Auckland, 1982;
145. The Information Philosopher Available online: <https://www.informationphilosopher.com/solutions/scientists/planck/>.

146. Travesi, J.; Maxwell, G.; Klaassen, C.; Holtz, M. Empirical validation of Iowa energy resource station building energy analysis simulation models. **2001**.
147. Sahlin, P.; Grozman, P. IDA Simulation Environment a tool for Modelica based end-user application deployment. *Proc. 3rd Int. Model. Conf. Linkoping, Novemb. 3-4 2003* **2003**, 105–114.
148. International Organization for Standardization ISO 13790:2008 Energy performance of buildings — Calculation of energy use for space heating and cooling 2008.
149. Rubitherm GmbH Technical data sheet for RT22HC 2018, 1.
150. American National Standards Institute; American Society of Heating Refrigerating and Air-Conditioning Engineers ANSI/ASHRAE Standard 140-2004 Building Thermal Envelope and Fabric Load Tests 2004.
151. European Committee for Standardization EN 15255:2007 Energy performance of buildings. Sensible room cooling load calculation. General criteria and validation procedures 2007.
152. European Committee for Standardization EN 15265:2007 Energy performance of buildings. Calculation of energy needs for space heating and cooling using dynamic methods. General criteria and validation procedures 2007.
153. European Committee for Standardization CEN 13791 Thermal Performance of Buildings - Calculation of Internal Temperatures of a Room in Summer Without Mechanical Cooling - General Criteria and Validation Procedures.
154. International Energy Agency CHC Task 34 Testing of Building Simulation Tools 2009.
155. Chartered Institution of Building Services Engineers (CIBSE) Technical Memorandum 33: Tests for software accreditation and verification 2006.
156. Modelica Association Available online: <https://www.modelica.org/> (accessed on Sep 13, 2020).
157. Sahlin, P.; Sowell, E.F. A neutral model format for building simulation models. *IBPSA Build. Simul. Conf.* **1989**, 1–10.
158. Sahlin, P. NMF handbook. **1996**.
159. Anderlind, G. A new model for calculating the effects of two and three-dimensional thermal bridges. In Proceedings of the The 5th Symposium Building Physics in the Nordic Countries; Chalmers University of Technology: Goteborg, 1999.
160. European Committee for Standardization EN 15377-1:2008 Heating systems in buildings. Design of embedded water based surface heating and cooling systems. Determination of the design heating and cooling capacity 2008.
161. Nageler, P.; Schweiger, G.; Pichler, M.; Brandl, D.; Mach, T.; Heimrath, R.; Schranzhofer, H.; Hochenauer, C. Validation of dynamic building energy simulation tools based on a real test-box with thermally activated building systems (TABS). *Energy Build.* **2018**, *168*, 42–55, doi:<https://doi.org/10.1016/j.enbuild.2018.03.025>.
162. Cornaro, C.; Pierro, M.; Roncarati, D.; Puggioni, V. Validation of a PCM simulation tool in IDA ICE dynamic building simulation software using experimental data from solar test boxes. In Proceedings of the Building Simulation Applications; 2017; Vol. 2017-Febru, pp. 159–166.